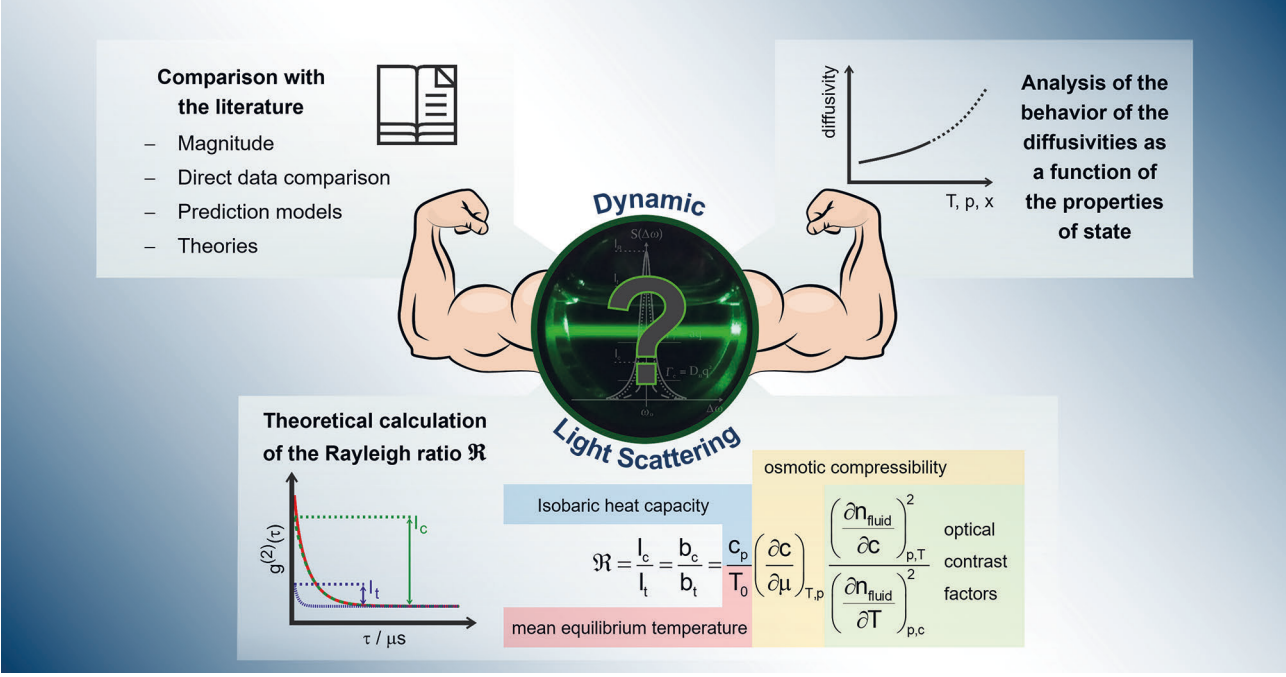

FAU Studies Chemical and Biological Engineering 5

Maximilian Piszko

Dynamic Light Scattering for Simultaneous Determination of Thermal and Mutual Diffusivities of Fluid Mixtures

FAU University Press

Maximilian Piszko

Dynamic Light Scattering for Simultaneous Determination of Thermal and Mutual Diffusivities of Fluid Mixtures

FAU Studies Chemical and Biological Engineering

Band 5

Herausgeber/-innen:
Prof. Dr. Kathrin Castiglione
Prof. Dr.-Ing. habil. Andreas Paul Fröba

Maximilian Piszko

Dynamic Light Scattering for Simultaneous Determination of Thermal and Mutual Diffusivities of Fluid Mixtures

Erlangen
FAU University Press
2025

Bibliografische Information der Deutschen Nationalbibliothek:
Die Deutsche Nationalbibliothek verzeichnet diese Publikation in der Deutschen Nationalbibliografie; detaillierte bibliografische Daten sind im Internet über http://dnb.d-nb.de abrufbar.

Kontakt: Maximilian Piszko, maximilian.piszko@fau.de, Friedrich-Alexander-Universität Erlangen-Nürnberg (ROR https://ror.org/00f7hpc57),
ORCID: 0000-0002-7929-8035

Bitte zitieren als
Piszko, Maximilian. 2025. *Dynamic Light Scattering for Simultaneous Determination of Thermal and Mutual Diffusivities of Fluid Mixtures*. FAU Studies Chemical and Biological Engineering Band 5. Erlangen: FAU University Press. DOI: 10.25593/978-3-96147-796-8.

Der vollständige Inhalt des Buchs ist als PDF über OPEN FAU
der Friedrich-Alexander-Universität Erlangen-Nürnberg abrufbar:
https://open.fau.de/home

Verlag und Auslieferung:
FAU University Press, Universitätsstraße 4, 91054 Erlangen

Druck: Docupoint

ISBN: 978-3-96147-795-1 (Druckausgabe)
eISBN: 978-3-96147-796-8 (Online-Ausgabe)
ISSN: 2940-6986
eISSN: 2940-6994
DOI: 10.25593/978-3-96147-796-8

Dynamic Light Scattering for Simultaneous Determination of Thermal and Mutual Diffusivities of Fluid Mixtures

Dynamische Lichtstreuung zur gleichzeitigen Bestimmung von Temperaturleitfähigkeit und Massendiffusionskoeffizienten in Fluidgemischen

Der Technischen Fakultät der
Friedrich-Alexander-Universität Erlangen-Nürnberg

zur Erlangung des Doktorgrades Dr.-Ing.

vorgelegt von
Maximilian Piszko, M. Sc. (Hons)
aus Rothenburg ob der Tauber

Als Dissertation genehmigt
von der Technischen Fakultät
der Friedrich-Alexander-Universität Erlangen-Nürnberg

Tag der mündlichen Prüfung: 02.08.2024

Gutachter: Prof. Dr.-Ing. habil. Andreas Paul Fröba
Prof. Dr.-Ing. Johannes Kiefer

Acknowledgement

The research presented in this thesis, as well as related work, were conducted at the Institute of Advanced Optical Technologies - Thermophysical Properties (AOT-TP) in the Department of Chemical and Biological Engineering (CBI) and at the Erlangen Graduate School in Advanced Optical Technologies (SAOT) at Friedrich-Alexander-Universität Erlangen-Nürnberg (FAU). Undertaking this research and producing meaningful work would not have been possible without financial support. Therefore, I extend my gratitude to the German Research Foundation (Deutsche Forschungsgemeinschaft, DFG) for their financial backing through projects FR 1709/11-1, FR 1709/11-2, and FR 1709/12-1. I also appreciate the support from the Arbeitsgemeinschaft industrieller Forschungsvereinigungen via the project 19028 BG/2. Furthermore, special thanks are due to Shell Global Solutions International BV for their financial support through a contracted research agreement. I also gratefully acknowledge the support provided by the Erlangen Graduate School in Advanced Optical Technologies (SAOT), funded by the Bavarian State Ministry for Science and Art.

I express my sincere gratitude to my doctoral supervisor Prof. Dr.-Ing. habil. Andreas Paul Fröba for providing me with the opportunity to conduct research in connection with my doctoral thesis at his research institute. I am particularly grateful for his honest discussions, scientific guidance, and the trust he placed in me and my work. He has motivated and challenged me, while also providing the necessary scientific opportunities and latitude conducive to my research activities.

I would like to thank all my colleagues, the numerous students who assisted me, and all members of AOT-TP for their support and contribution, which created a pleasant work atmosphere. In particular, my heartfelt thanks go to Dr. Cédric Giraudet and Dr.-Ing. Michael Rausch, who were valuable mentors, imparting knowledge regarding reliable laboratory work and scientific research. Their guidance significantly contributed to my development. Special appreciation is extended to Wenchang Wu, not only for becoming a good friend, but also for engaging in truly meaningful scientific discussions, and to Frances “The D.” Lenahan, for being a fellow sufferer in the shared projects. Furthermore, I want to acknowledge the Bachelor’s and Master’s thesis students in chronological order: Korbinian Batz, Maren Lang, Simon Hahn, Lukas Friedl, Claudio Dennstädt, and Sarah-Lena Steinacker. Their contributions were instrumental, and without them, this thesis would not have been possible.

I am also grateful to Prof. Dr.-Ing. Johannes Kiefer for agreeing to review my thesis.

Finally, I extend a very special thank you to my parents Gerlinde and Helmut, friends, and especially to Katharina for their patience and unwavering support throughout the past few years.

"There are many mistakes, but only one Nature"
~ researchers of Lab 5 at AOT-TP, 2022

In memory of Peter Krax and Harald Blumenstock

Abstract

Dynamic light scattering (DLS) stands as a powerful and well-established experimental technique for accurately determining transport and further thermophysical properties of pure fluids and fluid mixtures across a broad range of thermodynamic states. DLS, in contrast to conventional techniques relying on macroscopic gradients, proves particularly useful for determining thermal and mutual diffusivities near or within the two-phase region and in proximity to the critical point – where gradient-based techniques falter. Despite its utility, the DLS technique has limitations under certain conditions. It is not always possible to observe the expected number of signals or to unambiguously classify the signals obtained from experiments with respect to thermal and mutual diffusivities. Generally, the capabilities and limitations of DLS for the simultaneous determination of thermal and mutual diffusivities of fluid mixtures have not yet been fully explored.

This thesis aims to highlight which factors influence the feasibility of a simultaneous determination of thermal and mutual diffusivities in homogeneous molecular fluid mixtures through DLS. The focus is primarily on binary fluid mixtures, but certain aspects related to multicomponent mixtures are also discussed. Considering both theory and the experimental implementation of DLS, this thesis explores selected model systems consisting of methane and propane as well as binary mixtures of liquids with dissolved gases, facilitating fundamental investigations into different influencing factors. It also delves into various systems relevant for process and energy technologies which often have a technical nature. This includes systems relevant to the anticipated transition into a renewable energy economy, such as mixtures related to biofuels, electrolytes, and liquid organic hydrogen carriers, and to the geological storage of hydrogen. Additionally, mixtures related to natural gas and polymer melts with dissolved blowing agent are explored by DLS. Investigations are conducted across a wide range of thermodynamic states, encompassing temperatures between (280 and 560) K, pressures between (0.030 and 20) MPa, and compositions spanning mole fractions between about (0.002 and 0.995). This endeavor not only significantly expands the database of reliable diffusivity data but frequently showcases, for the first time, the applicability of DLS to the respective system.

The accessibility of specific diffusivities is strongly related to the location of the investigated thermodynamic state point relative to the phase

envelope of the mixture. In most cases, the simultaneous determination of thermal and mutual diffusivities hinges primarily on the signal-to-noise ratio, as well as the amplitudes and temporal spacing of the individual contributions. Drawing on insights gained from the various studies, an overview of the types of accessible diffusivities and their related uncertainties in different fluid classes and thermodynamic fluid states is presented. Relative experimental uncertainties of the diffusivities typically range between (0.6 and 15)%, but can also be as high as 100% under certain conditions. Additionally, a signal attribution strategy is developed, which is universally applicable to any binary fluid mixture.

Kurzdarstellung

Die Dynamische Lichtstreuung (DLS) ist eine leistungsfähige und etablierte experimentelle Technik zur genauen Bestimmung von Transporteigenschaften sowie weiterer thermophysikalischer Eigenschaften reiner Fluide und deren Gemische über weite Zustandsbereiche. Im Gegensatz zu konventionellen Techniken, die auf makroskopischen Gradienten basieren, erweist sich die DLS als besonders nützlich für die Bestimmung von Temperaturleitfähigkeit und Massendiffusionskoeffizienten in der Nähe oder innerhalb des Zweiphasengebietes sowie in der Nähe des kritischen Punkts – wo gradientenbasierte Techniken versagen. Trotz ihrer weiten Anwendbarkeit stößt die DLS unter bestimmten Bedingungen an ihre Grenzen, über die hinaus es nicht möglich ist, die erwartete Anzahl von Signalkomponenten zu beobachten oder die aus den Experimenten gewonnenen Signale bezüglich Temperaturleitfähigkeit und Massendiffusionskoeffizienten eindeutig zu klassifizieren. Bislang wurden die Möglichkeiten und Grenzen der DLS im Hinblick auf die gleichzeitige Bestimmung von Temperaturleitfähigkeit und Massendiffusionskoeffizienten in Fluidgemischen noch nicht vollständig erforscht.

Ziel der vorliegenden Arbeit ist es, zu einem besseren Verständnis der Faktoren beizutragen, die die gleichzeitige Bestimmung von Temperaturleitfähigkeit und Massendiffusionskoeffizienten in homogenen molekularen Fluidgemischen mittels DLS beeinflussen. Der Schwerpunkt liegt dabei in erster Linie auf binären Fluidgemischen, aber auch bestimmte Aspekte hinsichtlich der Untersuchung von Mehrkomponentengemischen werden diskutiert. Unter Berücksichtigung sowohl der Theorie als auch der experimentellen Umsetzung der DLS werden in dieser Arbeit ausgewählte Modellsysteme bestehend aus Methan und Propan, sowie binäre Gemische aus Flüssigkeiten mit darin gelösten Gasen untersucht, um grundlegende Untersuchungen verschiedener Einflussfaktoren durchzuführen. Darüber hinaus werden verschiedene in der Verfahrens- und Energietechnik relevante Systeme untersucht, die oft einen technischen Charakter aufweisen. Dies beinhaltet Systeme, die im Zusammenhang mit dem angestrebten Übergang zu einer erneuerbaren Energiewirtschaft stehen, wie z. B. Biokraftstoffe, Elektrolyte, flüssige organische Wasserstoffträger sowie der geologischen Speicherung von Wasserstoff. Darüber hinaus werden Gemische mit Bezug zu Erdgas sowie Polymerschmelzen mit darin gelöstem Treibmittel mittels DLS untersucht. Die Untersuchungen werden in einem breiten Spektrum thermodynamischer Zustände durchgeführt, das

Temperaturen von (280 bis 560) K, Drücke zwischen (0,030 und 20) MPa und Zusammensetzungen mit Molanteilen zwischen etwa (0,002 und 0,995) umfasst. Dieses Vorhaben erweitert nicht nur die Datenbank zuverlässiger Diffusionsdaten erheblich, sondern zeigt oft auch erstmalig die Anwendbarkeit der DLS auf das jeweilige System.

Die Zugänglichkeit spezifischer Diffusivitäten wird von der Lage des untersuchten thermodynamischen Zustandspunkts relativ zur Phasengrenzkurve des Gemisches beeinflusst. In den meisten Fällen hängt die gleichzeitige Bestimmung von Temperaturleitfähigkeit und Massendiffusionskoeffizienten in erster Linie vom Signal-Rausch-Verhältnis sowie von den Amplituden und zeitlichen Abständen der einzelnen Signale ab. Auf der Grundlage der aus den verschiedenen Studien gewonnenen Erkenntnisse wird ein Überblick über die Arten der zugänglichen Diffusivitäten und die zugehörigen Unsicherheiten für verschiedene Fluidklassen und thermodynamische Fluidzustände aufgezeigt. Die relativen experimentellen Unsicherheiten der Diffusivitäten liegen typischerweise zwischen (0,6 und 15)%, können aber unter bestimmten Bedingungen auch bis zu 100% betragen. Zusätzlich wird in dieser Arbeit eine Strategie zur Signalzuordnung entwickelt, die universell auf jedes binäre Fluidgemisch anwendbar ist.

Table of Contents

Symbols, Indices, and Abbreviations

Latin symbols

Symbol	Description	Unit
a	thermal diffusivity	$m^2 \cdot s^{-1}$
b	Fit parameter	
b_o	fit parameter; offset or base line in correlation function	
b_c	fit parameter; amplitude of signal related to concentration fluctuations in the correlation function	
b_t	fit parameter; amplitude of signal related to temperature fluctuations in the correlation function	
c	concentration	$mol \cdot m^{-3}$
c	weight or mass fraction	
c_o	speed of light in vacuo	$m \cdot s^{-1}$
c_{NaCl}	kg of sodium chloride per kg of water	
c_p	specific heat capacity at constant pressure	$J \cdot K^{-1} \cdot kg^{-1}$
c_s	sound speed	$m \cdot s^{-1}$
c_v	specific heat capacity at constant volume	$J \cdot K^{-1} \cdot kg^{-1}$
D_{11}	mutual or Fick diffusion coefficient	$m^2 \cdot s^{-1}$
D_{app}	apparent diffusion coefficient	$m^2 \cdot s^{-1}$
D_{eff}	effective diffusivity	$m^2 \cdot s^{-1}$
$\hat{D}_i$	eigenvalue of the Fick diffusion matrix with $i = 1$ or 2 for a binary mixture	$m^2 \cdot s^{-1}$
D_i or D	unidentified diffusivity, with $i = 1, 2$ for a binary mixture	$m^2 \cdot s^{-1}$
D_{ij}	components of the Fick diffusion matrix with i and $j = 1$ or 2 for a binary mixture	$m^2 \cdot s^{-1}$

D_m	mixed diffusivity	$m^2 \cdot s^{-1}$
D_p	barodiffusion coefficient	$m^2 \cdot s^{-1} \cdot Pa^{-1}$
D_{salt}	salt diffusion coefficient	$m^2 \cdot s^{-1}$
D_{self}	self-diffusion coefficient	$m^2 \cdot s^{-1}$
D_T	thermal diffusion coefficient (also referred to thermodiffusion coefficient in the literature)	$m^2 \cdot s^{-1} \cdot K^{-1}$
E	electric field	$V \cdot m^{-1}$
$G^{(2)}(\tau)$	second-order or intensity correlation function	$W^2 \cdot m^{-4}$
$g^{(2)}(\tau)$	normalized second-order or intensity correlation function	
$g_q(\tau)$	normalized time correlation function of the hydrodynamic fluctuations observed	
I	intensity or radiative flux	$W \cdot m^{-2}$
$I_{\{t,c\}}$	amplitude of signal related to fluctuations in temperature or concentration	
$\vec{j}^c$	linearized diffusion flux	$mol \cdot m^{-2} \cdot s^{-1}$
K	thermodynamic quantity defined in the text	
k	coverage factor	
k_B	Boltzmann constant	$J \cdot K^{-1}$
k_m	mass transfer coefficient	$m \cdot s^{-1}$
k_T	thermal diffusion ratio	
$\vec{k}$	wave vector	m^{-1}
l_o	mean free path length	m
Le	Lewis number	
l_{char}	characteristic length	m
M_i	molar mass of the component i	$g \cdot mol^{-1}$
N	number of (spherically symmetric) molecules or scatterer	

N_a	Avogadro constant	mol^{-1}
n_{air}	refractive index of air	
n_c	number of components	
n_{fluid}	refractive index of the fluid	
Nu	Nußelt number	
Pe	Péclet number	
Pr	Prandtl number	
p	pressure	Pa
q	modulus of the wave or scattering vector	m^{-1}
$\vec{q}$	scattering vector	m^{-1}
R_o	distance from the origin to the point of observation	m
$\mathcal{R}$	Rayleigh ratio = $I_c \cdot I_t^{-1}$	
$\vec{r}$	space variable	m
$S(\vec{q},\Delta\omega)$	generalized dynamic structure factor	s
$S(\Delta\omega)$	spectral power density	$W \cdot Hz^{-1}$
s	entropy per unit mass	$J \cdot K^{-1} \cdot kg^{-1}$
Sc	Schmidt number	
Sh	Sherwood number	
S_T	Soret coefficient	K^{-1}
T	measurement duration	s
T	temperature	K
t	time	s
u	velocity	$m \cdot s^{-1}$
u_f	flow velocity	$m \cdot s^{-1}$
w	$= \rho_o \nabla \cdot \vec{u}$	
x	variable thermodynamic quantity	
x	mole fraction	

z	complex Laplace variable
$z_{\pm}$	propagating modes
$z_{\pm}^{\circ}$	non-propagating modes

Greek symbols

$\alpha_{e,i}$	average molecular polarizability of component i	$Å^3$
β_S	solutal expansion coefficient	
β_T	thermal expansion coefficient	K^{-1}
Γ	spectral width of Lorentzian contribution	s^{-1}
γ	angle between the electric vector of the plane polarized incident light and R_o	rad
δx	fluctuating quantity x	
ε	dielectric constant of the medium	$C \cdot V^{-1} \cdot m^{-1}$
η_s	dynamic viscosity or shear viscosity	Pa·s
η_v	bulk viscosity	Pa·s
Θ_I	incident angle	rad
Θ_S	scattering angle	rad
κ	coupling parameter	
κ_c	thermal conductivity	$W \cdot m^{-1} \cdot K^{-1}$
Λ	wavelength of fluctuations	m
λ_o	wavelength of laser in vacuo	m
μ	chemical potential difference between two components in a mixture	$J \cdot mol^{-1}$
ν	kinematic viscosity	$m^2 \cdot s^{-1}$
ν_l	longitudinal viscosity $=(4/3\eta_s - \eta_v)\rho_o^{-1}$	$Pa \cdot s \cdot m^3 \cdot kg^{-1}$
$\Xi(\tau)$	arbitrary function to describe disturbances of the experimental correlation functions	

ρ	density of pure component or mixture	$kg \cdot m^{-3}$
τ	delay time	s
τ_C	characteristic decay time, mean lifetime, or relaxation time	s
ω	angular frequency	$rad \cdot s^{-1}$
ω_0	angular frequency of laser in vacuo	$rad \cdot s^{-1}$
$\Delta\omega$	change in angular frequency	$rad \cdot s^{-1}$

Indices

ad.	adiabatic
c	concentration fluctuations
c	critical
I	incident
LO	local oscillator
S	scattered
t	temperature fluctuations
o	in vacuo
o	mean equilibrium value

Abbreviations

A	aperture
ACF	autocorrelation function
AOT-TP	Institute of Advanced Optical Technologies – Thermophysical Properties
BSC	beam splitter cube
CF	correlation function
DCM	dicyclohexylmethane
DEF	double exponential fit

DLS	dynamic light scattering
DM	dichroic mirror
DPM	diphenylmethane
EoS	equation of state
G	gaseous region
GF	linear grey filter
IL	ionic liquid
L	liquid phase
LO	local oscillator
LOHC	liquid organic hydrogen carrier
M	mirror
ND	neutral density filter
PBS	polarization beam splitter
PMT	photomultiplier tube
PS	polystyrene
RID	refractive index difference
SaCe	sample cell
SC	supercritical phase
SEF	single exponential fit
SNR	signal-to-noise ratio
2P	two-phase region
λ/2	lambda-half wave plate

1 Introduction

The pursuit of increased efficiencies in the conversion, transport, and storage of energy has never been more economically and practically crucial. This scenario is fueled by the steadily escalating global demand for available energy and the anticipated transition into a renewable energy economy, all geared towards mitigating energy-related carbon emissions. Within the spectrum of industries, the highly diverse chemical sector stands out with the highest energy demand [1]. Specifically, the production of ammonia, which is of great importance in the fertilizer industry, constitutes about 2% of global energy usage, as outlined by a 2021 report from the International Energy Agency [2]. Given this background, the development and improvement of sustainable processes have assumed a position of immense interest. Consequently, precise knowledge of the thermophysical properties of fluids and fluid mixtures has emerged as a critical factor in numerous fields associated with energy and chemical engineering. This knowledge plays a pivotal role in designing and optimizing efficient processes and their corresponding apparatuses. Key among these properties are the transport properties, including kinematic viscosity ν, thermal diffusivity a or thermal conductivity κ_c, and mutual diffusivities of corresponding working fluids. These properties enable the characterization of momentum, heat, and mass transfer. In technical applications, ν determines the characteristics of lubricants [3] and the power requirements of pumps and mixers [4], a governs heat transfer rates [5], and molecular diffusive mass transport, expressed in terms of the Fick or mutual diffusion coefficient D_{11} for binary mixtures, often serves as the rate-limiting step in biological or chemical reactions [6–9]. The significance of ν, a, and D_{11} is highlighted by their role in defining several dimensionless engineering numbers that help elucidate various phenomena linked to heat and mass transfer as well as fluid dynamics. To give a few examples, the Lewis number $Le = a \cdot D_{11}^{-1}$ is of great importance for understanding and interpreting combustion phenomena where it exerts a significant influence on the speed of premixed flames [10]. The Prandtl $Pr = \nu \cdot a^{-1}$ and Schmidt $Sc = \nu \cdot D_{11}^{-1}$ numbers provide a means of incorporating transport properties into convective transport processes and have, for instance, a distinct effect on the temperature field within the combustion chamber [11]. The mass transfer related Péclet number $Pe = l_{char} \cdot u_f \cdot D_{11}^{-1}$, where l_{char} is the characteristic length and u_f is the flow velocity, serves as an indicator of whether advective or diffusive mass transport is the dominating phenomenon [12]. The Nußelt number $Nu = a \cdot l_{char} \cdot \kappa_c^{-1}$ is, for

example, used to analyze the heat transfer performance between a flowing fluid and a wall, such as in heat exchangers [13]. Similarly to *Nu* for heat transfer, for mass transfer the Sherwood number is defined as $Sh = k_m \cdot l_{char} \cdot D_{11}^{-1}$ where k_m represents the mass transfer coefficient. *Sh* is, for instance, a useful parameter for analyzing the efficiency of mass transfer across the gas-liquid interface in a gas absorption process [14].

The need for reliable transport properties, specifically for *a* and/or mutual diffusivities, is becoming increasingly apparent when examining processes in diverse application areas, involving various fluid classes and thermodynamic states. For example, knowledge regarding *a* and mutual diffusivities is generally required for optimizing separation processes [15–18] and catalytic reactions [19,20], which entail heat and mass transfer within fluid mixtures or across phase boundaries. The conversion of carbon monoxide (CO) and hydrogen (H_2) from fossil or renewable resources into liquid fuels and waxes via heterogeneous catalytic Fischer–Tropsch synthesis is a prominent example [21]. Here, the heat removal capacity and internal diffusion restrictions often act as limiting factors [22]. Additionally, diffusive mass transfer plays a significant role in enhanced oil recovery, wherein a light gas, such as carbon dioxide (CO_2), is injected into the oil reservoir to induce swelling and reduce the viscosity of the oil-rich phase [23,24]. To elucidate the dynamics of the evaporation process of multicomponent fuel droplets in direct injection engines after injection, precise knowledge of *a* and mutual diffusivities is essential to describe the intra-droplet heat and mass transfer [25]. In connection with the transition toward a renewable energy economy, electrolytes have become a crucial fluid class with substantial importance in numerous applications, including energy storage [26–28] and energy conversion [29,30]. The efficiency of such processes relies heavily on ion mobility and, thus, on the molecular transport of mass within the electrolyte [31,32], which can be described using mutual diffusivities. Furthermore, several processes related to the large-scale application of H_2-technologies, such as production, distribution, and storage, demand accurate *a* and mutual diffusivity data. For example, in the chemical storage of H_2 using liquid organic hydrogen carriers (LOHCs), exact knowledge of transport properties is essential for optimizing the design of catalyst materials involved in the hydrogenation and dehydrogenation processes [33]. Similarly, in the geological or subsurface storage of H_2, a field currently under detailed research, knowledge about diffusion in corresponding mixtures is necessary for modeling, designing, and optimizing the related processes, e.g., for estimating the leak rate of the storage facility [34–37]. The examples provided represent only a limited selection of the many applications that

require reliable data on transport properties. In this context, additional studies emphasize the importance of thermophysical property data with small uncertainties to prevent the design of undersized or oversized equipment, resulting in poor operations or increased capital costs [38–41].

In principle, there are three main approaches that help derive the required transport property data: experiments, simulations, and correlations or prediction models. Given the limitless number of possible working fluids, alongside a vast range of temperatures T, pressures p, and compositions, conducting experimental investigations of all possible process-relevant thermodynamic conditions is not feasible. Consequently, considerable efforts have been made to develop phenomenological approaches for elucidating heat, mass, and momentum transfer. However, corresponding correlations and prediction models are often only applicable within a specific range of fluid classes and/or thermodynamic states [42–48]. This limitation is partly due to the poor availability of experimental diffusivity data, crucial for establishing and applying phenomenological approaches to practical problems. In recent years, the increase in computational power has resulted in substantial efforts being devoted to developing theoretical methods for determining transport properties, such as molecular or atomistic simulation approaches that describe fluid behavior on a molecular or microscopic level [49–51]. These approaches offer clear advantages, including significantly lower costs compared to experimental approaches, the ability to study thermodynamic states not accessible experimentally, and potential insights into fluid structures at a molecular level. These insights can help to understand the influence of the molecule structure and inter- and intramolecular interactions on the studied thermophysical properties. Nonetheless, the success and reliability of such simulations depend strongly on the description of the pairwise inter- and intramolecular interactions between atoms, which can be expressed by force fields. For the development and, more importantly, the validation of these force fields, that is, the theoretical boundary condition, reliable experimental data remain indispensable. In summary, while experiments are not necessarily the first choice for obtaining transport property data, given their associated costs and time requirements, they serve as the foundation for all other available methods.

Given the crucial need and wide range of applications for experimental a and mutual diffusivity data with small uncertainties, numerous publications and monographs delve into various methods and techniques for the direct and indirect determination of diffusivities in fluids and fluid mixtures. Some commonly used methods for determining a include the laser flash method [52], laser-induced gratings or forced Rayleigh scattering

[53,54], hot-disk and (transient) hot-strip methods [55,56], and the transient hot-wire technique [57,58]. Additionally, techniques based on thermal wave interferometry [59], the Angstrom method [60], thermal lensing methods [61], and various thermographic methods [62], are also employed. Frequently, a is obtained indirectly using the relation $a = \kappa_c \cdot \rho^{-1} \cdot c_p^{-1}$, where ρ represents density and c_p denotes specific heat capacity at constant p. For determining D_{11} or self-diffusion coefficients D_{self} of species in the mixture, which are also referred to in the literature as intradiffusion coefficients, several experimental approaches are documented in the literature. Notably, approaching infinite dilution, D_{11} and D_{self} of the solute in the mixture converge to the same value [63–65]. Related measurement methods can be broadly categorized into stationary, quasi-stationary, and transient methods. Examples include methods based on Taylor dispersion [66], Raman spectroscopy [67], interferometry [68], nuclear magnetic resonance spectroscopy [69,70], Fourier-transform infrared spectroscopy [71], collapsing small bubbles [72], chromatography [73], steady flow methods [74], restricted diffusion [75], galvanostatic polarization [76], Moiré pattern analysis [77], pressure decay [78], beam deflection techniques [79], and non-equilibrium fluctuations analysis [80] (for instance, via the shadowgraph method). Each approach for determining either a or D_{11} has its merits and drawbacks. Overview articles are given, for instance, by Cernuschi et al. [81], Huang [82], Johnson and Babb [83], Dunlop et al. [84], and Winkelmann [85]. Importantly, most conventional experimental techniques for studying diffusivities have four major disadvantages. The primary drawback is that virtually all these techniques rely on analyzing the relaxation of macroscopic T, p, and c gradients. These gradients must be large enough to cause a measurable effect, yet small enough to induce minimal disturbance in the system under investigation. The application of macroscopic gradients often introduces additional flow contributions, that is, advection, which is mostly indistinguishable from pure diffusive contributions. These disturbance effects can result in systematic errors in the analysis, leading to potential overestimation of diffusivities and changes in the thermodynamic state. This complication is exacerbated in the vicinity of a phase transition or near the critical point. Here, even minor changes in the thermodynamic state can render reasonable measurements impossible. This is because, among other factors, the thermal expansion coefficient increases rapidly in the region around the critical point, resulting in a large Rayleigh number [86,87]. Nevertheless, information collected in these regions is of great scientific importance for both a fundamental understanding of the behavior of transport and other thermophysical properties as well as for establishing corresponding correlations and prediction models. Another

disadvantage of many techniques is their limited applicability. For instance, some techniques can only be applied to a certain range of fluid classes or fluid states, require previous knowledge of other fluid properties, or only provide D_{self} or a composition-independent average diffusion coefficient. Furthermore, most conventional techniques necessitate calibration, which typically requires an appropriate fluid with well-known properties. However, unlike transport properties such as κ_c [88,89] and viscosity [90,91], there are no internationally agreed-upon reference systems, standardized equipment, or universally established approach for measuring D_{11}. Thus, considering the complexity of the systems of interest nowadays, alongside associated problems with boundary conditions and assumptions made, erroneous measurements are indeed very likely. The last disadvantage to be discussed here concerns the center of mass changes in experiments that rely on the analysis of macroscopic gradients. Therefore, the results obtained for mutual diffusivities depend on the reference frame used [92–94]. This is a factor which must be considered, especially when comparing the results acquired through different techniques.

In contrast, dynamic light scattering (DLS) is a technique that can overcome these limitations and, from a theoretical point of view, even allows the simultaneous determination of a and mutual diffusivities in fluid mixtures. DLS, also known as photon correlation spectroscopy or quasi-elastic light scattering, is a contactless, non-invasive, optical method based on rigid working equations derived from classical hydrodynamic theory [95–97]. The diffusivities are absolutely determined by analyzing the dynamics of statistical microscopic fluctuations in T or entropy and c within the bulk of fluid mixtures in macroscopic thermodynamic equilibrium, without requiring any calibration procedure [96,98]. The basic justification for these relationships is Onsager's regression hypothesis [99,100], which states that, on a statistical average, the microscopic fluctuations are governed by the same transport equations as those for macroscopic systems. Fluctuation analyses are commonly performed in the time domain by calculating the second-order or intensity correlation function (CF) of the scattered light as a function of delay time τ [101]. Hence, for a binary mixture, the mean characteristic decay times or mean lifetimes of the two observable types of fluctuations in T and c obtained from the CF are governed by the corresponding transport properties, namely thermal diffusivity a and Fick or mutual diffusion coefficient D_{11}. For multicomponent mixtures with n_c components, scattered-light intensity is modulated by fluctuations in T governed by a, alongside the fluctuations in concentration c related to $n_c - 1$ independent mass fluxes described by the Fick diffusion matrix with $(n_c - 1)^2$

entries or diffusion coefficients. Thus, for a multicomponent mixture with n_c components, DLS gives access to a and the $n_c - 1$ eigenvalues of the Fick diffusion matrix [102,103].

Under most circumstances, DLS presents distinct advantages in comparison to conventional or standard techniques. DLS is versatile, applicable to any fluid or fluid mixture in any thermodynamic state and phase, and gives access to diffusivities over several orders of magnitude. DLS induces almost no energy input into the sample, is not prone to calibration errors, and determination of diffusivities typically takes 10 min for equimolar solutions and 1.5 h in the dilute range [104]. Due to its applicability in macroscopic thermodynamic equilibrium, DLS does not induce shift of the center of mass and is well-suited for determining thermophysical properties near the critical point as well as near or in the two-phase or multi-phase region, where gradient-based techniques fail. Numerous studies in the literature (see Chapter 2) affirm that DLS is a powerful and well-established technique for accurately determining diffusivities in mixtures of various fluid classes under process relevant conditions. For completeness, it should be mentioned that further properties are discernible by applying DLS to the bulk or interface of fluids and fluid mixtures [98]. These properties include sound speed and attenuation [105], the Landau-Placzek ratio [106] (which combines isobaric and isochoric heat capacities), activity coefficients of solutions [107,108], or ν or dynamic viscosity and interfacial tension [109,110]. Furthermore, DLS has become a standard technique for characterizing macromolecular systems, including polymer solutions [111–115], biological systems [116,117], colloidal suspensions and dispersions [118,119], and particulate systems [120,121]. However, as this thesis focuses on the simultaneous determination of a and mutual diffusivities, these topics will not be discussed further. Despite its utility, both experimental and theoretical studies in the literature have reported limitations of the DLS technique for determining diffusivities under certain conditions. For binary mixtures, it is not always possible to observe the expected number of signals or to unambiguously classify the signals obtained from experiments with respect to a and D_{11} [122–128]. For multicomponent mixtures, there is an ongoing debate on how many mass diffusive modes can be resolved experimentally by DLS for specific mixtures and how they can be interpreted [103,129,130]. To date, the capabilities and limitations of DLS for the simultaneous determination of a and mutual diffusivities of fluid mixtures have not yet been comprehensively explored.

This cumulative thesis aims to highlight which factors influence the feasibility of a simultaneous determination of a and mutual diffusivities by DLS

in the bulk of homogeneous molecular fluid mixtures. The focus is primarily on binary fluid mixtures, but certain aspects related to multicomponent mixtures are also discussed. To allow identification of limiting factors, both theory and experimental implementation of DLS are considered. A diverse range of systems and thermodynamic states is experimentally explored. This includes model or reference systems as well as technical systems relevant to process and energy technology. The research also delves into novel systems, for which the applicability of DLS has not yet been demonstrated. Drawing on insights gained from the various studies, an overview of the types of accessible diffusivities will be presented and a signal attribution strategy will be developed. The information collected within this thesis will be further used to facilitate a discussion on the range of accessible diffusivities and achievable uncertainty levels. Owing to the cumulative nature of this thesis, the results and discussion are primarily based on published studies. Accordingly, the corresponding list of publications is provided below. Each publication includes a brief statement regarding the authors' contributions. The structure of the thesis unfolds as follows: First, beginning with a historical overview, it outlines the current status of DLS applicability for simultaneous diffusivity determination. Subsequently, aspects related to the theory and experimental implementation of DLS are introduced, incorporating the signal attribution strategy developed in this work. Finally, the key findings are summarized, referencing the following publications.

Publications

A. Piszko, M.; Wu, W.; Will, S.; Rausch, M. H.; Giraudet, C.; Fröba, A. P. *Thermal and Mutual Diffusivities of Fuel-Related Binary Liquid Mixtures under Pre-Combustion Conditions*. Fuel **2019**, *242*, 562–572.

Author's contribution: The author was responsible for executing and evaluating the experimental investigations, as well as actively participating in the planning and writing of the entire publication.

B. Berger Bioucas, F. E.; Piszko, M.; Kerscher, M.; Preuster, P.; Rausch, M. H.; Koller, T. M.; Wasserscheid, P.; Fröba, A. P. *Thermal Conductivity of Hydrocarbon Liquid Organic Hydrogen Carrier Systems: Measurement and Prediction*. J. Chem. Eng. Data **2020**, *65*, 5003–5017.

Author's contribution: The author was responsible for the planning, execution, and evaluation of the DLS experiments. F. E. Berger Bioucas conducted the thermal conductivity measurements. Furthermore, the author composed all parts of the publication related to the DLS experiments in the bulk of fluids, alongside supporting the writing of the entire publication.

C. Piszko, M.; Batz, K.; Rausch, M. H.; Giraudet, C.; Fröba, A. P. *Diffusivities of Binary Mixtures Consisting of Carbon Dioxide, Methane, and Propane by Dynamic Light Scattering*. J. Chem. Eng. Data **2020**, *65*, 1068–1082.

Author's contribution: The author was responsible for planning, executing, and evaluating the experimental investigations and calculations, with additional support from K. Batz. Moreover, the author contributed to the planning and writing of the entire publication.

D. Piszko, M.; Giraudet, C.; Fröba, A. P. *Diffusivities of an Equimolar Methane–Propane Mixture Across the Two-Phase Region by Dynamic Light Scattering*. Int. J. Thermophys. **2020**, *41*, 1–25.

Author's contribution: The author took charge of planning, executing, and evaluating the experimental investigations and calculations. Additionally, the author was involved in the planning and writing of the entire publication.

E. Piszko, M.; Kankanamge, C. J.; Rausch, M. H.; Klein, T.; Fröba, A. P. *Dynamic Light Scattering for Studying Mutual Diffusion Coefficients in Electrolyte Systems Comprised Entirely of Ions*. J. Electrochem. Soc. **2020**, *167*, 133502

Author's contribution: The author was responsible for planning, executing, and evaluating the experimental investigations, with support from C. J. Kankanamge. Additionally, the author participated in the planning and writing of the entire publication.

F. Piszko, M.; Lenahan, F. D.; Hahn, S.; Rausch, M. H.; Koller, T. M.; Klein, T.; Fröba, A. P. *Diffusivities in Binary Mixtures of n-Hexane or 1-Hexanol with Dissolved CH_4, Ne, Kr, R143a, SF_6, or R236fa* Close to Infinite Dilution. J. Chem. Eng. Data **2021**, *66*, 2218–2232.

Author's contribution: The author was responsible for planning, executing, and evaluating the experimental investigations, with support from S. Hahn. The simulations were performed by F. D. Lenahan, and the author participated in the planning and writing of the entire publication.

G. Piszko, M.; Schaible, T.; Bonten, C.; Fröba, A. P. Mutual and *Thermal Diffusivities in Polystyrene Melts with Dissolved Nitrogen by Dynamic Light Scattering*. Macromolecules **2021**, *54*, 5662–5672

Author's contribution: The author was responsible for planning, executing, and evaluating the experimental investigations. Additionally, the author participated in the planning and writing of the entire publication.

H. Lenahan, F. D.; Piszko, M.; Klein, T.; Fröba, A. P. *Diffusivities in Binary Mixtures of n-Decane, n-Hexadecane, n-Octacosane, 2-Methylpentane, 2,2-Dimethylbutane, Cyclohexane, Benzene, Ethanol, 1-Decanol, Ethyl Butanoate, or n-Hexanoic Acid with Dissolved He or Kr Close to Infinite Dilution*. J. Chem. Eng. Data **2022**, *67*, 622–635.

Author's contribution: The author was responsible for the planning, execution, and evaluation of the experimental investigations. The simulations were performed by F. D. Lenahan, with the author writing all parts of the publication related to the experiments. Additionally, the author participated in the planning and writing of the entire publication.

I. Piszko, M.; Lenahan, F. D.; Friedl, L.; Klein, T.; Fröba, A. P. *Mutual and Thermal Diffusivities in Mixtures of Cyclohexane, n-Hexadecane, n-Octacosane, or n-Hexanoic Acid with Carbon Dioxide Obtained by Dynamic Light Scattering and Molecular Dynamics Simulations*. J. Chem. Eng. Data **2022**, *67*, 3059–3076.

Author's contribution: The author was responsible for the planning, execution, and evaluation of the experimental investigations. Experimental investigations were supported by L. Friedel, and simulations were performed by F. D. Lenahan, who also wrote the corresponding parts of the publication. The author wrote other parts and participated in the planning and writing of the entire publication.

J. Piszko, M.; Lenahan, F. D.; Dennstädt, C.; Klein, T.; Fröba, A. P. *Mutual and Thermal Diffusivities in Binary Mixtures of n-Hexane or 1-Hexanol with Krypton, R143a, or Sulfur Hexafluoride by Using Dynamic Light Scattering and Molecular Dynamics Simulations*. J. Chem. Eng. Data **2023**, *68*, 1343–1357.

Author's contribution: The author was responsible for the planning, execution, and evaluation of the experimental investigations. The experimental investigations were supported by C. Dennstädt. F. D. Lenahan performed the simulations and wrote the corresponding parts of the publication. The author wrote the other parts and participated in the planning and writing of the entire publication.

K. Piszko, M.; Schmidt, P. S.; Rausch, M. H.; Fröba, A. P. *Thermal Diffusivity and Fick Diffusion Coefficient in Mixtures of Hydrogen and Methane by Dynamic Light Scattering*. Int. J. Thermophys. **2023**, *44*, 146.

Author's contribution: The author was responsible for the planning, execution, and evaluation of the experimental investigations. The experimental investigations were supported by P. S. Schmidt. The author participated in the planning and writing of the entire publication.

L. Piszko, M.; Schmidt, P. S.; Rausch, M. H.; Fröba, A. P. *Diffusivities in Water or Aqueous Solutions of Sodium Chloride with Dissolved Hydrogen and Methane*. Int. J. Hydrogen Energy **2024**, *68*, 499–510.

Author's contribution: The author was responsible for the planning, execution, and evaluation of the experimental investigations. The experimental investigations were supported by P. S. Schmidt. The author participated in the planning and writing of the entire publication.

2 State of the Art

This chapter provides an overview of the current status of DLS applicability and limitations for accurately determining a and mutual diffusivities of molecular fluid mixtures. Notably, the goal is not to present a comprehensive historical review of all theoretical, experimental, and technical advances but rather to highlight crucial aspects. A broader historical context of the DLS method's evolution concerning the determination of thermophysical properties has been outlined by Fröba [98]. Additionally, exhaustive discussions on the modern theory of light scattering from bulk fluids are available in the standard works of Pecora [95], Berne and Pecora [96], and Chu [97]. These sources also proposed DLS as a unique diagnostic tool for exploring the dynamics and structural properties of various systems.

First, a concise historical review is provided, tracing the early development of DLS from its inception with bulk fluids, progressing towards the quantitative analysis of the Rayleigh component within the characteristically broadened spectrum of scattered light. This advancement enables the determination of diffusivities by DLS. Following this historical perspective, the discussion shifts to the examination of available experimental and theoretical studies. The evaluation centers on the applicability and limitations of DLS. Special emphasis is placed on the simultaneous determination of a and mutual diffusivities, without claiming completeness or delving into the interpretation of the diffusivity results and associated phenomena. The topic-specific terms used in the following sections are elucidated in more detail in Chapter 4.

2.1 Journey Towards the Quantitative Determination of Diffusivities via DLS

In 1930, Gross [131] conducted light scattering experiments on several pure homogeneous liquids (at large scattering angles Θ_S, i.e., 90°) under T significantly distant from the critical temperature T_c. They employed a mercury lamp and a spectrum analyzer based on an echelon grating. In addition to confirming the existence of the predicted Brillouin doublet [132], whose components are symmetrically shifted from the frequency of the incident light, Gross [131,133] spectroscopically revealed, for the first time, the existence of a third central, unshifted component in the spectrum of the scattered light. In 1934, Landau and Placzek [134] used a quasi-thermodynamic approach to present a theoretical explanation for the observed triplet

structure of light scattered from bulk fluids. They concluded that the unshifted contribution in the scattered light spectrum is governed by statistical fluctuations in the entropy or T of the liquid at constant p. They also predicted that the line should have a Lorentzian shape, with its width representing a measure of the lifetime of the spontaneous fluctuations. Thereafter, light scattering swiftly became an active research topic, and numerous experiments were conducted. At that time, various spectral discharge lamps were utilized for generating scattered light. Spectral analyses were performed using various devices based, for example, on gratings, Lummer-Gehrcke plates, or Fabry–Pérot interferometers. These approaches all utilized a pre-detection filtering scheme, whereby scattered light is first spectrally filtered, either spatially or temporally, before measuring the intensity at a certain frequency or angular frequency ω. However, applying a pre-detection filtering scheme, while seemingly straightforward for analyzing scattered light spectra, faced challenges. The width of the unshifted component, known as the Rayleigh line, is in the order of MHz or less for many fluids. This is often beyond the resolving power of such instruments. Thus, and given the limited linewidth and intensity of the available light sources, as a result, the achievable resolution and signal quality in these early experiments often hindered detailed investigations that would have allowed a sound analysis and interpretation of the spectral distribution of scattered light.

The advent of the Laser in 1960, providing a high intensity and narrow linewidth light source, along with the development of optical post-detection beating spectroscopy in the early 1960's [135], marked a significant advancement. Optical post-detection beating spectroscopy had a resolving power $\omega{\cdot}\Delta\omega^{-1}$ several orders of magnitudes greater than the best Fabry-Pérot spectrometer ($\omega{\cdot}\Delta\omega^{-1} \approx 10^7$). Consequently, this enabled the quantitative study of spectra governed by fluctuations in the bulk of fluids. In this context, especially the development of a setup using a helium-neon laser in combination with optical heterodyne detection techniques, exhibiting an optical resolving power of $\omega{\cdot}\Delta\omega^{-1} \approx 10^{14}$, was a milestone. This setup was presented by Cummins et al. [136] in the early part of 1964. Cummins et al. [136] investigated dilute solutions of monodisperse polystyrene molecules, demonstrating that the observed broadening of the spectrum depends both on the size of the scatterers and on the angle of observation. The earliest attempts at quantitative spectral measurements aiming to determine transport properties were performed in fluid systems near their critical point by Alpert et al. [137,138] (for a nearly equimass cyclohexane (C_6H_{12})-aniline mixture) and by Ford and Benedek [139] (for pure sulfur

hexafluoride (SF_6)), both in 1965. The study by Alpert et al. [137,138] was inspired by Pecora [140], who suggested that experiments near T_c in a binary liquid mixture could provide accurate information about the *c* fluctuations, because they become large and slow in the near-critical region [141,142]. Alpert [137] not only confirmed Pecora's [140] assumption, but also observed that the measurement signal related to *c* fluctuations is very strong in the immediate vicinity of the critical point and that it rapidly loses intensity with increasing distance. Due to the very strong scattered light signal in the immediate vicinity of the critical point, explained by the divergence of isothermal compressibility leading to large ρ fluctuations, many of the measurements were performed using the so-called homodyne method. Using the homodyne method, it is assumed that only light scattered by the sample is detected. In the following years, light scattering experiments on bulk fluids near the critical point were extensively performed [143–149].

The first attempts to investigate pure fluids and binary fluid mixtures far from their critical point began in 1966, spearheaded by researchers such as Lastovka and Benedek [150], Aref'ev et al. [151], Bergé et al. [152], Dubois et al. [153], and Dubois and Bergé [154]. To compensate for the expected low signal-to-noise ratio (SNR), most studies focused on specific systems selected for their high degree of scattering. They leveraged smaller Θ_S to increase the scattering volume (and, thus, the number of scatterers) and applied heterodyne detection schemes. Utilizing the heterodyne method, light scattered by the sample is superimposed with coherent reference light at the detection unit and may allow signal enhancement. Around the same time, Mountain [155–157] verified the results of Landau and Placzek [134] concerning the triplet structure of light scattered from bulk fluids by considering a coupling of the internal degrees of freedom of molecules with the translational degrees of freedom of a fluid. Additionally, in 1969, Mountain and Deutch [158] and Blum [102] provided a theoretical description of the Rayleigh–Brillouin spectrum for binary solutions and multicomponent fluids in the hydrodynamic regime using the approach suggested by Landau and Placzek [134]. In 1970, Bergé et al. [152] were the first to demonstrate the simultaneous determination of *a* and D_{11} via DLS for a binary mixture of carbon disulfide (CS_2) and acetone (C_3H_6O) using heterodyne photon beating spectroscopy. Additionally, by observing both Lorentzian lines simultaneously, it was possible to evaluate the total integrated intensity ratio of the light scattered through *c* fluctuations I_c and *T* fluctuations I_t. For the CS_2–C_3H_6O mixture, they found that $I_c \cdot I_t^{-1} = 2$, indicating that the contribution of *c* fluctuations to the scattered light signal has an amplitude

twice that of T fluctuations. In a follow up study, DuBois and Bergé [154] conducted further quantitative measurements on the intensity ratio, defining it as the Rayleigh ratio $\mathcal{R} = I_c \cdot I_t^{-1}$. They also demonstrated that a theoretical estimation of $\mathcal{R}$ is possible and discussed some associated influencing factors. Although some of these early experimental research activities affirmed the feasibility of applying light scattering techniques to bulk fluids and fluid mixtures for determining diffusivities and $\mathcal{R}$, their limited results did not conclusively establish DLS as a reliable and efficient tool for such purposes.

Technological advances, including the introduction of high-intensity argon-ion lasers in 1964, increased quantum efficiency of detection units (for example, single photon counting detectors like photomultiplier tubes (PMTs)), the establishment of autocorrelation techniques, and later the introduction of digital correlators played a crucial role in expanding these early research activities. In the first half of 1970s, the first results and data were presented that indicated that DLS from bulk fluids offered an accurate and convenient method for determining a in most pure liquids, along with a and/or D_{11} in a wide range of binary mixtures [126,159–161]. Jamieson and Walton [159] specifically determined D_{11} of binary liquid mixtures comprising linear alkanes, primary alcohols, nitrobenzene, CS_2, and C_3H_6O at infinite dilution and as a function of composition. They demonstrated that DLS provides results with uncertainties in the range of 5%, allowing for the study of the effects of c, chain length, and H_2 bonding on D_{11}. Gulari et al. [126] conducted investigations on various pure fluids and binary liquid mixtures as a function of composition at $T \approx 293$ K and compared their data with those obtained through conventional techniques. Apart from determining a of pure fluids, they demonstrated, for two out of the eight investigated systems, that a simultaneous determination of a and D_{11} was possible. For the remaining six systems, only D_{11} could be obtained in the mixtures. The authors suggested that the refractive index difference (RID) between the pure components is the major limitation of DLS for determining a and D_{11} simultaneously. The reported uncertainties for a and D_{11} were approximately (5 and 3)%. They posited that smaller uncertainties in the diffusivities could be obtained with increasing RID between the two components as well as by approaching equal composition of the two components. Corti and Degiorgio [160] explored a of pure liquid C_3H_6O, benzene (C_6H_6), and toluene ($C_6H_5CH_3$) at $T \approx 298$ K. They discussed various experimental difficulties related to laser power and intensity stability, PMTs, correlators, and the measurement of the $\mathcal{O}_S$ in connection with achievable uncertainties. Additionally, they demonstrated that the measurement time

for a single CF can be reduced from 2 h to 10 min [126] by using a fast digital correlator operating in real-time. Czworniak et al. [161] obtained D_{11} for 11 binary liquid mixtures of simple organic liquids as a function of composition at T = 293 K with uncertainties between (5 and 15)%. They also provided a theoretical interpretation of the composition-dependent behavior of D_{11}.

In addition to its extensive application in studying the decay rate of critical fluctuations [142,162–170], various theoretical and experimental aspects of the DLS technique related to determining diffusivities have witnessed continuous development over the subsequent four decades. The following sections provide a brief overview of these developments, along with a more detailed literature review focusing on the applicability of DLS for simultaneously determining a and mutual diffusivities. Various studies reported since the 1980s will be assessed, considering the type of system and thermodynamic conditions investigated. First, studies focusing on determining a of pure fluids and fluid mixtures will be discussed, followed by an examination of research on D_{11} in binary fluid mixtures. Thereafter, the evaluation will extend to studies focusing specifically on the simultaneous determination of a and D_{11} in binary fluid mixtures. Before delving into the investigation of multicomponent mixtures, this thesis will provide an overview of diffusivities obtainable near the critical plait point. Notably, the various aspects discussed are closely interlinked, and the division into sections is primarily for the sake of structure and readability.

2.2 Thermal Diffusivity of Pure Fluids and Fluid Mixtures

The majority of DLS studies in the literature focus on determining a of pure fluids and fluid mixtures. Apart from a few studies, such as that by Bohidar and Chopra [171], a substantial number of publications stem primarily from research groups led by Leipertz [125,172–193] and Straub [194–201], who both contributed significantly to the development of the DLS method for routine applications. Additionally, research groups led by Nishikawa [202–205] and, more recently, He. [206–216], Wu [217,218], and Ma [219,220], have employed the DLS method as a convenient tool for determining a.

Since the 1980s, Leipertz, Fiebig, and Simonsohn, in collaboration with other researchers, have presented numerous studies on the development and applications of the DLS method for investigating thermophysical properties. Some of their early studies [172,183,187] described the development of a DLS apparatus enabling fast and accurate determination of a of pure

transparent liquids over T and p ranges between (293 and 423) K and (0.1 and 11) MPa. It is worth noting that two PMTs were used for signal detection and the pseudo-cross CF was calculated, instead of using a single PMT and calculating the autocorrelation function (ACF). This method, proposed by Hiller and Simonsohn [221] in 1982, aims to limit distortions in the CF caused by after-pulse and dead-time effects of the PMTs, enhancing the overall signal quality. To validate their apparatus, Hendrix et al. [187] investigated $C_6H_5CH_3$ and methanol (CH_3OH), both characterized by relatively large scattering cross sections, leading to strong scattered light signals. Beside showcasing that DLS can yield a with uncertainties as low as 1%, they emphasized that deviations from the expected simple exponential decay in the measured CF serve as a reliable criterion for detecting systematic biases in measurements that could compromise the accuracy of the determined diffusivities. In subsequent work, the research group of Leipertz used the DLS method for determining a of several pure refrigerants. Ibreighith et al. [188] explored the refrigerants 2,2-dichloro-1,1,1-trifluoroethane (R123), 1,1,1,2-tetrafluoroethane (R134a), 1-chloro-1,1-difluoroethane (R142b), and 1,1-difluoroethane (R152a) in the liquid phase. Kraft and Leipertz determined a of saturated R134a [188], R152a [189], pentafluoroethane (R125) [190], and Round-Robin R134a [184], sometimes including the vicinity of the critical point. Fröba et al. investigated R143a [185,186], 1,1,1,3,3-pentafluorobutane (R365mfc) [191], and 1,1,1,2,3,3,3-heptafluoropropane (R227ea) [192] in the saturated liquid and saturated vapor phases over an extended T range between about (253 and 460) K, occasionally near the critical point. In all these studies, the typical average relative uncertainties of a were around 1%. In addition to refrigerants, Kraft et al. [193], Will et al. [173], and Fröba et al. [174,175] conducted investigations on $C_6H_5CH_3$ to expand the a database and test the accuracy of the method. They identified signal quality as the most crucial factor impacting achievable single-point accuracy. Signal quality is generally a function of the measurement duration, specific fluid under investigation, thermodynamic state, and experimental setup. To achieve higher accuracy, they recommended studying liquids with larger scattering cross section than $C_6H_5CH_3$ and conducting multiple measurements to partially average out the random errors arising from angle measurement and evaluation procedure of the CF.

Somewhat in parallel to the research group led by Leipertz, the research group led by Straub investigated a for pure fluids [194–200] and some selected binary mixtures [194,195] by DLS, covering a substantial range of T and ρ, including the vicinity of the critical point. Jany et al. [195,196] investigated a in pure CO_2, SF_6, ethane (C_2H_6), nitrous oxide, and the refrigerant

trifluoromethane (R23) as well as in mixtures of SF_6 with CO_2 or R23. They explored the liquid and vapor phases along the saturation line, as well as certain isotherms and the critical isochores. Their study range included T between about (298 and 323) K, p up to about 7 MPa, and covered a ρ range of $0.15 < \rho/\rho_c < 2$, where ρ_c is the critical density. The lower limit was attributed to the strongly decreasing scattering intensity at low ρ, while the upper limit was determined by the capabilities of the apparatus used. Kruppa et al. [197–199] devised a setup that could potentially facilitate future investigations at high T, specifically above 350 K. They explored pure chlorotrifluoromethane (R13), chlorodifluoromethane (R22), R134a, and R152a at T ranging between about (290 and 425) K, slightly extending the range of investigable ρ/ρ_c. Pitschmann and Straub [200] conducted similar investigations on the refrigerants difluoromethane (R32), R125, and R143a at T between (300 and 390) K. For many of the examined fluids, a values spanned a range of over four orders of magnitude. The corresponding uncertainties typically were between (0.5 and 5)%, depending on the investigated state region. In addition to providing a data, the research group led by Straub presented general guidelines for the experimental design, discussed limitations of DLS method applicability, and provided an estimate of the individual experimental contributions to the total uncertainty of a. They showed that by increasing laser power, utilizing smaller Θ_S, and improving the optical setup, accurate measurements were possible over an extended thermodynamic range, encompassing states points removed from the vicinity of the critical point. Furthermore, they noted that the homodyne technique was particularly applicable in the extended critical region and that the DLS method was unsuitable for assessing the gas region at about $\rho < 100\ \mathrm{kg \cdot m^{-3}}$, as increasing errors can be expected due to the low scattered light intensities. Regarding uncertainties, they evaluated influencing factors such as multiple scattering, laser heating, and gravitational influences, which become particularly important near the critical point. They also explored the effect of frequency stability of the laser, the definition of the scattering vector, and the influence of uncertainty in the refractive index, as well as the determined decay time or mean lifetime of the fluctuations on a. The research group led by Straub also showed that the absolute value of the refractive index has only a minor influence on the diffusivity result at small Θ_S and that, due to the statistical process, the main source of errors lies in determining the decay time. To allow an accurate estimation of uncertainties, they proposed performing six individual measurements at different angles, with the final diffusivity value obtained by averaging the individual results.

The determination of a in liquid mixtures has also been of scientific interest to the research group of Leipertz since the late 1980s. Their works are particularly relevant to this thesis, as they not only extend the applicability of DLS and provide accurate diffusivities, but also systematically evaluate the limitations of the DLS technique. Wu et al. [125,176] conducted a series of investigations, aiming to evaluate the influence of the RID of the pure components of binary mixtures on the determinability of a using DLS. Investigations were conducted on binary liquid mixtures of $C_6H_5CH_3$ and C_6H_6, decalin, carbon tetrachloride (CCl_4), or bromobenzene as well as mixtures of C_3H_6O and CCl_4. The RIDs of the pure components are (0.3, 1.0, 2.5, 4.2, and 7.4)%, respectively, and the mixtures were investigated as a function of composition at about room T and atmospheric p. In liquid mixtures at around room T, a is typically one to two orders of magnitude larger than D_{11}. Thus, the temporal spacing in the CF, which can be expressed by $Le = a \cdot D_{11}^{-1}$, is relatively large. For mixtures with RIDs < 5%, $\mathcal{R} = I_c \cdot I_t^{-1}$ was typically smaller than one. Therefore, the signal related to T fluctuations dominated the experimental CF. Wu et al. [125,176] stated that in this case, the additional contribution in the CF related to c fluctuations could be sufficiently described by an additional linear term. However, they also state that this simplification leads to unacceptable errors if I_c exceeds I_t, that is, if the RID exceeds 5%, as the contribution related to c fluctuations becomes too dominant. As an example, they stated that if $I_c = 3 \cdot I_t$ and $Le = 50$, an error of 2.5% can be observed in a. Thus, if the RID is surpassing 5%, either exact knowledge of D_{11} is required or the additional decay must be described with suitable mathematical terms in the CF for accurately determining a. A straightforward way would be fitting the CF with a sum of two exponentials, enabling the simultaneous determination of a and D_{11}. However, this requires that the CF is calculated over a large time range while maintaining a high temporal resolution to capture both signals related to T and c fluctuations. This necessitated a correlator exhibiting a large number of correlator channels to facilitate adjustment of a small sampling time. However, such correlators were not commercially available at that time, as they usually possessed only 100 correlator channels, and would have been very expensive. To overcome this measurement difficulty, Wu et al. [176] conducted two independent measurements of the CF in two different time domains sequentially by employing the same apparatus.

Similar to Wu et al. [125,176], Fröba et al. [177] obtained a of the binary refrigerant mixture R507 (50wt%. R125–50wt.% R143a) and proved, for the first time, the applicability of DLS for determining a in ternary systems by examining the refrigerant mixture R404A (44wt.% R125–52wt.% R143a–

4wt.% R134a). Heller et al. [181] assessed R417A (50wt.% R134a–46.6wt.% R125–3.4wt.% *n*-butane (R600)) and R417B (79wt.% R125–18.25wt.% R134a–2.75wt.% R600). Fröba et al. also explored binary and ternary mixtures of R125–R143a [179], R410A (50wt.% R125–50wt.% R32) [178], R407C (25wt.% R125–23wt.% R32–52wt.% R134a) [178], as well as of 1,1,1,3,3-pentafluorobutane (R365mfc) and perfluoropolyether (Galden® HT 55) [180]. Furthermore, Fröba et al. [182] demonstrated, for the first time, that a is also obtainable in the quaternary mixtures of R125–R143a–R32–R134a via DLS. In all these studies, the refractive indices of the pure components had comparable values. Thus, only one signal related to T fluctuations was fitted and the contributions of the c fluctuations to the CF were treated as low-amplitude disturbances and considered by including an additional linear term in the fitting process. Most of the measurements were performed at small Θs both in the saturated liquid and vapor phases at T between about (293 and 344) K, often including the liquid–vapor critical point. The typical average relative uncertainties of a were about 1%.

In the early 2000s, the research group of Nishikawa [202–205] focused mainly on ascertaining the temporal evolution of T fluctuations and on determining a of pure supercritical fluids such as ethylene, fluoroform, CH_3OH, C_2H_5OH, CO_2, and xenon. Most of the studies were conducted near the critical point, and aimed to analyze the influence of the relations between H_2 bonding, viscosity, and molecule type in each fluid on a.

From 2014 onwards, the research groups around He [206–216], Wu [217,218], and Me [219,220] applied the DLS method extensively as a convenient tool for determining a of various pure fluids at T between about (290 and 690) K and p up to about 11 MPa. The research group around He focused primarily on fluids relevant to combustion technology, such as fuels and fuel additives. They evaluated a of C_2H_5OH [206], ethyl decanoate [207], and ethyl myristate [209] in the compressed liquid phase; CO_2 [210] in the compressed liquid and supercritical phases; ethyl heptanoate [211] in the compressed liquid and saturated liquid phases; 2-methoxy-2-methylpropane [212], 2-ethoxy-2-methylpropane [213], and 2-methoxy-2-methylbutane [213] in the compressed liquid, saturated liquid, and saturated vapor phases; pentane [214,215] and dibutyl ether [216] in the saturated liquid, saturated vapor, and supercritical phases; and di-isopropyl ether [208] in the saturated liquid, saturated vapor, supercritical, and compressed liquid phases. The research group around Wu measured a of the refrigerants 2,3,3,3-tetrafluoroprop-1-ene (R1234yf) [217] and trans-1,3,3,3-tetrafluoroprop-1-ene (R1234ze(E)) [217] under saturation conditions, and trans-1-chloro-3,3,3-trifluoropropene (R1233zd(E)) [218] and dodecafluoro-2-

methylpentan-3-one (Novec1230) [218] in the saturated liquid phase at T between about (298 and 393) K. The research group around Ma obtained a of the refrigerants 3,3,3-trifluoropropene (R1243zf) [220] and R1233zd(E) [220] close to saturation conditions and for several methyl esters and ethyl esters [219], used as fuel additives, in the compressed liquid phase at T between about (303 and 473) K. In these studies, the average relative uncertainties in a were between about (1 and 3)%.

2.3 Mutual Diffusion Coefficient in Binary Fluid Mixtures

Most of the studies in the literature focus on determining D_{11} in the liquid phase. Starting in 1981, Bohidar and Chopra [171] delved into aqueous solutions of urea, dextrose, sucrose, sodium chloride (NaCl), ammonium nitrate, and zinc sulphate, as well as binary liquid mixtures of C_3H_6O and H_2O or C_6H_6, C_6H_6 and CCl_4 or CH_3OH, as well as CH_3OH and CCl_4 as a function of mixture composition at T between about (307 and 311) K. The measurements conducted at Θ_S between (8 and 19)° generally took between (0.5 and 1) h, with typical uncertainties of D_{11} ranging between (1 and 2)%. Schmitz et al. [128] explored mixtures of 2-butoxyethanol and H_2O at different compositions and as a function of T between about 285 K and that of liquid–liquid phase separation, which was in the range of 323 K for these mixtures. ACFs were obtained at Θ_S between (35 and 145)°. A statement regarding the uncertainties has not been provided. To study the effect of molecular association on D_{11}, McKeigue and Gulari [222] investigated the binary liquid mixtures of CH_3OH and C_6H_6 or CS_2 as well as C_2H_5OH and C_6H_6 or CS_2. DLS experiments were performed over the entire c range and for T from approximately (298 to 353) K. ACFs were calculated at different Θ_S between (4 and 18)° using a homodyne detection scheme. Since I_c was significantly greater than I_t in concentrated solutions, under most circumstances they could determine the D_{11} with low uncertainty by performing a single exponential fit (SEF). In dilute solutions, I_c and I_t had comparable magnitudes, necessitating the experimental CF to be fitted by a double exponential fit (DEF). Additionally, they observed that the amount of scattered light was greatly reduced in dilute solutions compared to concentrated solutions, resulting in a smaller SNR and, thus, generally higher experimental uncertainty. Consequently, McKeigue and Gulari [222] concluded that the achievable uncertainty of D_{11} is approximately 1% in concentrated solutions and approximately 5% for samples where the mole fraction x of either component is below about 0.05. Krahn et al. [104] measured

the D_{11} in binary liquid mixtures of CH_3OH, C_6H_6, *n*-hexane (*n*-C_6H_{14}), C_3H_6O, and CS_2 at T between (293 and 298) K and x between about (0.03 and 0.97). ACFs were obtained at Θ_S in a heterodyne detection scheme wherein heterodyning was performed by using window flares. Since a and D_{11} for the investigated systems differed by some orders of magnitude, they claimed that they were able to fit the experimental correlator data with a single exponential. However, the signal contribution resulting from T fluctuations can be expected to have a non-negligible influence, especially for low and high c. They demonstrated that the determination of D_{11} required approximately 10 min for equimolar solutions and 1.5 h in the dilute range. Uncertainties of D_{11} were about 2% in the ranges of $0 < x < 0.1$ and $0.9 < x < 1$ and 0.5% in equimolar solutions. Like many other authors, they observed a decrease in scattering intensity in dilute solutions, leading to larger uncertainties, and pointed out that the main limitation of DLS is a sufficient RID of the pure components. Siddiqi et al. [223] examined binary liquid mixtures of CS_2 with CCl_4, C_6H_{12}, or $C_6H_5CH_3$, as well as of pyridine and H_2O at $T = 293$ K. For these systems, the measurements in the two diluted areas of $x < 0.1$ and $x > 0.9$ could not be conducted as the amplitude related to c fluctuations in the CF was too small. Same as other researchers, the authors found that the amplitude of the c fluctuations was dependent on the RID of the two components, since the amplitude is a function of the partial derivative of dielectric constant with respect to c. For equimolar solutions the partial derivative was at its maximum, and its value decreased with dilution toward the two ends of the composition range. Most importantly, they also observed that this limitation did not apply to all types of mixtures, but was critical for mixtures that exhibited a small variation in chemical potential with c. Indeed, the term $(\partial\mu/\partial c)$, which is the reciprocal of the osmotic compressibility, will also be of particular interest later when discussing the limits of DLS pertaining to the simultaneous determination of a and D_{11}. In $(\partial\mu/\partial c)$, μ denotes the difference in the chemical potential of the two components, and c represents the weight fraction of the heavier component. Fiedel et al. [224] investigated the binary liquid mixtures of bromobenzene with acetonitrile, *n*-C_6H_{14}, or C_2H_5OH at $T = 293$ K, with x between (0.05 and 0.95). ACFs were obtained using a heterodyne detection scheme at $\Theta_S = 7°$. Relative uncertainties in D_{11} ranged from 0.8% in concentrated mixtures to 16% in the dilute regime. In agreement with other authors, they reported that the amplitude related to c fluctuations in the CF is rather small at extreme c, resulting in considerable experimental noise. For improved signals, they recommended increasing the experimental time (45 min in their study). Moreover, Fiedel et al. [224] stated that

the primary source of inaccuracy in such measurements was poor sample quality because of dust or uncertainties in composition due to different evaporation rates of the components during preparation. Wu et al. obtained D_{11} in binary mixtures of C_3H_6O and CCl_4 as a function of composition at T = 296 K [176] (discussed in detail in Section 2.2) and in a binary separation system comprising n-C_4H_{14} and nitrobenzene [225] with a miscibility gap below about T = 292.6 K. Depending on the intensity of the scattered light at different T, ACFs were determined using either a homodyne or heterodyne detection scheme. They also presented an approach that allows the disturbing influences of the heterodyne part to be corrected in homodyne measurements.

In 1984, Saad and Gulari published two articles in which they demonstrated, for the first time, the determination of D_{11} (and a) in mixtures of liquids with dissolved gases [226] (discussed in the next section), as well as in mixtures of liquid hydrocarbons in supercritical fluids [127] using DLS. Saad and Gulari [127] investigated D_{11} of C_6H_6 and n-heptane (n-C_7H_{16}) in supercritical CO_2 along isochores in the dense gas region at x < 0.05 of hydrocarbon. ACFs were calculated at Θ_S between (6 and 11)° leveraging a homodyne detection scheme. Since these investigations were performed in the vicinity of the critical point, the use of a homodyne detection scheme was deemed appropriate. The measured CFs exhibited single exponential behavior over the reported range of data. This observation is not in agreement with the results reported by Ackerson and Hanley [122], who investigated a mixture of x = 0.7107 methane (CH_4) and x = 0.2893 C_2H_6 near the critical point, observing two exponential contributions to the CFs. Their work will be discussed in more detail in Section 2.5. In the near-critical region, along the critical isochore, the diffusion coefficient vanishes like the inverse of the correlation length to the power of 0.67 [170]. The attribution of the observable single contribution to D_{11} by Saad and Gulari [127] was partly based on the obtained critical exponent. The obtained critical exponent was found to be in fair agreement with the data derived from pure fluids and their mixtures along the critical isochore and with predicted values obtained using the renormalization-group theory [227]. In 1988, Bender and Pecora [228] determined the D_{11} for mixtures of 2-butoxyethanol and H_2O as a function of composition at T between about (283 and 313) K and atmospheric p. ACFs were calculated at Θ_S between (35 and 125)° employing a homodyne detection scheme.

Although most available studies report on D_{11} in rather simple liquid systems, the research group of Fröba [229–233] significantly extended the applicability of DLS to more complex technical systems. Rausch et al.

[229,230] examined binary liquid mixtures of several ionic liquids (ILs) with C_2H_5OH, C_3H_6O, H_2O, acetonitrile, or dichloromethane as a function of mixture composition at T between about (278 and 323) K and atmospheric p. Furthermore, Rausch et al. [231] determined D_{11} of liquid glycerol–H_2O mixtures at T between (323 and 448) K, different compositions, and ambient p. Pseudo-cross CFs were obtained at Θ_S exceeding 63° using a heterodyne detection scheme. Large angles were chosen to ensure that the computed intensity CFs are governed only by c fluctuations, facilitating the use of a SEF. Uncertainties from 1.3% for mixtures with a strong scattering signal and up to 69% for mixtures with weak signals were acquired with a confidence interval of 95% (k = 2). They also stated that considerably smaller uncertainties could be achieved by utilizing lasers with higher powers for a given measurement time. In this context, they conducted experiments with different laser output powers (500–1500 mW) and different measuring times (15–200 min) to investigate their influence on the D_{11} and find the optimum measurement conditions. Heller et al. [232] demonstrated that DLS can be used to determine D_{11} in the binary LOHC system dibenzyltoluene–perhydrodibenzyltoluene. Investigations were performed in the liquid phase at different compositions and T between (264 and 571) K. Pseudo-cross CFs were computed at Θ_S = 90° using a heterodyne detection scheme. The DLS method was found to be a suitable tool for such technical systems, providing reliable data on D_{11} over four orders of magnitude with an expanded uncertainty of (3 to 25)%. Knoll et al. [233] highlighted that DLS could be used to simultaneously assess molecular and micelle diffusion in a technical microemulsion system. Consequently, research was conducted at T between (314 and 353) K and p between (10 and 16) MPa. For a microemulsion consisting, for example, of CO_2 and polyol or CO_2, polyol, and a surfactant, both the translational micelle diffusion coefficient and a faster apparent molecular diffusion coefficient describing the diffusion of CO_2 were obtained. Leveraging homodyne and heterodyne detection schemes, they showcased that the micelles could generate a local oscillator field, enabling simultaneous heterodyne measurements of the molecular diffusivities.

Regarding rather technical systems, recently, Tang et al. [234,235] determined D_{11} of mixtures comprising the lubricant polyalkylene glycol with dissolved R32 or R1234yf at T between (293 and 353) K and p between about (0.1 and 3.4) MPa Measurements were performed at several Θ_S between (3.0 and 3.2)° under heterodyne conditions. Whether pseudo-cross CFs or ACFs were computed is not clear. The signal associated with T fluctuations was

visible in the CFs of the binary mixtures but was not evaluated further. The uncertainty of D_{11} was estimated to be 4% (k = 2).

2.4 Simultaneous Determination of Thermal Diffusivity and Mutual Diffusion Coefficient for Binary Fluid Mixtures

Compared to studies reporting specifically on either a or D_{11} of pure fluids or fluid mixtures, few studies demonstrate the simultaneous determination of both properties. As mentioned in Section 2.1, Bergé et al. [152] were the first to demonstrate the simultaneous determination of a and D_{11} using DLS in 1970. The first related study with a focus on transport property determination was published by Saad and Gulari [226] in 1984. They investigated the saturated liquid phase of mixtures of n-C_7H_{16} with dissolved CO_2 at corresponding T between (283 and 323) K and p between about (1 and 8) MPa. The amount of the dissolved CO_2 ranged between x = (0.3 and 0.9). Mixtures consisting of liquids with dissolved gases facilitate the simultaneous determination of a and D_{11}. This is because, for many related systems, the light-scattering signals originating from T and c fluctuations appear at similar time scales. ACFs were obtained at various Θ_S between (6 and 11)° using a homodyne detection scheme. However, it is questionable whether true homodyne conditions could be achieved for such a relatively weakly scattering molecular system – especially at low c of CO_2. In agreement with the work of Wu et al. [176], who investigated the influence of the RID of pure components on the determination of a, I_c was dominant in the concentrated mixtures examined by Saad and Gulari. This was because the refractive indices of CO_2 and n-C_7H_{16} differed by about 30%. Thus, they performed a DEF that allowed them to simultaneous determine a and D_{11}. Given the related relative signal amplitudes, the typical relative uncertainties of a and D_{11} were (24 and 2)% and the smallest uncertainty of D_{11} was about 0.7% for the concentrated mixtures.

Next, it is important to mention the work by Leipertz [236] in 1988. Rather than presenting new diffusivity data, Leipertz provided a comprehensive state of the art report on the DLS technique, including an evaluation of the limitations regarding the simultaneous determination of a and D_{11} in transparent binary liquid mixtures. Leipertz reported that measurement times for a CF typically ranged from 1 to 2 h when far from the critical point to several seconds when nearby. Here, low-power lasers could be employed under homodyne conditions. Leveraging small Θ_S arrangements, the application of the heterodyne detection technique is highly recommended for

obtaining small uncertainties in the diffusivities. For both transport properties, uncertainties exceeding 2% for a single measurement could be achieved via DLS. Based on the findings by Wu et al. [125,176], Leipertz concluded that if the RID of both pure components is less than or equal to 5%, a can be measured independently of D_{11}, and D_{11} cannot be determined. If the RID is (5 to 15)%, a can only be measured with exact knowledge of D_{11}, which must be measured first. If the RID is (10 to 15)% or higher, only D_{11} can be obtained via DLS. Here, it should be noted that these statements can be true in many cases; however, as it will be demonstrated later, other influencing factors, such as the osmotic compressibility or *Le*, must also be considered.

In 1995, Li et al. [237] investigated an equimolar liquid mixture of $C_6H_5CH_3$ and n-C_6H_{14} at T = 298 K. Pseudo-cross CFs were measured at Θ_S between (2 and 3)° in a heterodyne detection scheme. A new feature incorporated into their experiments was the use of a digital multiple-tau correlator (MTC), which exhibited a quasi-logarithmic spacing of the correlator channels, rendering it especially well-suited for resolving multiple relaxation times in the CF. In earlier experiments, correlators with a constant spacing between the correlator channels, that is, linear-tau correlators (LTCs), were commonly used. Each run lasted about (6 to 10) h. Although the obtained pseudo-cross CFs at different Θ_S contained both signals, the authors chose to analyze the signals related to T and c fluctuations separately employing SEFs. This was because the decay time of these two modes differed by a factor of 30. Therefore, they did not perform a true simultaneous determination of a and D_{11}. In addition, Li et al. [237] reported $\mathcal{R}$ = 3.7 for the equimolar liquid mixture of $C_6H_5CH_3$ and n-C_6H_{14}, which indicated that the signal related to c fluctuations was approximately four times stronger than that related to T fluctuations. The uncertainties reported for a, D_{11}, and $\mathcal{R}$ were around (1, 7, and 8)%, respectively. A reason for the relatively large uncertainty of D_{11}, despite $\mathcal{R} > 1$, was not provided.

The research group of Fröba [238–244] made significant progress in the simultaneous determination of a and D_{11}. In their work, the pseudo-cross CF was generally calculated rather than the ACF. In context of the simultaneous determination of a and D_{11}, especially the doctoral thesis of Heller [245] and related publications have markedly contributed to an improved understanding. In 2014, Heller et al. [238] investigated the binary mixtures of n-octacosane (n-$C_{28}H_{58}$) with CO, H_2, or H_2O in the saturated liquid phase at T ranging from (398 to 523) K and p between (0.5 to 3.0) MPa at small Θ_S. The decay times related to a and D_{11} differed by factors below about three. Various data evaluation strategies, including a multi-fit

procedure, were evaluated to minimize uncertainties in the resulting transport properties. The relative expanded uncertainties reported ranged from (4 to 15)% for a and (4 to 30)% for D_{11}. In the same year, Rausch et al. [239] reported a and D_{11} for mixtures of the IL 1-butyl-3-methylimidazolium tricyanomethanide or 1-butyl-3-methylimidazolium tetracyanoborate with dissolved CO_2 at T between (303 and 333) K and p between (0.2 and 2.6) MPa. Investigations were performed at small and large Θ_S. Unlike Heller et al. [238], the decay times related to T and c fluctuations differed by more than a factor of 100 for these mixtures. Because the associated signals appeared on different time scales, the simultaneous determination of a and D_{11} from one CF was only possible using a MTC. To obtain both properties from the LTC, two separate measurements were taken under a specific thermodynamic state leveraging different sampling times. The relative expanded uncertainties ranged from (4.1 to 21)% for a and (3.1 to 28)% for D_{11}. Similar to previous reports, the relative uncertainty of D_{11} was generally observed to decrease with an increase in the mole fraction of the dissolved CO_2 due to a rise in I_c.

In the subsequent years, Heller et al. [240] and Koller et al. [241] studied similar systems via DLS. Heller et al. [240] investigated binary mixtures of n-dodecane (n-$C_{12}H_{26}$) or n-tetracontane with dissolved CO, H_2, or H_2O in the saturated liquid phase at small Θ_S, T between (398 and 524) K, and p up to 4.2 MPa. Each measurement lasted between (10 and 120) min, depending on the light scattering intensities. a and D_{11} were determined simultaneously with expanded relative uncertainties (k = 2) ranging from approximately (2 to 12)% and (3 to 25)%, respectively. These authors also made important statements regarding signal attribution. For many systems and thermodynamic states, a and D_{11} differed by two to three orders of magnitude, facilitating a clear separation of the two corresponding exponentials. In most cases, the faster decaying exponential could be attributed to T fluctuations associated with a, while the slower decaying exponential was ascribed to c fluctuations associated with D_{11}. Given that most systems exhibit an observable increase in D_{11} and a decrease in a with increasing T, a region exists where these trends intersect. Heller et al. [241] observed such an intersection of the diffusivities for mixtures of n-$C_{12}H_{26}$ with dissolved H_2 and H_2O. In the intersection region, they observed only one hydrodynamic mode and assumed that a and D_{11} were identical. After intersecting, the faster decaying exponential was ascribed to c fluctuations, whereas the slower mode was attributed to T fluctuations. These results demonstrate the need for careful attribution of obtained signals. Without further knowledge, it is initially difficult, if not impossible, to determine which

contribution is related to which type of fluctuation for a given thermodynamic state and system. Koller et al. [241] investigated binary mixtures of the IL 1-ethyl-3-methylimidazoliumtetracyanoborate with the dissolved gases CO_2, N_2, CO, or H_2 at T from (298 to 363) K and p up to 6.3 MPa. The expanded relative uncertainties (k = 2) ranged from approximately (4 to 28)% for a and (3 to 40)% for D_{11}, respectively. Furthermore, Koller et al. [242] examined a binary liquid mixture of n-$C_{28}H_{58}$ and C_2H_5OH. They demonstrated, for the first time, the simultaneous analysis of equilibrium fluctuations in the bulk and at the surface of a binary liquid mixture via DLS. Thus, the simultaneous determination of a, D_{11}, viscosity, and surface tension was achieved. Giraudet et al. [47] delved into binary mixtures of n-C_6H_{14} or n-decane (n-$C_{10}H_{22}$) with dissolved H_2, He, N_2, or CO at T ranging from (303 to 423) K and p up to 6 MPa, corresponding to a gas mole fraction of x < 0.06, that is, close to infinite dilution. The authors revealed, for the first time, that even for x = 0.007 and Le close to unity, reliable D_{11} data can be obtained via DLS in such mixtures with an average expanded uncertainty (k = 2) of 13%. Similar to Heller et al. [240], the authors encountered situations where only one hydrodynamic mode was observable in the CF. They discovered that, in general, when $Le \geq 1.6$ or $Le \leq 0.6$, which is valid for numerous systems and thermodynamic states, both contributions could be resolved, and the CF could be well-fitted by the sum of two exponentials. However, in the vicinity of Le = 1, both hydrodynamic modes could not be distinguished from one another due to the convergence of their decay times. In addition, for some cases the associated amplitudes of the modes also converged, that is, $\mathcal{R} = I_c \cdot I_t^{-1} \approx 1$, hindering the determination of two individual diffusivities. Wu et al. [48] conducted similar investigations for binary mixtures comprising the gases H_2, He, N_2, CO, or CO_2 dissolved in C_2H_5OH, 1-hexanol (1-$C_6H_{14}OH$), or 1-decanol (1-$C_{10}H_{22}OH$) in the same range of T. Regarding the limits of DLS, identical findings as those for the n-alkane based mixtures [47] were observed. In addition to systems at close to infinite dilution of the dissolved gas, Klein et al. [243] and Wu et al. [244] investigated binary mixtures of CO_2 dissolved in n-C_6H_{14} or 1-$C_6H_{14}OH$ over a wide range of compositions, including x of dissolved CO_2 between approximately x = (0.005 and 0.98) at T ranging from (303 to 353) K. Although Klein et al. [243] reported only D_{11} in their publication, they also simultaneously determined a. Wu et al. [80] later reported some of these values. For these mixtures, the expanded relative uncertainties (k = 2) were around 20% for a and 3% for D_{11}. Similar to Saad and Gulari [226], Klein et al. [243] and Wu et al. [244] observed that I_c strongly increased with an increase in dissolved CO_2, as shown in the CFs presented in the respective

publications. This increase in I_c was responsible for the generally larger uncertainties of a.

Heller [245] provided in his doctoral thesis a comprehensive evaluation of the maximum and minimum permissible difference between the two observed decay times, allowing fitting with a sum of two exponentials. In addition, certain guidelines regarding the experimental conditions were presented. A brief summary is as follows: Heller discussed two cases where $\tau_{C,c} >> \tau_{C,t}$ and $\tau_{C,c} \approx \tau_{C,t}$. Here, $\tau_{C,t}$ and $\tau_{C,c}$ are the mean lifetimes of the fluctuations in T and c. For $\tau_{C,c} >> \tau_{C,t}$, the MTC is generally preferred over the LTC when the simultaneous determination of both properties a and D_{11} from one CF is desired. For an accurate determination, appropriate scattering geometries, that is, Θ_S must be selected. For this, the expected magnitudes of a and D_{11} must be considered, and, consequently, their relaxation times and the behavior of observable disturbances in the CF. Although small Θ_S are generally favored, increasing the incident angle can diminish the relaxation time and circumvent significant disturbances in the event that D_{11} yields numerical values that result in relaxation times exceeding 500 µs. Measurements with Θ_S = 90° might also be suitable to reduce the observable relaxation time and obtain CFs free of disturbances. However, this may hinder the simultaneous determination of both diffusivities. Furthermore, scattering geometries leading to relaxation times of less than 1 µs should be avoided because, with smaller sampling times, artefacts introduced by the PMTs become visible within calculated CFs. Although these artifacts are limited by using a pseudo-cross correlation scheme, they cannot be completely avoided. For $\tau_{C,c} \approx \tau_{C,t}$, Heller [245] concluded that the likelihood of separating two superimposed exponential modes on the time scale using nonlinear regression analysis is highly dependent on the signal statistics, that is, the SNR. To obtain high-quality DLS signals with excellent signal statistics, both long measurement durations and transparent, particle-free samples are required. Heller concluded that the interplay between the overall signal quality, individual decay times, and individual amplitudes of the signals related to the T and c fluctuations determine whether a simultaneous determination of both a and D_{11} is possible. According to Heller, a simultaneous determination is feasible if the ratio of the decay times $\tau_{C,c} \cdot \tau_{C,t}^{-1}$ is either > 1.5 or < 0.7. These values are similar to those reported by Giraudet et al. [47] for the corresponding *Le*.

Recently, Cui et al. investigated a and D_{11} in the saturated liquid phase of mixtures of CO_2 dissolved in n-C_7H_{16} [246], n-tetradecane (n-$C_{14}H_{30}$) [247], or n-eicosane (n-$C_{20}H_{42}$) [248] as a function of composition at T between

(298 to 473) K and p up to 5.6 MPa. The reported average expanded uncertainty of a and D_{11} were about (10 and 5)%. Furthermore, leveraging a method similar to that previously reported by Koller et al. [242] for binary liquid mixtures, Cui et al. [249] demonstrated the simultaneous determination of a, D_{11}, viscosity, and interfacial tension via DLS in mixtures of n-C_7H_{16} with dissolved CO_2. In 2023, Gao et al. [250] presented a study that aimed to elucidate the influence of sampling time, Θ_S, viscosity, RID of the pure components, and Le on the reliability and obtainable uncertainties for the simultaneous determination of a and D_{11} via DLS. They investigated the binary mixtures of n-C_6H_{14} and n-$C_{10}H_{22}$ at x = 0.5 as well as of n-C_6H_{14} and n-hexadecane (n-$C_{16}H_{34}$) at x = (0.06 and 0.85), respectively. Here, the first and third systems had similar viscosities but different RIDs for the pure components. In contrast, the second and third systems exhibited identical RIDs for the pure components but different viscosities. The authors stated that the measurements were taken under saturation conditions. They concluded that both the a and D_{11} of the binary mixtures could be obtained with an uncertainty of less than 5% if the sampling time was 1.5 to 3 times that of the relaxation time, Θ_S was between 8° and 12°, and the system had a relatively low viscosity. Moreover, the authors assert that a simultaneous determination of the a and D_{11} is feasible if the pure components had a RID > 4% and Le was between 10 and 80. These findings are, however, somewhat questionable.

2.5 Diffusivities in the Vicinity of the Critical Point of Binary Fluid Mixtures

Critical phenomena in fluids are a separate and extensive area of research [251–253], and play an important role in the field of transport properties [141]. The vicinity of the critical point of binary fluid mixtures is a somewhat special topic, not only because of the peculiar behavior of several physical quantities, but also because the interpretation of the signals accessible via DLS can be complicated in the near-critical region. Only the most important features relevant to the accessibility and interpretation of diffusivities of binary fluid mixtures via DLS will be highlighted. In 1980, Ackerson and Hanley [122] studied a mixture of x = 0.7107 CH_4 and x = 0.2893 C_2H_6 near the critical point using DLS. They observed two relaxation modes, and their associated decay rates were attributed to pure D_{11} and a. In 1984, Miura et al. [167] investigated mixtures of helium-3 and helium-4 at different compositions along their respective critical isochores near the vapor–liquid critical point. Unlike Ackerson and Hanley [122], they were only able to detect

a single, relatively slow decay rate. In the 1990s, Anisimov et al. [124,254–256] presented new theoretical aspects of light scattering from bulk fluids, demonstrating that in near-critical binary fluid mixtures neither of the two observable diffusivities could be associated with pure D_{11} or a. Instead, owing to a coupling of the hydrodynamic modes, two effective diffusivities $D_{\mathrm{eff},\{1,2\}}$ could be observed. The strength of the coupling was determined by the coupling parameter, which varies considerably depending on the thermodynamic state and fluid properties. According to Anisimov et al. [124], the two diffusivities are only decoupled in special cases, such as in the limit of infinite dilution, where they become a and D_{11}. They compared their calculations with the experimental data reported by Ackerson and Hanley [122] and suggested that the experimental data represented two effective diffusivities and not pure D_{11} and a. Fröba et al. [123] investigated an equimolar mixture of CH_4 and C_2H_6 at T ranging from (265 to 310) K. They observed two contributions, that is, two hydrodynamic diffusion modes, which exhibited the typical behavior expected for a and D_{11} in the vicinity of the critical point. For clarification, the authors calculated the expected $D_{\mathrm{eff},1}$ and $D_{\mathrm{eff},2}$. However, owing to large uncertainties in the input quantities required to calculate the coupling parameter, a wide range of possible $D_{\mathrm{eff},1}$ and $D_{\mathrm{eff},2}$ were found. Therefore, they could not confirm whether the observed diffusivities should be interpreted as effective diffusivities or not.

2.6 Diffusivities in Multicomponent Fluid Mixtures

Although numerous studies in the literature demonstrate that determining a in molecular multicomponent mixtures is straightforward (see Section 2.2), few studies discuss the application of DLS for studying mutual diffusivities in non-polymer multicomponent mixtures. In 1993, Leaist and Hao [257] investigated the diffusion of sodium dodecyl sulfate micelles in aqueous salt solutions using DLS and Taylor dispersion experiments. They found that the supposed diffusion coefficient of the micelles obtained via DLS was larger than the coefficient determined via Taylor dispersion. To interpret the results, the authors formally extended the theoretical approach reported by Mountain and Deutch [158] for a binary mixture and developed an expression for the spectrum of light scattered by the c fluctuations in a multicomponent solution, while disregarding T fluctuations. They found that multi-exponential decays are generally observable in the CF of DLS experiments for a multicomponent solution, where the respective decay times are governed by the eigenvalues of the diffusion coefficient matrix. For the chosen system, the authors were able to only resolve a single exponential decay related to c fluctuations. This was explained by the

strong scattering of the micelles resulting from the large RID and thermodynamic driving forces. The authors concluded that if the cross-diffusion coefficients can be safely neglected, for their studied system, the single obtained eigenvalue will be equal to the mutual diffusion coefficient of the polymer component. In summary, the authors recommend caution when interpreting DLS diffusion data for multicomponent solutions, unless coupled diffusion is known to be insignificant.

DLS experiments on low-molecular weight ternary fluid mixtures were performed in the mid-2000s by Ivanov et al. [129,258,259], who investigated mixtures consisting of glycerol, C_3H_6O, and H_2O in the near-critical region in a series of studies, and by Das et al. [260], who studied aqueous solutions of mixtures containing decylsulfobetaine and dodecylsulfobetaine. Both groups compared their DLS results with data obtained from the Taylor dispersion, similar to Leaist and Hao [257]. Ivanov et al. [129,258,259] found only one eigenvalue of the Fick diffusion matrix using DLS measurements that coincided with their Taylor dispersion measurements. A second DLS signal that was observed and attributed to mass diffusion yielded an eigenvalue that differed by a factor of more than 1000 from their Taylor dispersion results. Das et al. [260] found good agreement between their DLS and Taylor dispersion results. However, they did not prove that their DLS signals were associated with hydrodynamic modes. Bardow [130] proposed a simple theory that described the observable signals in the spectrum for ternary mixtures and provided a potential explanation for the observation of a single signal related to mass diffusion in ternary mixtures. The theory suggested that even though two hydrodynamic modes associated with mass diffusion contributed to the overall signal, one mode was strongly enhanced for situations typically encountered in DLS experiments.

Motivated by the ongoing debate mentioned above, Heller et al. [103] investigated ternary fluid mixtures consisting of *n*-$C_{12}H_{26}$, *n*-$C_{28}H_{58}$, and the solutes CO, H_2, or H_2O at T up to 523 K and p up to 4.1 MPa via DLS using a heterodyne detection scheme. They were able to separate three individual contributions for the first time and demonstrated that these were related to hydrodynamic modes. The fastest decaying mode was associated with T fluctuations and, thus, a. The two slower decaying modes originated from c fluctuations. A comparison of the DLS results and calculations using molecular dynamic simulations and an equation of state (EoS) based on statistical associating fluid theory indicated that the eigenvalues of the Fick diffusion matrix could be obtained via DLS measurements. Furthermore, the authors found that for the studied systems, the slow mass diffusivities (i.e., eigenvalues of the Fick diffusion matrix) coincided with the mutual

diffusivities of the binary subsystems. To the best of my knowledge, there are no studies available in the literature that aim to resolve the individual contributions in DLS experiments for quaternary mixtures, quinary mixtures, or mixtures with even more components.

3 Aim of this Thesis

The preceding literature survey reveals certain limitations in the applicability of DLS for the simultaneous determination of a and mutual diffusivities in fluid mixtures. For various reasons, situations may arise wherein the expected number of signals cannot be resolved, and/or the unambiguous classification of the signals obtained from DLS experiments may not be possible with respect to a and mutual diffusivities. In general, the capabilities and limitations of DLS for the simultaneous determination of a and mutual diffusivities of fluid mixtures have not yet been fully explored.

The main objective of this thesis is to explore which factors in the DLS technique influence the feasibility of a simultaneous determination of a and mutual diffusivities in the bulk of homogeneous molecular fluid mixtures. The focus is primarily on binary fluid mixtures, which are the most studied systems that allow for the simultaneous determination of a and D_{11}. However, certain aspects related to multicomponent mixtures will also be discussed. To allow identification of limiting factors, both theory and experimental implementation of DLS are considered. The theory can provide a general understanding of the various contributions to the observed signals including the expected signal amplitudes of the studied fluctuations, their interrelationships, and possible coupling of heat and mass transfer. With respect to the experimental implementation, aspects such as measurement equipment, sample preparation, processing and characteristics, and data evaluation are considered. To facilitate a comprehensive discussion, a diverse range of systems will be experimentally explored over a wide range of thermodynamic states, encompassing T between (280 and 560) K, p between (0.030 and 20) MPa, and compositions spanning x between about (0.002 and 0.995).

Equimolar CH_4–propane (C_3H_8) mixtures, as well as various binary mixtures of liquids with dissolved gases were selected as model systems and should facilitate fundamental investigations into different influencing factors. The equimolar CH_4–C_3H_8 mixtures will be investigated across the two-phase envelope including the gas, liquid, and supercritical states, as well as the liquid and vapor phases under saturation conditions and in the vicinity of the plait critical point. This should provide a better understanding regarding the different types of diffusivities in the different fluid regions and enable the identification of the effect of the location of the investigated thermodynamic state point relative to the phase envelope of the mixture on the simultaneous accessibility of a and D_{11}. In this context, to the best of

my knowledge, the dilute gas region within the hydrodynamic regime has not yet been investigated using DLS. The systematic investigation of liquids with dissolved gases under conditions close to infinite dilution of the gas should serve to identify the influence of fluid properties such weight, size, shape, and polarity of the constituents on the simultaneous determination of a and D_{11}. Studies covering a wide range of compositions under saturation conditions can reveal the relationship between light scattering signal amplitudes and concentration. Additionally, this thesis also delves into various systems relevant for process and energy technologies which often have a technical nature. This includes liquid mixtures, liquids with dissolved gases, and gaseous and supercritical mixtures and should allow to evaluate the transferability of the previously determined relationships and applicability of DLS. These systems include particularly systems that are currently being discussed in connection with the anticipated transition into a renewable energy economy such as mixtures related to biofuels, electrolytes, LOHCs, and to the geological storage of H_2. Electrolytes have to be considered a special class because they may contain multiple species that might be represented in a binary mixture consisting of two salts with up to four different ions. Additionally, mixtures related to natural gas and polymer melts with dissolved blowing agent are explored. In addition to the main aim, this endeavor should not only significantly expand the database of reliable diffusivity data but often evaluate, for the first time, the applicability of DLS to the respective system.

Drawing on insights gained from the various studies, this thesis aims to: (1) highlight which factors influence the feasibility of a simultaneous determination of thermal and mutual diffusivities in homogeneous molecular fluid mixtures through DLS; (2) provide an overview of the types of accessible diffusivities and their related uncertainties in different fluid classes and thermodynamic fluid states; (3) develop tools and strategies which allow for the attribution of the signals obtained through DLS experiments on arbitrary binary fluid mixtures.

4 Applied Strategy and Methods Used

This chapter provides an overview of the principles of the DLS method and applied strategies used in this thesis. Further details can be found in the respective publications that are identified in this work. First, the fundamentals of hydrodynamic fluctuations, which form the basis of DLS, will be briefly outlined. This is because the spectrum of the fluctuations that can be derived provides information on resolvable diffusivities. Thereafter, various aspects of light scattering from the bulk of (binary) fluid mixtures will be briefly discussed. This includes the very principles, scattered light spectrum, time domain analysis, and homodyne and heterodyne techniques. Before presenting a typical setup and introducing experimental procedures, a summary will be provided on the theoretical calculation of the Rayleigh ratio, which represents one of the pillars of the mode allocation strategy developed in this thesis. Finally, data evaluation, limiting factors, and the strategies for signal attribution in DLS experiments are presented and discussed.

4.1 Hydrodynamic Fluctuations in the Bulk of Fluids

In the bulk of a fluid or fluid mixture in macroscopic thermodynamic equilibrium, microscopic statistical fluctuations in the variables of state can be observed. These fluctuations occur naturally with a distribution of wavelengths and frequencies. Local perturbations resulting from these fluctuations disturb the equilibrium state of the system on a microscopic level. In the hydrodynamic regime, where the mean free path length l_0 of the molecules is considerably smaller than the reciprocal value q^{-1} of the modulus of the scattering vector ($q \cdot l_0 << 1$), the relaxation of each degree of freedom – also known as mode – toward its equilibrium value obeys the same laws as those for the relaxation of macroscopic systems. The basic justification for this relationship is Onsager's regression hypothesis [99,100], which states that, on average, microscopic fluctuations are governed by the same transport equations as the macroscopic ones. Thus, the decay of entropy or T fluctuations is governed by a. p fluctuations in fluids move at the speed of sound c_s, and their decay is governed by the sound attenuation. In the case of a binary fluid mixture, the decay of c fluctuations is governed by D_{11}. The notation D_{11} is chosen to be consistent with the generalized formulation of Fick's first law for diffusion in multicomponent mixtures where, in a ternary mixture, D_{12} and D_{21} are the off-diagonal elements of the diffusion

matrix [245]. To describe the fluid mechanics, that is, motion of molecules, in a nonrelativistic binary fluid medium, four basic laws are required: the continuity equation, which expresses the conservation of matter; force equation, which expresses the conservation of momentum; heat transport equation, which expresses the conservation of energy; and diffusion equation. To analyze the fluctuating quantities and their spatiotemporal behavior, the hydrodynamic equations are first linearized because the fluctuations, denoted as $\delta x = x - x_o$, around their mean equilibrium value (index o) are assumed to be small. In principle, any chosen variable of state could be represented by x. Herein, the primary interest lies in evaluating the evolution or dynamics of the fluctuations in the state variables. Because the dynamics of a fluid system are fully contained in the CFs of the fluctuations [261,262], the time dependence of the CFs of the local thermodynamic variables is computed according to the linearized hydrodynamic equations. The following derivations include several assumptions and utilize mathematical operations with well-established thermodynamic relationships. The detailed derivations and discussions can be found in the works of Mountain and Deutch [158], Boon and Yip [261], Cohen et al. [263], and Berne and Pecora [96].

The linearized hydrodynamic equations for a binary mixture within the framework of the Navier–Stokes hypothesis and Fourier's law are expressed as function of the space variable ($\vec{r}$) and time (t) [107,158,261,263]. These equations are the continuity equation

$$\frac{\partial \rho(\vec{r},t)}{\partial t} = -\rho_o \psi(\vec{r},t); \tag{4.1}$$

the longitudinal part of the Navier–Stokes equation

$$\rho_o \frac{\partial \psi(\vec{r},t)}{\partial t} = -\nabla^2 p + \left(\frac{4}{3}\eta_s - \eta_v\right)\nabla^2 \psi \; ; \tag{4.2}$$

the diffusion equation

$$\rho_o \frac{\partial c(\vec{r},t)}{\partial t} = -\nabla \cdot \vec{j}^c \, , \tag{4.3}$$

where $\vec{j}^c$ is the linearized diffusion flux, presented as

$$\vec{j}^c = -\rho_o D_{\text{п}} \left[\nabla c + \frac{k_T}{T_o}\nabla T + \frac{k_p}{p_o}\nabla p \right]; \tag{4.4}$$

and the entropy transport equation [96, 158, 261, 263]

$$\rho_o c_p \frac{\partial T}{\partial t} - \rho_o k_T \left(\frac{\partial \mu}{\partial c}\right)_{p,T} \frac{\partial c}{\partial t} + \rho_o T_o \left(\frac{\partial s}{\partial p}\right)_{T,c} \frac{\partial p}{\partial t} = \kappa_c \nabla^2 T \,. \tag{4.5}$$

In Equations 4.1 to 4.5, $\psi(\vec{r},t) = \nabla\cdot\vec{u}\,(\vec{r},t)$, $\rho(\vec{r},t)$ denotes the local mass density, $\vec{u}\,(\vec{r},t)$ represents the local fluid velocity, $c(\vec{r},t)$ indicates the local mass fraction of one component, s is the entropy per unit mass, c_p refers to the heat capacity per unit mass at constant p and c, and μ signifies the difference in the chemical potential of the two components. The term $(\partial\mu/\partial c)$ represents the inverse of osmotic compressibility, which will later be of particular significance. The transport coefficients appearing in these equations are the dynamic or shear viscosity η_s, bulk viscosity η_v, thermal conductivity κ_c, and the Fick or mutual diffusion coefficient D_{12}. κ_c, the thermal diffusion ratio k_T, and the thermodynamic quantity k_p can be expressed via

$$\kappa_c = a\rho c_p \,, \tag{4.6}$$

including thermal diffusivity a,

$$\frac{k_T}{T_o} = -\frac{D_T}{D_{12}} c(c-1) \,, \tag{4.7}$$

with the thermal diffusion coefficient D_T, and

$$\frac{k_p}{p_o} = \left(\frac{\partial \mu}{\partial p}\right)_{c,T} \left(\frac{\partial \mu}{\partial c}\right)^{-1}_{T,p} = \frac{D_p}{D_{12}} c(c-1) \tag{4.8}$$

with the barodiffusion coefficient D_p.

In the next step, three statistically independent fluctuating thermodynamic variables have to be selected to characterize the state of a binary system. The two obvious candidate choices p, c, and T or p, c, and s do, however, not satisfy the criterion of statistical independence. Instead, the three variables p, c, and ϕ according to [263]

$$\phi = T - \frac{T_o}{\rho_o} \frac{\beta_T}{c_p} p \tag{4.9}$$

are selected. In Equation 4.9, the thermal expansion coefficient β_T can be expressed as

$$\beta_T = -\frac{1}{\rho}\left(\frac{\partial \rho}{\partial T}\right)_{c,p} \,. \tag{4.10}$$

Thereafter, the linearized, coupled differential hydrodynamic equations are rewritten for the fluctuations δp, δc, $\delta\phi$, and $w = \rho_o \nabla \cdot \vec{u}$ and Laplace-Fourier transformed [96,261]. Following the procedures as outlined in the literature, a dispersion equation can be obtained for a binary mixture which, for a given wave number of the fluctuations q observed, can be expressed as [261,263]

$$\begin{bmatrix} \left[z + D_{\text{II}} q^2\right] & \varphi D_{\text{II}} q^2 & T_o^{-1} k_T D_{\text{II}} q^2 & 0 \\ c_{s,ad.}^2 \rho_o^2 \left(\frac{\partial \mu}{\partial c}\right)_{T,p} \varphi D_{\text{II}} q^2 & \left\{ z + \left[c_{s,ad.}^2 \rho_o^2 \left(\frac{\partial \mu}{\partial c}\right)_{T,p} \varphi D_{\text{II}} + c_{s,ad.}^2 \beta_T^2 T_o c_p^{-1} a \right] q^2 \right\} & \left[c_{s,ad.}^2 \rho_o^2 \frac{k_T}{T_o} \left(\frac{\partial \mu}{\partial c}\right)_{T,p} \varphi D_{\text{II}} + c_{s,ad.}^2 \rho_o \beta_T a \right] q^2 & \rho_o c_{s,ad.}^2 \\ \frac{k_T}{c_p} \left(\frac{\partial \mu}{\partial c}\right)_{T,p} D_{\text{II}} q^2 & \left[\frac{k_T}{c_p} \left(\frac{\partial \mu}{\partial c}\right)_{T,p} \varphi D_{\text{II}} + c_p^{-1} T_o \beta_T \rho_o^{-1} a \right] q^2 & \left\{ z + \left[a + \frac{k_T^2}{T_o c_p} \times \left(\frac{\partial \mu}{\partial c}\right)_{T,p} D_{\text{II}} \right] q^2 \right\} & 0 \\ 0 & -\rho_o^{-1} q^2 & 0 & \left[z + \nu_l q^2\right] \end{bmatrix} = 0 \tag{4.11}$$

with z as the complex Laplace variable; the adiabatic sound speed

$$c_{s,ad.} = \left(\frac{\partial \rho}{\partial p}\right)_{s,c}^{-1/2}; \tag{4.12}$$

longitudinal viscosity

$$\nu_l = \left(\frac{4}{3}\eta_s - \eta_v\right)\rho_o^{-1}; \tag{4.13}$$

and

$$\varphi = \frac{k_p}{p_o} + \frac{k_T}{T_o}\left(\frac{\beta_T T_o}{c_p \rho_o}\right). \tag{4.14}$$

Solving Equation 4.11 to the order q^2 provides two propagating modes

$$z_{\pm} = \pm i c_{s,ad.} q - K q^2, \tag{4.15}$$

with

$$K = \frac{1}{2}\left[\nu + \left(\frac{c_p}{c_v} - 1\right)a + \sigma D_{\text{II}}\right], \tag{4.16}$$

where c_v denotes the specific heat capacity at constant volume, ν the kinematic viscosity

$$\nu = \eta_s \rho_o^{-1}, \tag{4.17}$$

and σ the quantity

$$\sigma = \left(c_{s,ad.}\rho_o\varphi\right)^2 \left(\frac{\partial\mu}{\partial c}\right)_{T,p}, \tag{4.18}$$

as well as two non-propagating modes

$$z_{\pm}^{\circ} = -\frac{1}{2}\left(a + D'\right)q^2 \pm \frac{1}{2}\left(a + D'\right)q^2 \left[1 + \frac{4a\Delta}{\left(a - D'\right)^2}\right]^{1/2}, \tag{4.19}$$

with

$$D' = D_{11} + \Delta = D_{11}\left[1 + \frac{k_T^2}{T_o c_p}\left(\frac{\partial\mu}{\partial c}\right)_{T,p}\right]. \tag{4.20}$$

The interested reader will note that Equations 4.19 and 4.20 imply that the two non-propagating modes are related to the pure thermal diffusivity a and pure mutual diffusion coefficient D_{11} only when $k_T \to 0$. This topic has been analyzed in detail by Anisimov et al. [124] for near-critical binary fluid mixtures and will later be discussed in more detail.

4.2 Light Scattering from the Bulk of Fluids

In general, light is scattered by optical inhomogeneities. Optical inhomogeneities in the bulk of pure fluids and fluid mixtures in macroscopic thermodynamic equilibrium are caused by statistical microscopic fluctuations in the state variables, such as T, c, and p. These fluctuations cause concomitant fluctuations in the local dielectric constant of the medium ε. These fluctuations can be expressed as

$$\delta\varepsilon\left(\vec{r},t\right) = \left(\frac{\partial\varepsilon}{\partial p}\right)_{c,\phi} \delta p\left(\vec{r},t\right) + \left(\frac{\partial\varepsilon}{\partial c}\right)_{\phi,p} \delta c\left(\vec{r},t\right) + \left(\frac{\partial\varepsilon}{\partial\phi}\right)_{p,c} \delta\phi\left(\vec{r},t\right), \tag{4.21}$$

following the above path and notation. These sources of time-dependent optical inhomogeneities modulate the scattered light and lead to a time-dependent scattered electric field. Thus, the scattered electric field contains information on the above-described modes related to the fluctuation

dissipation processes and, thus, the transport properties of the scattering medium.

In DLS experiments, the sample fluid in macroscopic thermodynamic equilibrium is irradiated with coherent laser light, and the scattered light associated with a certain wavelength of fluctuations Λ is then analyzed under a well-defined scattering geometry. The scattering geometry can be expressed in terms of the scattering angle Θ_S, which can be described using wave vectors. Figure 4.1(a) represents a simple schematic of the scattering geometry. Here, the scattering vector $\vec{q} = \vec{k}_I - \vec{k}_S$ is defined by the wave vector $\vec{k}_I$ of the incident laser light with a frequency ω_0 and wavelength λ_0 in vacuo and the wave vector of the scattered light $\vec{k}_S$. Assuming the scattering process is quasi-elastic, that is, $\left|\vec{k}_I\right| \approx \left|\vec{k}_S\right|$, and using trigonometric functions, the modulus of the wave vector can be expressed as

$$q = \frac{2\pi}{\Lambda} = \left|\vec{q}\right| = \frac{4\pi n_{\text{fluid}}}{\lambda_0} \sin\left(\frac{\Theta_S}{2}\right), \tag{4.22}$$

where n_{fluid} is the refractive index of the fluid at a given thermodynamic state. Equation 4.22 indicates that the chosen scattering geometry is directly linked to the size of the fluctuations being studied. In a realistic experiment, Θ_S is defined as the angle between the detection direction of scattered light and the direction of the incident laser light in the sample fluid. The experimentally accessible incident angle Θ_I is the angle between the scattering direction and the direction of the incident laser light outside the sample cell. Θ_I can be measured using an autocollimation method with an estimated expanded uncertainty ($k = 2$) of 0.01°. The RID between the sample and ambient air ($n_{\text{air}} \approx 1$) requires the Snell–Descartes law of refraction to express the relationship between Θ_S and Θ_I, leading to

$$q = \frac{4\pi n_{\text{fluid}}}{\lambda_0} \sin\left(\frac{\arcsin\left(n_{\text{air}} / n_{\text{fluid}} \sin\Theta_I\right)}{2}\right), \tag{4.23}$$

which represents the principal work equation of DLS for experiments at small Θ_S. Evidently, the use of an approximation for q without n_{fluid} for small Θ_S is common practice [125,235,247]. However, using an approximation can lead to inaccuracies and is not recommended. For small angles, estimating n_{fluid} and using Equation 4.23 is sufficient and introduces an error in the diffusivities that is far below the typical related uncertainties [264,265] – and in any case smaller than by using the approximation. At large scattering

angles, that is, $\Theta_S \approx 90°$, q is calculated using Equation 4.22. In this case, n_{fluid} is an important quantity, with exact knowledge necessary for the correct determination of diffusivities via DLS. In the work related to this thesis, when measuring at Θ_S around 90°, n_{fluid} was determined using an Abbe refractometer or obtained from the literature.

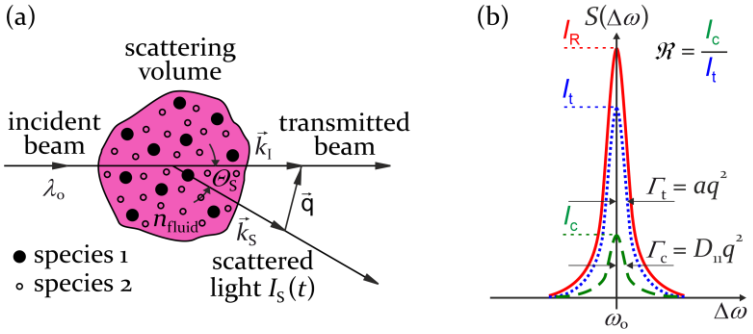

Figure 4.1: (a) Simple schematic of the scattering geometry at small Θ_S. The two different species comprising the binary mixture are indicated by filled and open circles of different sizes. (b) Schematic of the spectral power density of the central Rayleigh component of the characteristically broadened spectrum observable for a binary mixture.

4.2.1 Scattered Light Spectrum

In light scattering experiments, the intensity I_S of the scattered light is measured, not the electric field E_S. I_S can be represented as [107,158,263,266]

$$I_S\left(\vec{R}_o,\vec{q},\Delta\omega\right) = I_I\left[\frac{k_I^4 N \sin^2\gamma}{32\pi^3 R_o^2}\right] S\left(\vec{q},\Delta\omega\right), \tag{4.24}$$

where N denotes the number of (spherically symmetric) molecules or scatterer, R_o represent the distance from the origin to the point of observation, γ indicates the angle between the electric vector of the plane polarized incident light of intensity I_I and R_o, and $\Delta\omega = \omega_o - \omega_S$ is the change in angular frequency that the incident light experiences upon scattering. The generalized dynamic structure factor $S\left(\vec{q},\Delta\omega\right)$, also known as spectral density, refers to the space and time Fourier transform of the CF of fluctuations in ε. It can be expressed as [107]

$$S(\vec{q},\Delta\omega) = 2\,\mathrm{Re}\int_0^\infty dt \int d\vec{r}\,d\vec{r}\,' \left\langle \delta\varepsilon(\vec{r}+\vec{r}\,',t)\,\delta\varepsilon(0,0)\right\rangle \exp\left[i(\vec{q}\vec{r}-\Delta\omega t)\right]. \tag{4.25}$$

In terms of Fourier–Laplace transforms [158]

$$S(\vec{q},\Delta\omega) = 2\,\mathrm{Re}\left\langle \hat{\varepsilon}(\vec{q},i\Delta\omega)\,\varepsilon(-\vec{q})\right\rangle, \tag{4.26}$$

with

$$\hat{\varepsilon}(\vec{q},z) = \int_0^\infty dt \int d\vec{r}\,\delta\varepsilon(r,t)\exp\left[i\vec{q}\vec{r}-zt\right] \tag{4.27}$$

and

$$\varepsilon(\vec{q}) = \int d\vec{r}\,\delta\varepsilon(\vec{r},0)\exp(i\vec{q}\vec{r}). \tag{4.28}$$

In these equations, the caret indicates a Laplace-time transform. If only $\vec{q}$ is a variable, a time-independent initial value is implied. The angular bracket $\langle\ldots\rangle$ indicates an average over the initial states of the system. Since the shape of the characteristic broadened spectrum is contained in $S(\vec{q},\Delta\omega)$ and the intensity of the scattered light is proportional to the ACF of the fluctuations in ε [96,261], the main interest is in calculating $S(\vec{q},\Delta\omega)$. To obtain $S(\vec{q},\Delta\omega)$ related to the ε fluctuations in macroscopic thermodynamic equilibrium, the linearized Laplace–Fourier transformed hydrodynamic equations described above are solved to construct a set of CFs [158,261,263]. By following the steps outlined in the literature, the dielectric fluctuation CF is calculated, leading to the spectral distribution. This distribution comprises a central, frequency-unshifted line, also known as the Rayleigh line, and a frequency-shifted Brillouin doublet, which is not further considered in this thesis. The Rayleigh line, owing to contributions arising from the *T* or entropy and *c* fluctuations, is general expressed as

$$S^{cen}\left(\vec{q},\Delta\omega\right)=\frac{k_{\mathrm{B}}T_{\mathrm{o}}^{2}}{c_{\mathrm{p}}}\left(\frac{\partial\varepsilon}{\partial T}\right)_{p,c}^{2}\left(\frac{2}{z_{+}^{\circ}-z_{-}^{\circ}}\right)\left[\frac{z_{-}^{\circ}\left(D_{\mathrm{II}}q^{2}+z_{-}^{\circ}\right)}{\Delta\omega^{2}+\left(z_{-}^{\circ}\right)^{2}}-\frac{z_{+}^{\circ}\left(D_{\mathrm{II}}q^{2}+z_{+}^{\circ}\right)}{\Delta\omega^{2}+\left(z_{+}^{\circ}\right)^{2}}\right]$$
$$+\frac{k_{\mathrm{B}}T_{\mathrm{o}}}{\left(\frac{\partial\mu}{\partial c}\right)_{T,p}}\left(\frac{\partial\varepsilon}{\partial c}\right)_{T,p}^{2}\left(\frac{2}{z_{+}^{\circ}-z_{-}^{\circ}}\right)\left[\frac{z_{+}^{\circ}\left(D_{\mathrm{II}}q^{2}+s_{-}^{\circ}\right)}{\Delta\omega^{2}+\left(z_{+}^{\circ}\right)^{2}}-\frac{z_{-}^{\circ}\left(D_{\mathrm{II}}q^{2}+z_{+}^{\circ}\right)}{\Delta\omega^{2}+\left(z_{-}^{\circ}\right)^{2}}\right]$$
$$+2k_{\mathrm{T}}\frac{k_{\mathrm{B}}T_{\mathrm{o}}}{c_{\mathrm{p}}}\left(\frac{\partial\varepsilon}{\partial T}\right)_{p,c}\left(\frac{\partial\varepsilon}{\partial c}\right)_{T,p}\left(\frac{2}{z_{+}^{\circ}-z_{-}^{\circ}}\right)\left[\frac{z_{+}^{\circ}D_{\mathrm{II}}q^{2}}{\Delta\omega^{2}+\left(z_{+}^{\circ}\right)^{2}}-\frac{z_{-}^{\circ}D_{\mathrm{II}}q^{2}}{\Delta\omega^{2}+\left(z_{-}^{\circ}\right)^{2}}\right]$$

,(4.29)

where k_{B} is the Boltzmann constant. The central distribution is a relatively complicated feature because the contributions arising from T and c fluctuations are coupled. Evidently, as expected from Equations 4.19 and 4.20, the spectral distribution can only be decomposed into a (close to) sum of two Lorentzian contributions with the widths Γ_{t} and Γ_{c} proportional to a and D_{II} if $k_{\mathrm{T}}\to 0$. This condition is, for instance, sufficiently met in the very dilute limit of one component [96,261,263]. Comprehensive discussion is given by Cohen et al. [263]. From Equation 4.19, the following equations can be obtained:

$$z_{-}^{\circ}\xrightarrow[k_{\mathrm{T}}\to 0]{}-aq^{2}\ \text{ and }\ z_{+}^{\circ}\xrightarrow[k_{\mathrm{T}}\to 0]{}-D_{\mathrm{II}}q^{2}, \tag{4.30}$$

and the central part of the spectrum becomes [154,158,261,263]

$$\lim_{k_{\mathrm{T}}\to 0}S^{cen}\left(\vec{q},\Delta\omega\right)=\frac{k_{\mathrm{B}}T_{\mathrm{o}}^{2}}{c_{\mathrm{p}}}\left(\frac{\partial\varepsilon}{\partial T}\right)_{p,c}^{2}\left[\frac{2aq^{2}}{\Delta\omega^{2}+\left(aq^{2}\right)^{2}}\right]$$
$$+\frac{k_{\mathrm{B}}T_{\mathrm{o}}}{\left(\frac{\partial\mu}{\partial c}\right)_{T,p}}\left(\frac{\partial\varepsilon}{\partial c}\right)_{T,p}^{2}\left[\frac{2D_{\mathrm{II}}q^{2}}{\Delta\omega^{2}+\left(D_{\mathrm{II}}q^{2}\right)^{2}}\right]. \tag{4.31}$$

Here, the Lorentzian contributions are denoted by square brackets, with the prefactors related to the amplitude of the respective signal. As visible from Equation 4.31, the scattered light signal related to T fluctuations is proportional to k_{B}, T^{2}, inverse of c_{p}, and $(\partial\varepsilon/\partial T)^{2}$ at constant p and c. Similarly, the scattered light signal related to c fluctuations is proportional to k_{B}, T, $(\partial\varepsilon/\partial c)^{2}$ at constant T and p, and osmotic compressibility. Although in the literature $(\partial\varepsilon/\partial c)^{2}$ is often accounted in terms of the RID of the

species in the mixture, the influence of osmotic compressibility is usually not considered. The individual signal amplitudes translate to the signals observable in the experiment and will be of particular interest when considering the calculation of the Rayleigh ratio $\mathcal{R}$, as described in Section 4.3.

As previously mentioned, in DLS experiments, the scattered light intensity is analyzed under a well-defined scattering geometry, and, thus, (in principle) a single q. Figure 4.1(b) illustrates a schematic of such a spectral distribution for a binary mixture based on Equation 4.31 for a given q, indicated by the red solid line. The blue dotted and green dashed lines in Figure 4.1(b) are related to T and c fluctuations. Here, each contribution is characterized by its amplitude I and width Γ, which can be related either to a or D_{11} via the squared modulus of the wave vector q^2. It is important to note, however, that in an experiment, it may not be immediately clear which spectral contribution corresponds to which type of fluctuation. Furthermore, situations may arise where one amplitude is significantly larger or smaller than another. In the extreme case, one signal may no longer be observable within the achieved SNR. Where contributions can be attributed to the respective fluctuations, $\mathcal{R}$ can be determined.

4.2.2 Time Domain Analysis and Homodyne and Heterodyne Technique

For numerous fluid mixtures, spectral broadening caused by the fluctuations is in the range of MHz (compared to laser frequency in the order of 6×10^{14} Hz). A straightforward analysis that measures the spectrum using a charge-coupled device spectrometer or Fabry–Pérot scanning interferometer is usually not feasible. This is because the broadening of the scattered light spectrum is too small to be resolved in the frequency domain. According to the Wiener–Chintschin Theorem, the power-spectral density is the inverse Fourier transform of the time ACF of the scattered electric field. Given that common detectors measure intensity rather than the electric field ($I_S \propto E_S^* E_S$), an elegant and commonly applied approach to overcome this limitation is the time domain analysis. This is achieved by calculating the time-dependent intensity ACF, also known as the second-order ACF, as a function of the delay time τ

$$G^{(2)}(\tau) \equiv \langle I(0) I(\tau) \rangle = \lim_{T\to\infty} \frac{1}{2T} \int_{-T}^{T} I(t) \cdot I(t+\tau)\, dt \,, \tag{4.32}$$

where the brackets indicate the time average of the product $I(t)I(t + \tau)$ of the time-dependent intensity at the two time periods, t and $t + \tau$. In Equation 4.32, T denotes the measurement duration. The time dependent intensity, or more precisely the radiative flux, is a function of the electric field given by

$$I(t) = \frac{c_0 \varepsilon}{2} E^*(t) E(t), \tag{4.33}$$

where c_0 is the speed of light and * represents the complex conjugate variable.

In a realistic experimental situation, the scattered light from the sample is superimposed with coherent stray light, also known as a local oscillator (LO) or reference light, which is generated by imperfections in the optical path or cell windows. To provide a general description, a superposition $E(t) = E_S(t) + E_{LO}(t)$ of the scattered electric field $E_S(t)$ with the LO field $E_{LO}(t)$ is considered. Thus, the intensity measured by a detector is given by

$$I(t) = \frac{c_0 \varepsilon}{2} \left| E_S(t) + E_{LO}(t) \right|^2 = I_S(t) + I_{LO}(t) + \frac{c_0 \varepsilon}{2} \left[E_S^*(t) E_{LO}(t) + E_{LO}^*(t) E_S(t) \right]. \tag{4.34}$$

Here, $I_S(t)$ and $I_{LO}(t)$ are the intensities of the scattered light and LO. $E_S(t)$ and $E_{LO}(t)$ can be quantified by the electric field of the incident light and characteristic time behavior of the fluctuations observed, which is discussed in detail by Chung et al. [267] and Leipertz and Fröba [268]. Using mathematical manipulations and fundamental relations, the $G^{(2)}(\tau)$ obtained from light scattering experiments can be shown to provide access to the CF of the observed fluctuations. Considering the intensity of scattered light and the LO, Equation 4.32 becomes for a single diffusive process related to a single type of fluctuations

$$G^{(2)}(\tau) = \left(I_S + I_{LO} \right)^2 + I_S^2 \left| g_q(\tau) \right|^2 + 2 I_S I_{LO} g_q(\tau), \tag{4.35}$$

where I_S, I_{LO}, and $g_q(\tau)$ are the time average of the scattered light intensity, the time average of the LO intensity, and normalized CF of the hydrodynamic fluctuations observed, respectively. The hydrodynamic fluctuations can be obtained by using the linearized hydrodynamic equations and applying a Fourier–Laplace analysis [96] as mentioned previously.

Since the power spectral density and ACF are Fourier-transformed pairs, the individual Lorentzian lines according to Equation 4.31 are transformed

into simply exponentially decaying functions in the time domain. Each function exhibits a characteristic decay time τ_C, also known as the relaxation time or mean lifetime of the fluctuations. Consequently, the normalized time CF for a single diffusive process can be expressed as

$$g_q(\tau) = \exp(-\tau/\tau_C). \tag{4.36}$$

The analysis in the time domain is particularly advantageous for studying relatively slow diffusive processes between about (10^{-14} and 10^{-6}) $m^2 \cdot s^{-1}$, such as those found in many liquid but also gaseous systems. This is because the narrower the spectral broadening, the larger the value of τ_C. If the diffusivities are in the range of 10^{-5} $m^2 \cdot s^{-1}$ or more, such as in low-density gaseous mixtures, the spectral broadening increases significantly. This can result in a decay time that is too small to accurately determine diffusivities. In such cases, analysis in the frequency domain can be a better choice. Considering Equation 4.35, the idealized second-order CF for a single diffusive process and where light scattered from the sample and a LO field are present takes the form of

$$G^{(2)}(\tau) = (I_S + I_{LO})^2 + I_S^2 \exp(-2\tau/\tau_C) + 2I_S I_{LO} \exp(-\tau/\tau_C). \tag{4.37}$$

Equation 4.37 is composed of three terms. The first term represents the static part of the CF. The second term, known as the homodyne term, describes the signal from purely scattered light from the sample. The last term represents the signal of scattered light multiplied by an additional contribution from stray or reference light, called the heterodyne term. Extracting reliable information from a sum of two exponentials with similar time constants is exceedingly difficult Thus, the experimenter has to realize a situation where one of the exponentials clearly dominates, that is, where $I_S >> I_{LO}$ (homodyne) or where $I_S << I_{LO}$ (heterodyne). Establishing homodyne conditions for studying molecular fluctuations can be challenging, if not impossible. This is due to the significantly weaker magnitude of the scattered light from the molecular inhomogenities compared to the imperfections in the optical path or stray light from the windows of the sample cell (SaCe), dust on other optical components, or any particle-like impurities present in the SaCe. Thus, the defined heterodyne conditions are the experimenter's choice when studying diffusion in molecular systems. Heterodyne conditions can be realized by superimposing direct coherent laser light with scattered light onto the detector or by intentionally using stray light from the SaCe windows. The heterodyne technique has the additional advantage that the field of the LO acts as an amplifier, as presented in Equation 4.37. Normalized to its value for $\tau \to \infty$, the idealized

normalized second-order CF for a single diffusive process obtained under heterodyne condition takes the form of

$$g^{(2)}(\tau) = 1 + \frac{2I_S}{I_{LO}} \exp(-\tau/\tau_C). \tag{4.38}$$

Here, $\tau_C = (D \cdot q^2)^{-1}$ is related to the diffusion constant D that can be identified by thermal diffusivity a, the mutual or Fick diffusion coefficient D_{11}, or the particle diffusion coefficient, which is not considered in this thesis. In a realistic experiment, effects caused by the imperfect signal collection occur [268]. Therefore, fit parameters are introduced in practice, and the normalized intensity CF takes the form of

$$g^{(2)}(\tau) = b_o + b \exp(-\tau/\tau_C), \tag{4.39}$$

where b_o accounts for a shift in the baseline and b is the amplitude of the exponential. Equation 4.39 is used in the experimental evaluation of pure fluids and binary mixtures where the experimental CF is governed by only one relaxation process. Generally, the two relaxation processes that can be found in binary mixtures give rise to a second exponential. Thus, the normalized intensity CF related to the Rayleigh component and recorded in a heterodyne detection scheme, wherein considerably stronger reference light is coherently superimposed with the scattered light from the sample, takes the form

$$g^{(2)}(\tau) = b_o + b_t \exp(-\tau/\tau_{C,t}) + b_c \exp(-\tau/\tau_{C,c}). \tag{4.40}$$

Here, b_o, b_t, and b_c are the experimental constants defined by the characteristics of the experimental setup, the thermodynamic state, and the ratio of the intensities of the scattered light to that of the reference light. Furthermore, b_t, and b_c are the amplitudes of the exponentials related to T and c fluctuations. The decay times $\tau_{C,t}$ and $\tau_{C,c}$, which are equivalent to the mean lifetimes of the observed microscopic T and c fluctuations, are related to a and D_{11} by

$$a = (\tau_{C,t} q^2)^{-1} \text{ and } D_{11} = (\tau_{C,c} q^2)^{-1}. \tag{4.41}$$

Generally, situations can occur where either $\tau_{C,t} << \tau_{C,c}$, $\tau_{C,t} >> \tau_{C,c}$, or $\tau_{C,t} \approx \tau_{C,c}$. Thus, as previously mentioned in relation to the discussion on Figure 4.1(b), importantly, it is not immediately clear which type of fluctuation is related to which of the two exponential functions.

The theory discussed above is applicable to most experimental cases related to pure fluids or binary mixtures. However, as reported by Anisimov et al.

[124] and Fröba et al. [123], the situation becomes more complex when mode coupling cannot be neglected, that is, where k_T does not tend toward zero. In such cases, neither a nor D_{11}, but two effective diffusivities are obtained according to the hydrodynamic fluctuation theory as

$$D_{\mathrm{eff},\{1,2\}} = \frac{1}{2}\left\{\left[a + D_{11}\left(1+\kappa\right)\right] \mp \sqrt{\left[a + D_{11}\left(1+\kappa\right)\right]^2 - 4aD_{11}}\right\} \qquad (4.42)$$

and the strength of the coupling between heat and mass transfer is described by the coupling parameter

$$\kappa = \frac{k_T^2}{Tc_p}\left(\frac{\partial \mu}{\partial c}\right)_{p,T} = c^2\left(1-c\right)^2 T \frac{S_T^2}{c_p}\left(\frac{\partial c}{\partial \mu}\right)_{p,T}^{-1}, \qquad (4.43)$$

where the Soret coefficient $S_T = D_T \cdot D_{11}^{-1}$.

For low-molecular weight multicomponent mixtures with n_c components, the scattered-light intensity is governed by fluctuations in T related to a, as well as $n_c - 1$ individual contributions from c fluctuations related to the eigenvalues of the Fick diffusion matrix. For ternary non-electrolyte fluid mixtures, the scattered light spectrum can be derived from Fick's second law [158,269] and the differential equation for the T field [103]. Assuming that coupling between the T and c fluctuations can be neglected, an expression for the eigenvalues of the 2 × 2 Fick diffusion matrix can be given by [103]

$$\hat{D}_{1,2} = \frac{1}{2}\left[D_{11} + D_{22} \pm \sqrt{\left(D_{11} - D_{22}\right)^2 + 4D_{12}D_{21}}\right], \qquad (4.44)$$

where D_{ij}, with i and j = 1 or 2, are the components of the Fick diffusion matrix. The normalized intensity CF for ternary fluid mixtures comprises a superposition of three exponentials according to

$$g^{(2)}\left(\tau\right) = b_o + b_t \exp\left(-\tau/\tau_{C,t}\right) + b_{c,1}\exp\left(-\tau/\tau_{C,c,1}\right) + b_{c,2}\exp\left(-\tau/\tau_{C,c,2}\right), \qquad (4.45)$$

where the relaxation times $\tau_{C,t}$, $\tau_{C,c,1}$, and $\tau_{C,c,2}$ are related to a, $\hat{D}_1$, and $\hat{D}_2$ in the same manner as expressed by Equation 4.41. Although the above theory is generally valid, Bardow [130] presented additional theoretical considerations. He demonstrated that in some cases only one mass diffusive mode might be resolvable in DLS experiments on ternary mixtures due to the relatively weak scattering from the c fluctuations associated with the

second mass diffusive mode. More details on the theory of DLS for ternary fluid mixtures can be found in the doctoral thesis of Heller [245].

4.3 Calculation of the Rayleigh Ratio

The amplitudes of the signals obtained for a binary mixture typically cannot be determined experimentally in an absolute manner due to unknown experimental constants. However, the Rayleigh ratio $\mathcal{R}$, also known as the Rayleigh factor ratio, which represents the ratio of signal amplitudes b_c and b_t or I_c and I_t related to the c and T fluctuations, can be determined experimentally. When $\mathcal{R}$ is greater than one, the larger amplitude signal in the CF is associated with c fluctuations, whereas the smaller amplitude signal is associated with T fluctuations. Conversely, when $\mathcal{R}$ is less than one, the larger amplitude signal is associated with T fluctuations, and the smaller amplitude signal is associated with c fluctuations.

The Rayleigh ratio was established by DuBois and Bergé [154], and is defined as [154,262]

$$\mathcal{R} = \frac{I_c}{I_t} = \frac{b_c}{b_t} = \frac{c_p}{T}\left(\frac{\partial c}{\partial \mu}\right)_{p,T} \frac{\left(\frac{\partial n_{\text{fluid}}}{\partial c}\right)^2_{p,T}}{\left(\frac{\partial n_{\text{fluid}}}{\partial T}\right)^2_{p,c}}. \tag{4.46}$$

Here, the optical contrast factors, $(\partial n_{\text{fluid}}/\partial T)_{p,c}$ and $(\partial n_{\text{fluid}}/\partial c)_{p,T}$, can be computed using the following well-established analytical expressions [270–272]

$$\left(\frac{\partial n_{\text{fluid}}}{\partial T}\right)_{p,c} = \frac{\left(n^2_{\text{fluid}}-1\right)\left(n^2_{\text{fluid}}+2\right)}{6n_{\text{fluid}}}\frac{1}{\rho}\frac{\partial \rho}{\partial T} = \frac{\left(n^2_{\text{fluid}}-1\right)\left(n^2_{\text{fluid}}+2\right)}{6n_{\text{fluid}}}\beta_T \tag{4.47}$$

and

$$\left(\frac{\partial n_{\text{fluid}}}{\partial c}\right)_{p,T} = \frac{\left(n^2_{\text{fluid}}-1\right)\left(n^2_{\text{fluid}}+2\right)}{6n_{\text{fluid}}}\left(\frac{1}{\rho}\left(\frac{\partial \rho}{\partial c}\right)_{T,p} + \frac{\frac{\alpha_{e,1}}{M_1}-\frac{\alpha_{e,2}}{M_2}}{\frac{c\alpha_{e,1}}{M_1}-\frac{(1-c)\alpha_{e,2}}{M_2}}\right), \tag{4.48}$$

where the term

$$\frac{1}{\rho}\left(\frac{\partial \rho}{\partial c}\right)_{T,p} = \beta_S \tag{4.49}$$

is also known as the solutal expansion coefficient. The refractive index of the binary mixture can be estimated using the Lorentz–Lorenz equation [273] combined with a linear mixing rule by applying a simple mass-weighting scheme [272,274]

$$\frac{n_{\text{fluid}}^2 - 1}{n_{\text{fluid}}^2 + 2} = \frac{N_\text{a}}{3\varepsilon_\text{o}} \rho \left(\frac{c\alpha_{\text{e},1}}{M_1} + \frac{(1-c)\alpha_{\text{e},2}}{M_2} \right). \tag{4.50}$$

In Equations 4.47 to 4.50, N_a is the Avogadro constant; ε_o denotes the permittivity of free space; ρ represents the density of the mixture; and $\alpha_{\text{e},i}$ and M_i are the average molecular polarizability and molar mass of the component i. According to Equation 4.46, a decrease in c_p and osmotic compressibility, as well as an increase in T, will result in a decrease in $\mathcal{R}$ to some extent.

Accurately calculating $\mathcal{R}$ requires relatively precise knowledge of the input quantities mentioned above, which can be a challenging task. Some optical contrast factors can be found in the literature for some systems and thermodynamic states, e.g., in Refs. [271,272], whereas others must be calculated. The $\alpha_{\text{e},i}$ values derived through experiments or theoretical methods can be obtained from the literature, see, e.g., [272,275,276]. Calculations performed as part of this thesis revealed that the parameter $\alpha_{\text{e},i}$ has a significant influence on $\mathcal{R}$ and, therefore, must be chosen carefully. Mixture properties, such as ρ, c_p, and μ, can be obtained from the literature or estimated using an EoS like the GERG-2008 EoS [277] or volume-translated Peng–Robinson (VT-PR) EoS [278]. The REFPROP database [279] is a very useful tool in this regard. Values for β_T and β_S, the partial derivatives of ρ contained in β_T and β_S, and osmotic compressibility $(\partial c/\partial \mu)_{p,T}$ are scarcely available in existing literature. However, the partial derivatives of ρ and osmotic compressibility can be determined through the mass fraction or T dependencies of μ and ρ around the experimental T and composition using a first- or second-order polynomial [265,280]. Furthermore, mathematical expressions or an EOS can help calculate osmotic compressibility [123,154]. However, the applicability of such approaches must be evaluated for each specific situation. Determining reliable values for osmotic compressibility was the most difficult part of the $\mathcal{R}$ calculations performed for this thesis.

4.4 Setup and Experiment

For this thesis, several experimental setups were developed and applied to achieve its aims. These setups are described in detail in the corresponding publications [264,280–282]. However, the essential components, basic optical and electronic arrangements, and approach for maintaining macroscopic thermodynamic equilibrium will be briefly discussed.

Figure 4.2 depicts the optical and electronic arrangement of a DLS apparatus for the analysis of scattered light at small Θ_S between (3 and 12)° as well as at $\Theta_S = 90°$. A single-mode continuous wave laser with a wavelength of, for instance, $\lambda_0 = 532$ nm was directed into the SaCe using a set of mirrors to generate scattered light. In addition to true single mode operation with sufficient coherence length, also stable output power, low RMS noise, defined linear polarization, excellent beam quality, and pointing stability are important laser properties when aiming for an accurate determination of diffusivities via DLS. The incident angle Θ_I was set at M2 for small scattering angles, whereas for large scattering angles (that is, $\Theta_S = 90°$), M2 was removed. The detection direction of the scattered light was determined by using two apertures (A), one positioned behind the SaCe and one in front of the detection unit. The detection unit comprised two PMTs that were operated in a pseudo-cross correlation scheme to suppress after pulsing and dead-time effects. The PMT pulses were discriminated, amplified, and then directed to two different digital correlators. A heterodyne detection scheme was realized by using either an external reference beam, which was separated from the main beam by a beam splitter (BS) or by using the window flares. To adjust intensity and polarization, combinations of lambda-half wave plates ($\lambda/2$) and polarization beam splitters (PBS) located in both the main and reference beam paths were used. A neutral density filter (ND) and linear grey filter (GF) were inserted into the path of the reference beam for further intensity attenuation.

Although not the focus of this thesis, most of the setups used herein allowed for Raman scattering experiments in addition to DLS. This enabled the sample characteristics and composition to be analyzed. Raman scattered light was detected either at a 90° angle or via a backscattering scheme using a dichroic mirror (DM). For more information, please refer to the publications related to this thesis [264,265,280–292].

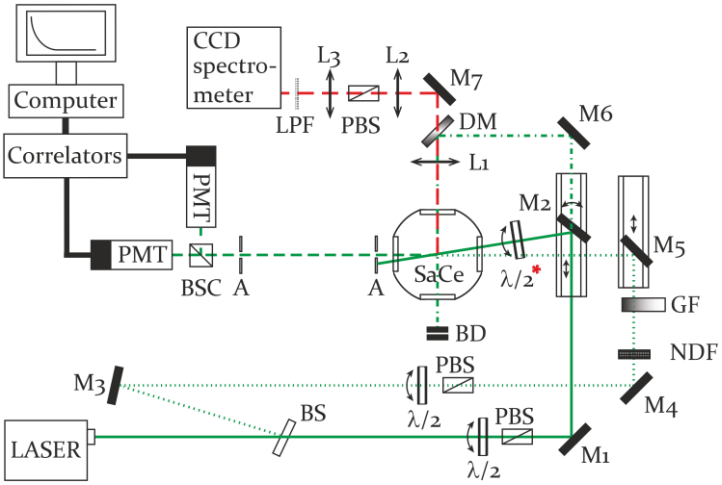

Figure 4.2: Optical and electronic arrangement of a typical setup for DLS and Raman spectroscopy experiments. The components include mirror (M), lens (L), beam splitter (BS), beam splitter cube (BSC), dichroic mirror (DM), lambda-half wave plate (λ/2), polarization beam splitter (PBS), neutral density filter (ND), linear grey filter (GF), aperture (A), photomultiplier tube (PMT), and sample cell (SaCe). λ/2* is only inserted in the beam path for Raman spectroscopy experiments and allows the polarization of the incident laser light to be adjusted. The green solid and dashed-dotted lines represent the main beam, which generates the scattered light, at small or large scattering angles, respectively. The green dotted and dashed lines denote the reference beam or LO and the detection beam path of the scattered light, respectively, for the DLS experiments. The red dashed line indicates the detection beam path for the Raman spectroscopy experiments under 90°.

This thesis utilized two types of digital correlators with different evaluation schemes. The LTC had 2048 equally spaced correlation channels. The complete time range analyzed was manually fixed by adjusting the sampling time, that is, the time interval between individual channels. The MTC had 263 channels with a static and quasi-logarithmic time structure. The LTC was used to resolve specific signals with the highest possible temporal resolution whereas the MTC was additionally used to identify signals at different time scales. To evaluate the correlation data obtained by the MTC, a weighting scheme had to be applied. The simultaneous utilization of LTC and MTC enhanced the statistical analysis. The time range for acquiring CFs was adjusted based on the expected decay times. As a general rule, the observed time interval, also known as lag-time, should be adjusted between $7 \cdot \tau_C$ and $10 \cdot \tau_C$ of the largest decay time observed. Therefore, selecting appropriate Θ_I or Θ_S for each system and thermodynamic state is also necessary. If long-term disturbances are observed in the experimental CF, selecting even larger time intervals might be preferable to accurately describe

them. Due to the direct relationship between sampling time and integration time, it is preferable to tune Θ_S to use rather higher sampling times. This often allows for an improved SNR with a shorter experimental time. However, sampling times exceeding 2.5 µs should not be used because long-term artifacts of the correlators can appear. If high sampling times are required, the application of a random input scaler may be helpful.

Maintaining macroscopic thermodynamic equilibrium is a crucial prerequisite for studying transport properties via DLS. Therefore, regulating T and p to maintain the fluid sample in the desired equilibrium state is a significant challenge, particularly when the system is processed under conditions far from ambient. In this thesis, the T of the SaCe was measured using an AC bridge and at least two Pt100 resistance probes. The probes were calibrated with an absolute expanded uncertainty (k = 2) of either (20 or 15) mK. The Pt100 resistance probe, located in the cell wall near the resistance heating element, was used to establish the T control loop. To measure T of the fluid, a second resistance probe was placed inside the cell material close to the fluid. The p was measured by using calibrated pressure transducers with absolute expanded uncertainties (k = 2) of either (0.015 or 0.002) MPa. In certain instances, the p was regulated indirectly by utilizing an additional heating loop. To allow more than two T probes to be used in conjunction with a two-channel millikelvin thermometer, a four-wire test point switch was developed. This device, known as a stepper, facilitated the management of multiple four-wire T probes, which could be probed sequentially on a single measurement channel. As a special feature, this device included an adjustable constant current source for each channel. This source was used to imitate the self-heating property of the resistance probes induced by power dissipation of the applied measurement current. The experimental procedures varied among the different studies, and corresponding information is provided in the respective publications. For each thermodynamic state at macroscopic thermodynamic equilibrium, six individual measurements were typically taken at different Θ_S. This approach is in agreement with that suggested by Kruppa et al. [197] and Pitschmann and Straub [200] and should allow for a reliable estimation of the uncertainties of the diffusivities. For each experiment, the pseudo-cross CFs were calculated simultaneously using the two correlators.

4.5 Signal Evaluation and Limiting Factors

This section presents the general data evaluation scheme, which, in addition to thorough sample preparation and experimentation, is essential for obtaining reliable results. Thereafter, the limiting factors for simultaneously determining a and D_{11} will be evaluated, with strategies presented for attributing the obtained signals for different experimental situations.

4.5.1 General Data Evaluation

The CF data obtained from the DLS experiments were analyzed using nonlinear regression software based on the Levenberg–Marquardt algorithm, which was developed by Heller [245] for this specific purpose. Under ideal experimental conditions, the fit model was obtained either by using Equation 4.39, 4.40, or 4.45, depending on the number of exponential contributions expected or resolved. In a realistic experiment, the obtained signals are often superimposed with additional disturbing signals. These disturbances must be considered to accurately determine the experimental constants and mean lifetimes. Such signals may originate, for instance, from particulate-like impurities, vibrations, or incoherent external light. For a binary mixture, the CF is expected to comprise a sum of two exponentially decaying functions that reflect the mean lifetimes of T and c fluctuations. The corresponding fit model accounting for the disturbing signals can be expressed as

$$g^{(2)}(\tau) = b_o + b_t \exp\left(-\tau/\tau_{C,t}\right) + b_c \exp\left(-\tau/\tau_{C,c}\right) + \Xi(\tau). \qquad (4.51)$$

The researcher must select the mathematical description of the disturbance term, denoted by $\Xi(\tau)$, based on their knowledge of the physical cause or origin of the observed disturbance. This step is crucial because the researcher's selection may significantly alter the obtained parameters for strongly non-ideal signals. This is clearly a weak point in the DLS technique. In principle, $\Xi(\tau)$ can be any arbitrary function. Yet, most common linear or second-order polynomial terms are selected to account for disturbing signals if necessary. Notably, the inclusion of a linear or quadratic term into the fit will result in slightly smaller or larger decay times than that of the hypothetical fit without a disturbance term. This is especially true if $\mathcal{R}$ is either considerably small or large. Therefore, a combination of linear and quadratic terms may be appropriate for an accurate evaluation of the experimental CFs. However, this is only valid when the SNR is relatively high because the introduction of additional fit parameters will

increase the fit uncertainty. If the SNR is relatively low, incorrect diffusivity results may be obtained due to the increased number of degrees of freedom. Heller [245] provided a more in-depth discussion on fit-related topics, which will not be reiterated here. In general, the fit is considered appropriate only if the residuals, that is, the differences between the experimental data and corresponding fit, do not exhibit any systematic deviations in the time ranges of the signals of interest. In some cases, the disturbances were too complex to be described by simple functions, making it impossible to provide a reliable fit; thus, the corresponding CFs were dismissed. In such cases, the experimental conditions were modified, where possible, to obtain a clearer CF signal without disturbances. For each system investigated, the obtained signals in the CFs were found to be related to the hydrodynamic modes, and the underlying working equations were valid. This investigation was conducted by varying Θ_S to determine whether the inverse of the mean lifetimes of the fluctuations studied were proportional to q^2, which is applicable in the hydrodynamic regime.

Figure 4.3(a) presents a typical experimental normalized CF recorded via LTC. The CF was obtained in the compressed liquid phase of an equimolar CH_4–C_3H_8 mixture at T = 283.17 K, p = 12.000 MPa, and Θ_I = 4.00°.

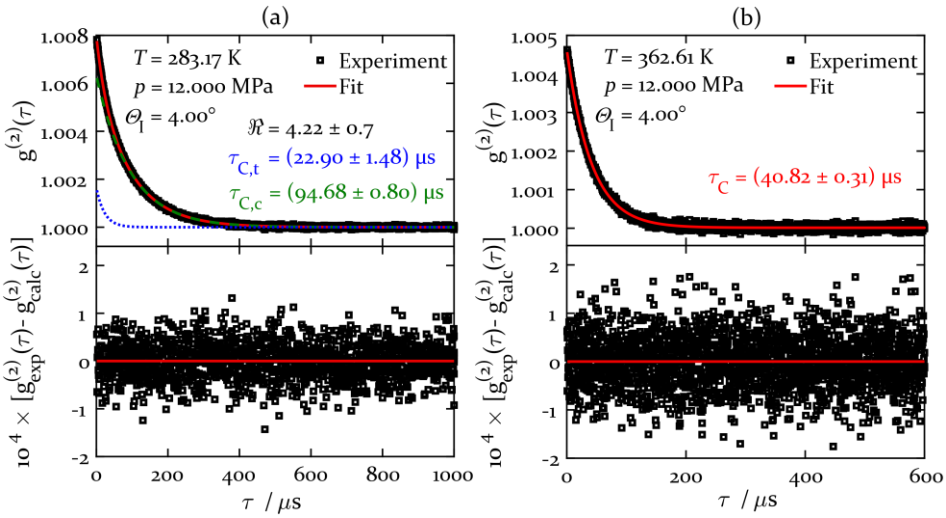

Figure 4.3: Fit to CFs (upper parts) and residuals from the fit to CFs (lower parts) recorded via LTC for an equimolar CH_4–C_3H_8 mixture at T = 283.17 K, p = 12.000 MPa, and Θ_I = 4.00° (a) as well as at T = 362.61 K, p = 12.000 MPa, and Θ_I = 4.00° (b).

The correlator data and global fit according to Equation 4.40 are denoted by squares and a red solid line. The blue dotted and green dashed lines in Figure 4.3(a) indicate the two individual exponential contributions related to the *T* and *c* fluctuations. The residuals of the measured data from the fits to the CF, which are shown in the lower part of the figure, confirm that the signal can be expressed by the sum of two exponentials and are free of systematic deviations. Assuming that the decay times, $\tau_{C,t}$ and $\tau_{C,c}$, are related to *T* and *c* fluctuations, the experimental Rayleigh ratio of $\mathcal{R} = 4.22$ can be obtained. The top section of Figure 4.3(b) highlights a normalized CF for the same equimolar CH_4–C_3H_8 mixture at the same *p* and Θ_1 as that for Figure 4.3(a), with only *T* changed to $T = 362.61$ K. The respective fit residuals illustrated in the lower part of Figure 4.3(b) reveal that only one hydrodynamic mode is resolvable in the experimental CF, and the correlator data can be represented by Equation 4.39. There are several reasons why only one hydrodynamic mode might be resolvable for binary mixtures in the DLS experiment; these will be discussed in the next section.

The final diffusivity data were determined by averaging the results from typically 12 independent CFs obtained via the DLS experiments using the LTC and MTC. A weighting scheme based on the inverse relative uncertainties of the individual diffusivity data was applied that considered the statistical uncertainty of the correlator data, along with uncertainty regarding the Θ_1 or Θ_S measurement. This scheme is described in Ref. [285]. The experimental uncertainties reported in the publications and associated error bars shown in the figures have a confidence level of 0.95 ($k = 2$). The reported *T* and *p* are mean values obtained from data recorded for a complete DLS measurement series performed in the corresponding thermodynamic state.

4.5.2 Limits to the Simultaneous Determination of Thermal and Mutual Diffusivities

Whether or not two contributions related to pure *T* and *c* fluctuations and, thus, *a* and mutual diffusivities can be simultaneously resolved experimentally in a binary mixture via DLS depends mainly on five factors: (1) possible coupling of hydrodynamic modes, (2) Lewis number $Le = a \cdot D_{11}^{-1}$, (3) Rayleigh ratio $\mathcal{R}$, (4) SNR, and to a certain extent (5) the strength of disturbances in the CFs. Although under real experimental conditions, these influencing factors occur in tandem, for improved structure and readability, they will be discussed separately as follows.

Influence of Mode Coupling

The influence of mode coupling is straightforward. Equation 4.42 provides two effective diffusivities that can be obtained for binary mixtures when mode coupling is present. If mode coupling is eliminated, the simultaneous determination of both a and D_{11} is theoretically possible. However, the input quantities required to calculate the mode coupling parameter κ, as specified in Equation 4.43, are not widely available in the literature. This factor combined with the specified uncertainties in the input parameters often make a comprehensive evaluation impossible. However, by considering the reported general behavior of the diffusivities and properties that influence κ, such as S_T, c_p, and $(\partial c/\partial \mu)$, and considering theoretical studies [124], general guidelines can be established for binary mixtures [265]. In the liquid state far from the plait critical point, a is at least one order of magnitude larger than D_{11} and κ tends toward 0. Consequently, the two hydrodynamic modes are on different time scales and can be associated with a and D_{11}. In the gas state far from the plait critical point and dew point line, a and D_{11} have the same order of magnitude and κ tends toward 0. Typically, a and D_{11} do not differ by more than a factor of 2; thus, the two hydrodynamic modes appear on the same time scale. In the vicinity of the plait critical point of a binary mixture, D_{11} vanishes, a is nearly constant, S_T and $(\partial c/\partial \mu)$ diverge, and c_p remains constant [254,293]. In the near-critical region along the critical isochore, there is a temperature $T > T_c$, for which Le is unity. The smaller the c of the solute, the larger the influence of the mode coupling parameter κ and the closer this temperature is to T_c [124,294]. As a criterion, mode coupling is non-negligible until Le is considerably larger than κ. In general, the divergence of κ approaching T_c is weaker than the divergence of Le [124].

Influence of Le, $\mathcal{R}$, and SNR

Various theoretical scenarios are constructed as examples to evaluate the effect of different mutual influencing factors on the simultaneous determination of a and D_{11} in binary mixtures. For this evaluation, Le, $\mathcal{R}$, and noise level, that is, SNR, were fixed, and a mock-up CF for a binary mixture based on Equation 4.51 was first constructed and then fitted using nonlinear regression based on the Levenberg–Marquardt algorithm. All cases discussed herein assume that the coupling of hydrodynamic modes can be neglected. The number of artificial correlator channels was fixed at 2048, and the channel spacing was constant to simulate a signal obtained using LTC. For

signal construction, the term $\Xi(\tau)$ was set to zero. The decay times reported for the initial conditions were obtained by fitting the constructed CFs. Thereafter, noise was incorporated in the form of normally distributed (Gaussian) random numbers, and the signal was fitted with a DEF or SEF. The noise level was adjusted to obtain a SNR of approximately 50, and the initial fit parameters were assumed to be appropriately chosen. For the fitting, $\Xi(\tau)$ was set to a linear term; this is a common practice in many experiments. In Figures 4.4–4.7, the data points are indicated by black squares, the global fit by a red solid line, and the two individual fit contributions represented by green dashed and blue dotted lines. The corresponding decay times, indicated using the same color-code, and the obtained $\mathcal{R}$ from the fit is reported. To obtain $\mathcal{R}$, the contribution indicated by the green dashed line and the associated decay time $\tau_{C,1}$ is assumed to be related to c fluctuations, whereas $\tau_{C,2}$ is related to T fluctuations. The corresponding fit residuals (res) are shown below the respective CFs and were calculated in the same manner as indicated in the y-axis label of Figure 4.3.

First, the influence of *Le* was investigated, starting with an ideal case scenario where *Le* = 30, $\mathcal{R}$ = 1, and no long-term disturbance exists. Figure 4.4(a) depicts the constructed CF without noise, whereas Figures 4.4(b) and 4.4(c) highlight the DEF and SEF of the noisy signal. The fit residuals indicate that DEF represents the signal well, and the decay times can be reproduced within fit uncertainties. However, smaller values are observed in comparison to the initial decay times. This is a typical behavior that results from using a linear term to describe a long-term disturbance (which is not even present in this case). This behavior is enhanced in this example because the lag-time selected was less than 7 to 10 times the largest decay time. Therefore, some information on the baseline is missing. The systematic deviations observable in the fit residuals indicate that SEF is unable to represent the signal. Figures 4.4(d)–(f) and 4.4(g)–(i) highlight cases where $\mathcal{R}$ remains 1 but *Le* is either (1.5 or 0.6), respectively. The decay times of the initial conditions without noise could be reconstructed through fitting, indicating that in the (unrealistic) case where no noise is present, two exponentials can be resolved despite *Le* being close to unity. For a SNR of about 50, SEF appears to be adequate for both *Le* = (1.5 and 0.6) because no clear systematic deviations are observable in the fit residuals. In both cases, the decay time obtained through SEF was similar to the average of the two initial decay times. The situation regarding DEF is ambiguous. Although the decay times obtained through fitting corresponded with the initial conditions when considering the fit uncertainties, the uncertainties are large. When fitting is executed multiple times (with different initial values),

different decay times are consistently found. In addition, the value of $\mathcal{R}$ obtained through fitting is erroneous. Evidently, a researcher is responsible for obtaining reproducible results. Therefore, DEF cannot be used in the accurate evaluation of these discussed cases.

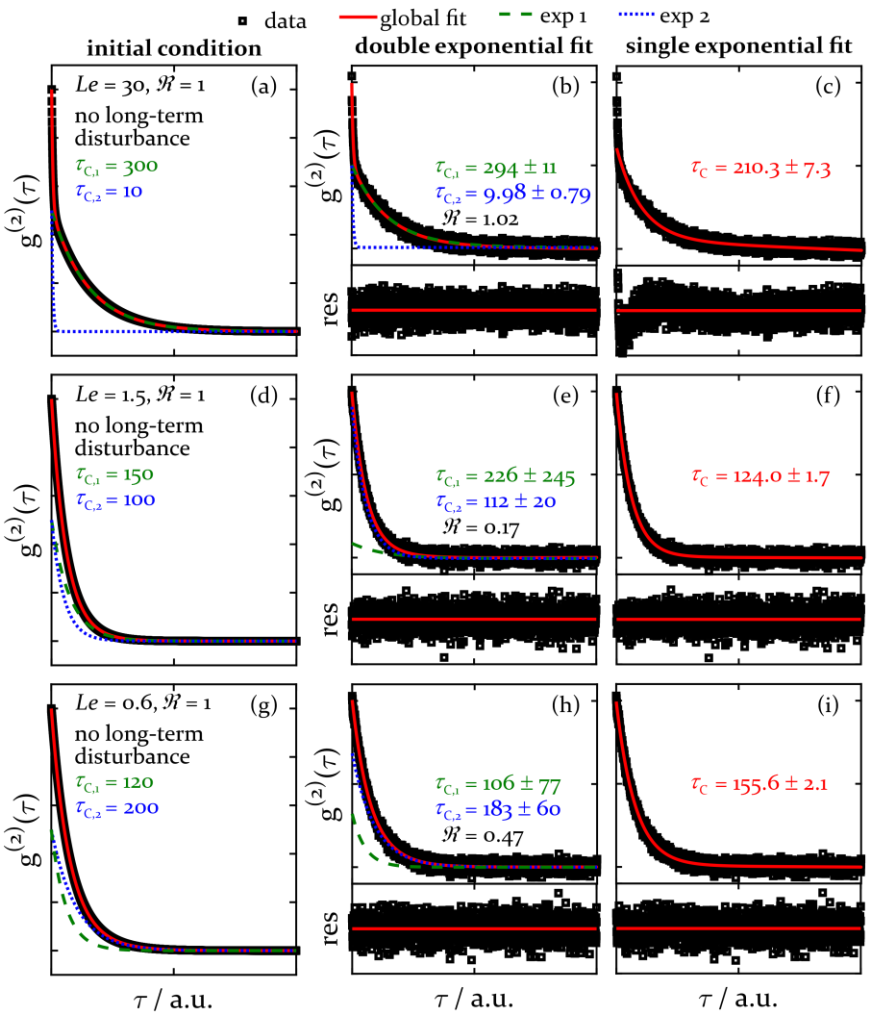

Figure 4.4: Variation of *Le*. (a), (d), and (g) mock-up CF for a binary mixture based on Equation 4.51 under various conditions. (b), (e), and (h) DEFs of the noisy signals and fit residuals. (c), (f), and (i) SEFs of the noisy signals and fit residuals.

Second, the value of $\mathcal{R}$ was varied. Figures 4.5(a)–(c) and 4.5(d)–(f) demonstrate the initial cases where *Le* = 30, no long-term disturbances exist, and

$\mathcal{R}$ is either (9 or 0.1), respectively. In both cases, DEF resulted in decay times that were close to the initial values, as expected. The relative uncertainties in the decay times were larger for the signal with the smaller amplitude. Interestingly, in both cases, the decay time obtained from the fit was overestimated for the signal with the smaller amplitude and underestimated for the signal with the larger amplitude. The $\mathcal{R}$ value obtained from the fitting is in relatively good agreement with the initial conditions. As anticipated, SEF was unable to accurately represent the data, as evidenced by the fit residuals, and the single obtained decay time was relatively close to that of the signal with the larger amplitude. However, for an increase in the level of noise or increase/decrease of $\mathcal{R}$, a fit with a single exponential can be appropriate based on the fit residual evaluation. In this case, the farther $\mathcal{R}$ is from unity, the closer the single obtainable contribution will be to either a or D_{11}.

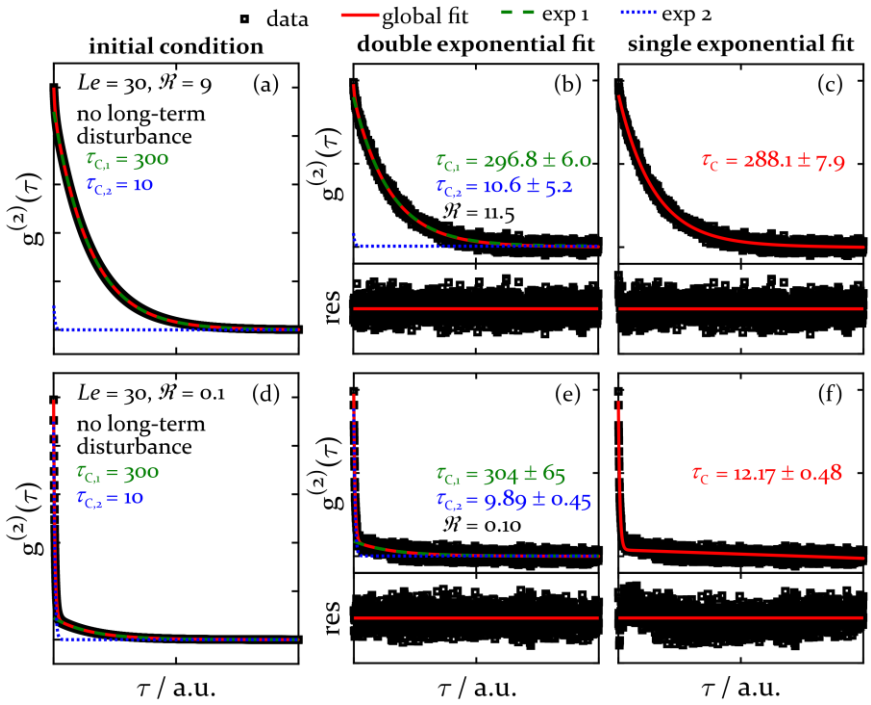

Figure 4.5: Variation of $\mathcal{R}$. (a) and (d) mock-up CF for a binary mixture based on Equation 4.51 under various conditions. (b) and (e) DEFs of the noisy signals and fit residuals. (c) and (f) SEFs of the noisy signals and fit residuals.

Figures 4.6(a)–(i) illustrate the cases wherein $\mathcal{R}$ = 0.1 and *Le* is either (10, 3, or 1.5). When *Le* = 10, the situation is similar to that of *Le* = 30, as shown in Figures 4.5(d)–(f). However, when *Le* is further reduced, as shown in Figures 4.6(d)–(i) where *Le* is either (3 or 1.5), the fit residuals of DEF and SEF are almost identical.

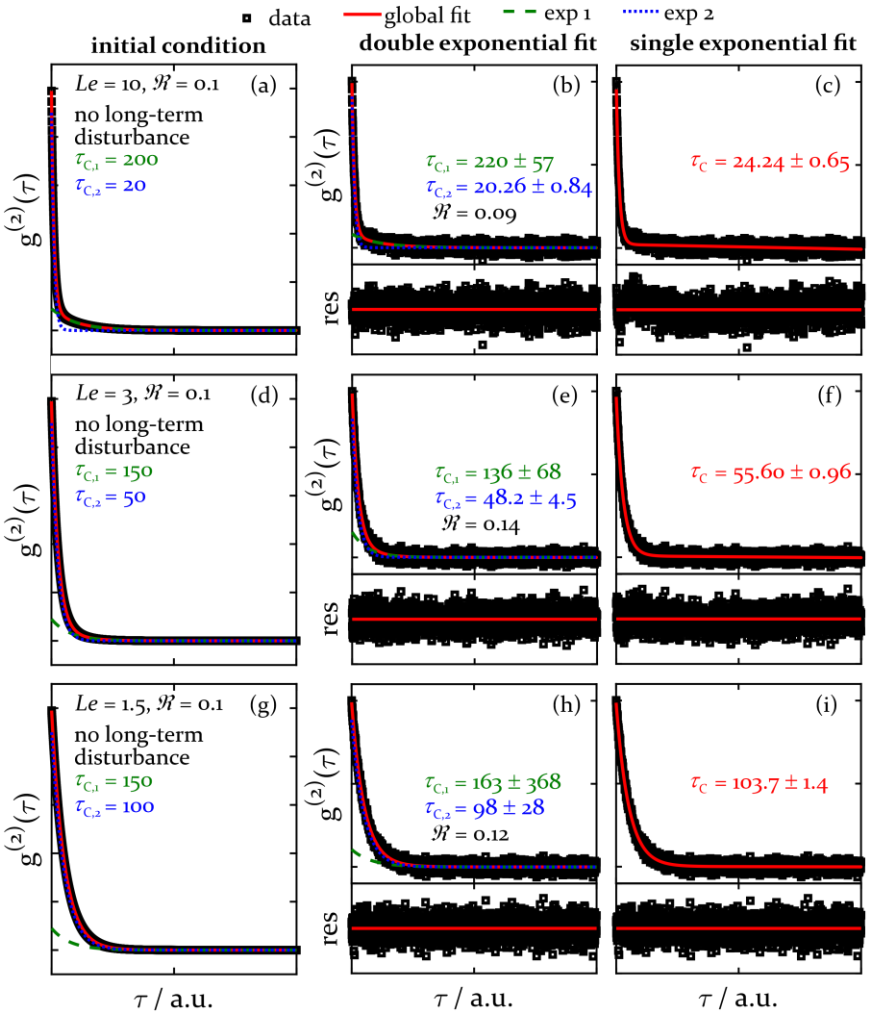

Figure 4.6: Variation of *Le* and $\mathcal{R}$. (a), (d), and (g) mock-up CF for a binary mixture based on Equation 4.51 under various conditions. (b), (e), and (h) DEFs of the noisy signals and fit residuals. (c), (f), and (i) SEFs of the noisy signals and fit residuals.

The experimental situations shown in Figures 4.6(d)–(i) is a challenge for researchers, as they must decide whether to perform a fit with one or two exponentials. Although SEF produced smaller uncertainties in the decay time than DEF, for the scenarios presented here, the initial decay times were obtained via DEF despite the large uncertainties. For DEF, larger fit uncertainties will be acquired since *Le* approaches unity. Similar to the cases where *Le* was larger, the decay time obtained via SEF was closer to the signal contribution with a larger amplitude. To evaluate whether DEF or SEF is the correct choice, CFs must be obtained for several Θ_S to assess the stability and reproducibility of both. This may provide insight into which fit equation to use.

Two features that were not directly discussed in connection with Figures 4.4–4.6 are the influence of SNR, and the case where *Le* becomes considerably large (or extremely small). In fact, when mode coupling is excluded, SNR plays the most important role in the simultaneous determination of a and D_{11}. This is particularly evident in the cases presented above; even when $Le = 1.5$ and $\mathcal{R} = 0.1$, the two initial decay times were obtained by fitting the constructed CF in the absence of noise (see Figure 4.6(g)). Larger SNR values can be obtained by increasing the c; sampling time, which is related to the integration time; scattering volume, that is, smaller scattering angles; by investigating molecules with larger scattering cross sections; and by increasing the laser power. When increasing the laser power, the researcher must ensure that there is no laser heating present, which might induce a thermal lens effect. The limitations presented by a considerably large *Le* is not straightforward because in using MTC, two decay times can in principle be resolved on a time scale between about (1 and 10^8) μs. When using LTC, the maximum *Le* at which two contributions can still be reliably resolved again depends on $\mathcal{R}$. For different situations, studies in the literature report that a and D_{11} can be simultaneously determined for maximum *Le* values up to approximately 80 [250].

Influence of Long-Term Disturbances

So far, only signals without long-term disturbances have been considered. Such signals can typically be obtained for model systems. However, in realistic experiments, signals are usually superimposed by additional contributions. This is especially true when studying technical systems. The disturbances can be considerably weak or considerably strong. There are two main difficulties associated with the presence of long-term disturbances in the fit. First, relating the observed disturbance to a specific physical origin

and, thus, to define an (perfectly) adequate function for the term $\Xi(\tau)$ in Equation 4.51 is usually not possible. Even if the disturbance can be accurately described, the second issue is that the introduction of more fit parameters owing to the inclusion of $\Xi(\tau)$ leads to a larger degree of freedom for the fit. Therefore, the fit uncertainties will be larger, and situations may arise where certain signal contributions are incorrectly fit due to an insufficiently large SNR. To allow for a basic discussion, mock-up CFs were constructed with an additional quadratic term before adding noise, as shown in Figure 4.7. Fits were then performed with an additional quadratic term as well. Certainly, the situation here is quite simple because the initial disturbance is identical to the fit function. For Le = 10 and $\mathcal{R}$ = (1 or 0.1), as shown in Figures 4.7(a)–(c) and 4.7(d)–(f), the signal can be well represented by DEF and the obtained decay times with uncertainties match the initial ones. The SEFs provide clear systematics in the fit residuals. Here, the general behavior of the magnitude of the decay times and associated uncertainties is as discussed in the previous scenarios where no long-term contribution existed.

The case where Le = 3 and $\mathcal{R}$ = 0.1 is shown in Figures 4.7(g)–(i). According to the fit residuals, both DEF and SEF appear to be adequate. Although the decay times obtained via DEF agree with the initial values when considering the uncertainties, SEF again results in a decay time that is closer to the contribution with the larger amplitude. Comparing this situation with the case where Le = 3, $\mathcal{R}$ = 0.1, and no disturbance exists, as shown in Figures 4.6(d)–(f), the situations are extraordinarily similar. However, the decay time obtained for the CF with the long-term disturbance was slightly larger than that of the CF without the disturbance because a quadratic term was used in the fit equation (see Section 4.5.1). These results indicate that if the disturbance can be accurately described, the decay times can be reliably accessed even under such conditions. However, as noted above, the disturbances in the experiment often do not follow strict mathematical expressions. Thus, a researcher must carefully evaluate the long-term contribution when aiming for the accurate determination of diffusivities via DLS.

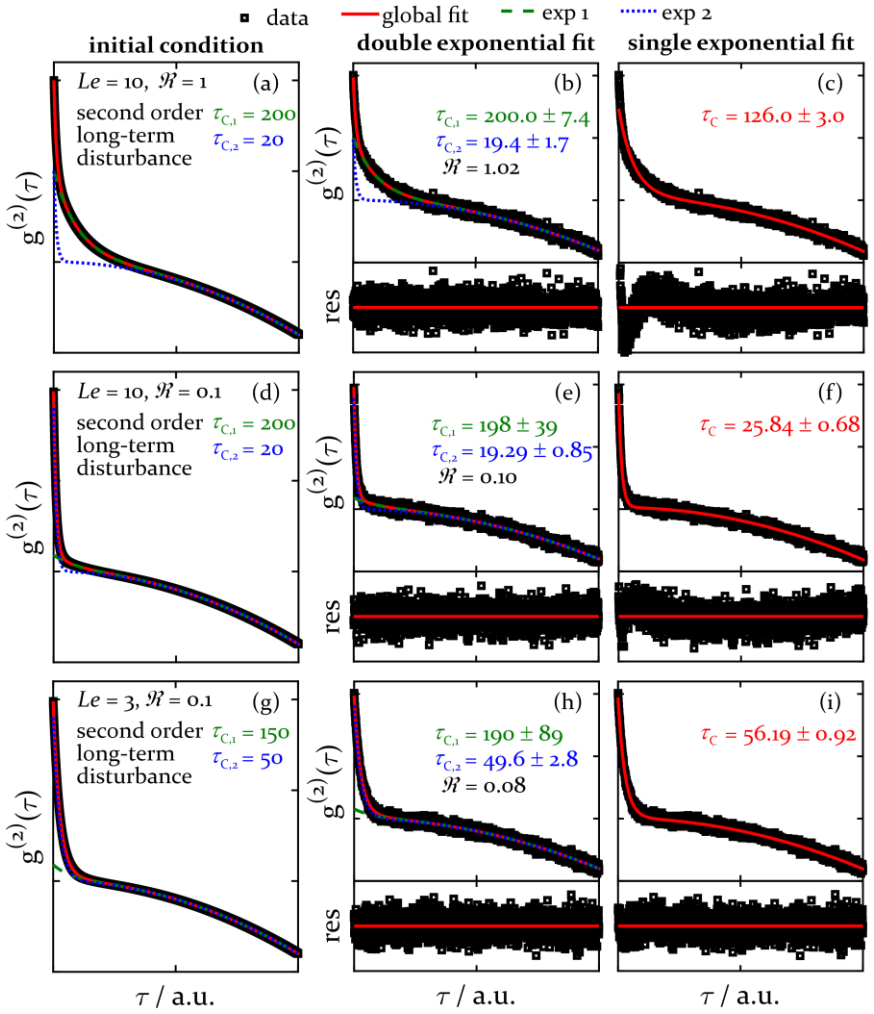

Figure 4.7: Variation of *Le*, $\mathfrak{R}$, and additional long-term disturbances in the CF. (a), (d), and (g) mock-up CF for a binary mixture based on Equation 4.51 under various conditions. (b), (e), and (h) DEFs of the noisy signals and fit residuals. (c), (f), and (i) SEFs of the noisy signals and fit residuals.

Summary

The discussed theoretical scenarios for binary mixtures clearly exhibit some limiting cases where only one signal can be resolved. However, in a real experiment, parameters *Le*, $\mathfrak{R}$, and the achievable SNR, as well as the influence of a long-term disturbance, are initially unknown and may also not be clearly evaluable. Nevertheless, based on the previous evaluation and

considering state-of-the-art technical equipment such as lasers, detectors, and correlators, some general statements can be made for binary mixtures.

A first indication of whether two contributions can be resolved is the Lewis number $Le = a \cdot D_{11}^{-1}$, which should be either greater than 1.5 or less than 0.5 to ensure a sufficient temporal separation of the two modes. For *Le* very close to unity, only one apparent diffusivity related to both transport properties, that is, a and D_{11}, can be obtained and is denoted as mixed diffusivity D_m. In addition, none of the signal amplitudes associated with the fluctuations in T, b_t, or c, b_c, should be considerably large or considerably small. In general, the closer the Rayleigh ratio $\mathcal{R} = b_c \cdot b_t^{-1}$ is to unity, the larger should the deviation of *Le* from unity be to enable detection of both contributions. When *Le* is quite close to unity, for instance, for approximately $0.4 < Le < 0.9$ or $1.1 < Le < 1.6$, either two modes and, thus, a and D_{11} or only a single mode and, thus, D_m can be obtained. Here, D_m represents a if $b_t >> b_c$ or D_{11} when $b_c >> b_t$. The greater the differences in b_t and b_c, the better the agreement between D_m and a or D_{11}. Furthermore, even if *Le* is far from unity, only a single mode may be obtained if either b_t or b_c tends toward zero. As long as a long-term disturbance in the CF can be accurately described, it has little effect on the simultaneous determination of a and D_{11}. Finally, given the conditions discussed above, the most important factor affecting the simultaneous determination of a and D_{11} is a large SNR. However, the required SNR depends on the specific conditions. The smaller SNR is, the larger the deviation of *Le* from unity and the closer $\mathcal{R} = 1$ should be in most cases. Additionally, if $Le >> 1$ or $Le << 1$, the temporal spacing between the two signal contributions may be too large to be obtained in a single CF using LTC. In the case of multicomponent mixtures, the situation is considerably more complex. Section 5 will provide further details on attribution of signals in binary and multicomponent mixtures.

4.6 Strategies for Signal Attribution

In the examples above, the conditions were clear in terms of coupling of hydrodynamic modes, temporal spacing, and relative amplitudes of the two contributions. However, in actual experiments, these factors are initially unknown. Attribution to a particular diffusivity remains a challenge, especially when the expected number of signals cannot be resolved in the DLS experiment. To facilitate signal attribution, appropriate strategies were developed in this thesis for binary fluid mixtures. These strategies will be discussed below.

First, it is important to distinguish between the types of diffusivities that can be obtained in two scenarios: when two hydrodynamic modes are accessible (a) or when only a single hydrodynamic mode is accessible (b). Figure 4.8 shows the corresponding flow charts. When two hydrodynamic modes are accessible (see Figure 4.8(a)), it is necessary to examine whether a coupling of hydrodynamic modes can be excluded. If the signals observed are solely related to T and c fluctuations, a and D_{11} can be obtained. If there is a coupling of hydrodynamic modes, only two effective diffusivities $D_{\mathrm{eff},1}$ and $D_{\mathrm{eff},2}$ can be obtained, as discussed in Section 4.2.2. Importantly, even if mode coupling is excluded, which hydrodynamic mode is related to which type of fluctuation may initially be unclear. The strategies for answering this question will be given below.

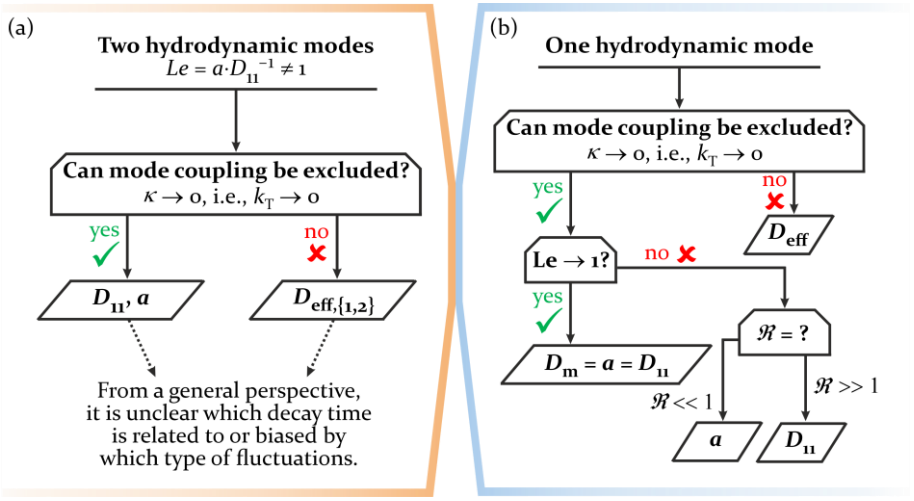

Figure 4.8: Schematic flow charts of the diffusivities that can be obtained via DLS for a binary mixture: (a) if two contributions or hydrodynamic modes are resolvable, or (b) if one hydrodynamic mode is resolvable.

If only one contribution is observed in a binary mixture, attributing diffusivities becomes more complex (see Figure 4.8(b)). If a coupling of hydrodynamic modes exists, only one effective diffusivity D_{eff} can be obtained. If a coupling of hydrodynamic modes can be excluded, whether Le is unity should be determined. If Le is unity, which represents an ideal case, D_m can be obtained, which represents both a and D_{11}. In this case, if $\mathfrak{R} > 1$, the single obtained diffusivity is closer to D_{11}. Contrastingly, if $\mathfrak{R} < 1$, the single obtained diffusivity is closer a. For the cases $\mathfrak{R} >> 1$ or $\mathfrak{R} << 1$, it can be assumed

that the single obtained diffusivity is equal to D_{11} or a. Note that the interpretation of D_m is associated with extended uncertainties, which are hard to quantify. If *Le* is not unity, the ratio of amplitudes must be considered in terms of $\mathcal{R}$. If $\mathcal{R} << 1$, the hydrodynamic mode is related to a. If $\mathcal{R} >> 1$, the hydrodynamic mode is related to D_{11}. In reality, attributing the diffusivity by using *Le* or $\mathcal{R}$ can be challenging because knowledge of both parameters may not be available and situations can arise where, for example, *Le* is close to unity and $\mathcal{R}$ is only slightly larger or smaller than one. This can introduce bias with regards to the obtained diffusivity, favoring one type of fluctuation over the other. In addition, resolving two individual contributions becomes less likely as SNR decreases.

The above schemata provide a theoretical guideline for mode allocation. However, there are still some unanswered questions. If two hydrodynamic modes are accessible and mode coupling can be excluded, a method must be found to relate the obtained signals to specific fluctuations and diffusivities. Thus, the general mode allocation strategy consists of the schemata depicted in Figure 4.8 in combination with the three pillars shown in Figure 4.9. The first aspect is comparison with the literature. For instance, in the compressed liquid phase far away from the critical plait point, the mode coupling parameter is known to approach zero, and D_{11} is some orders of magnitude smaller than a. Sometimes, a direct comparison with literature diffusivity data obtained via other techniques may be possible or well-established prediction methods and theories may be used to estimate diffusivities. The second aspect involves analyzing how the diffusivities behave as state variables change. For instance, in most fluid mixtures, a decreases while D_{11} increases with increasing T and decreasing p. In general, experiments can be started in a region where the physical mechanism related to the diffusivities are well understood and the behavior of the diffusivities analyzed as a function of T, p, and mixture composition. The composition-dependent trend or behavior of the diffusivities in the critical region can also aid in signal attribution. Furthermore, investigating the a in pure components and dilute mixtures can be helpful. The final aspect involves the theoretical calculation of $\mathcal{R}$, which is particularly useful for mode allocation when only one hydrodynamic mode can be resolved in the CF. The calculation details are provided in Section 4.3. The calculation of $\mathcal{R}$ can be validated by comparing the calculated values for $\mathcal{R}$ with the experimental values, which are naturally obtained via DLS in cases where two hydrodynamic modes are accessible. Thereafter, the calculations can be used to attribute the single diffusivity if only one hydrodynamic mode is observable in the experiment. Additionally, the calculation of $\mathcal{R}$ allows to use the flow chart

shown in Figure 4.8(b) in reverse. In the case where one mode is resolvable, mode coupling can be excluded, and $\mathcal{R}$ is approximately unity, *Le* should be close to unity as well. Furthermore, if $\mathcal{R} << 1$ or $\mathcal{R} >> 1$ and only one mode is observed, no further information on *Le* is required for signal attribution.

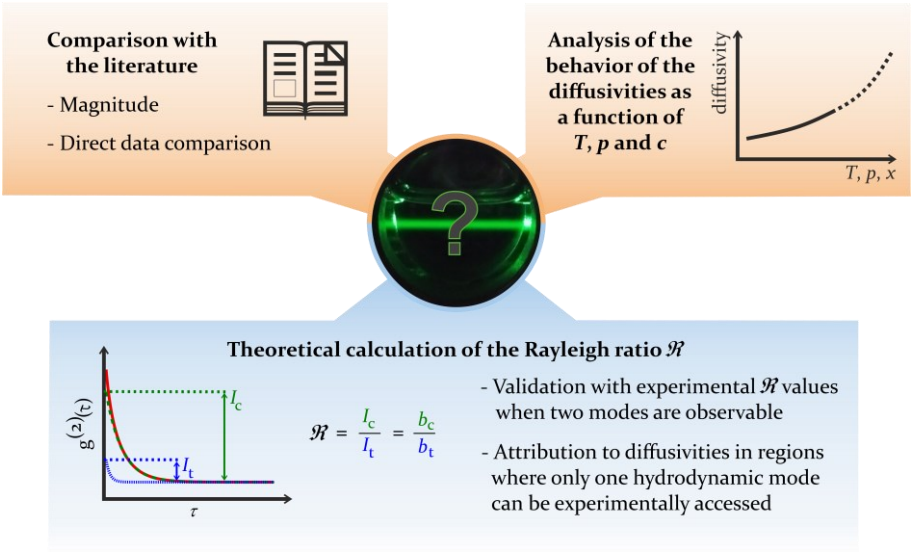

Figure 4.9: Overview of the overall mode allocation strategy for a binary mixture.

5 Results and Discussion

This chapter summarizes the most important results of the work performed in this thesis regarding the simultaneous determination of a and mutual diffusivities, as well as the applicability of DLS for systems in process, chemical, and energy technology. For a full discussion of the results of this work, the reader is referred to the publications listed in the Appendix. First, the results are presented for model systems, allowing a fundamental investigation of the various factors influencing the simultaneous determination of a and D_{11}, and demonstrating the types of diffusivities that can be obtained under different conditions. Thereafter, the applicability of DLS for systems that have a technical nature, often related to the transition toward a renewable energy economy, will be evaluated for various types of fluid classes and thermodynamic states. In all cases, depending on the individual situation, the developed strategies and toolset, which was briefly described in Section 4.6, were applied for signal identification and attribution.

5.1 Selected Model Systems

To gain a fundamental understanding of how different factors such as thermodynamic state, molecular properties, and experimental conditions influence the diffusivities accessible via DLS, the results of selected binary model mixtures will first be presented. The study of such systems should allow different limitations to be identified in an isolated manner.

5.1.1 Equimolar CH_4–C_3H_8 Mixture

The equimolar mixture of CH_4 and C_3H_8 has a T_c and critical pressure of approximately T_c = 314 K and p_c = 8.6 MPa. The proximity to ambient T facilitates experimental access of different fluid phases. Therefore, the accessibility of diffusivities via DLS experiments can be examined across the two-phase region in a general manner. Figure 5.1 showcases the two-phase boundary line of the mixture calculated using the GERG-2008 EoS [277] as implemented in the REFPROP database version 10 [279], represented by the solid blue line. The red circle in Figure 5.1 represents the plait critical point. The dashed, dotted-dashed, and dotted lines in Figure 5.1 denote selected theoretical isochores corresponding to the critical isochore with a critical density ρ_c = 239.61 kg·m^{-3}, $\rho = \rho_c \pm 10$ kg·m^{-3}, and $\rho = \rho_c \pm 33$ kg·m^{-3}, respectively. Heterodyne DLS experiments were performed at 125 different

thermodynamic states at small Θ_S, T ranging between (283 and 363) K, and p from (0.5 to 12) MPa. The investigated state points included 36 state points in the compressed liquid state (L, squares), 53 in the supercritical state (SC, circles), 21 in the gas state (G, diamonds), and 15 in the two-phase region (2P, triangles), as shown in Figure 5.1. Investigations in the low-density gaseous regime were included, which to the best of my knowledge have not previously been investigated via DLS. In the two-phase region, both the saturated liquid (2P-L) and saturated vapor (2P-V) phases were investigated whenever possible. Note that the compositions of both phases change with T and p, whereas the overall (global) mixture composition remains constant. The thermodynamic states investigated herein include the (distant) vicinity of the plait critical point, but not the vicinity where the sample becomes opalescent and gravity induces density gradients [295].

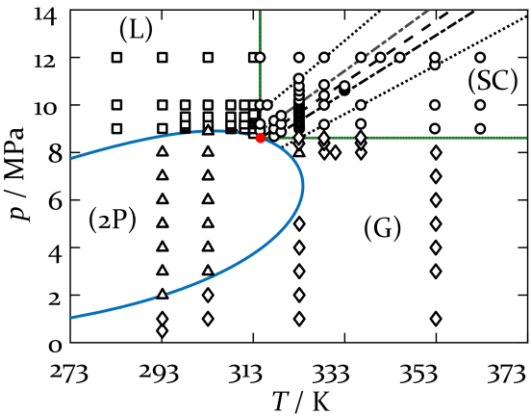

Figure 5.1: Two-phase boundary line (solid blue line) and plait critical point (closed red circle) of the equimolar CH_4–C_3H_8 mixture calculated using the GERG-2008 EoS [277]. The black dotted and/or dashed lines denote selected isochores. The different symbols indicate all state points investigated in this work. The figure was adapted from the respective publication [265].

Diffusivities in the Liquid and Supercritical States Along Isobars

Since the signal assignment to each type of fluctuation is initially unknown, two unidentified diffusivities, D_1 and D_2, are observable in a binary mixture according to the theory of DLS. The results obtained for D_1 and D_2 along three isobars as a function of T, crossing the liquid and super-critical states of the mixture, are shown in the top and bottom parts of Figure 5.2(a). The p of (9, 10, and 12) MPa are depicted by red, orange, and green symbols,

respectively. The dashed lines in the lower part of Figure 5.2(a) represent a taken from REFPROP [279]. Figure 5.2(a) shows that D_1 and D_2 could be simultaneously resolved in the liquid state. The ratio between the fast diffusivity D_2 and slow diffusivity D_1 varied between 4 and 13. The larger the ratio, the closer ρ was to ρ_c. In the supercritical state, only one hydrodynamic mode was resolved for most T and p. For the three isobars, the behavior of the resulting diffusivity followed that of D_1, and the T dependence across the liquid and supercritical states was well represented by a third-order polynomial, as indicated by the solid lines in the upper part of Figure 5.2(a). In the compressed liquid phase, D_{11} is typically some orders of magnitude smaller than a. Because the magnitude of D_1 in the compressed liquid phase was smaller than that of D_2, D_1 could be presumed to be related to c fluctuations. Based on this assumption for the three isobars, Figure 5.2(b) showcases the theoretical and experimental $\mathcal{R}$ as a function of T. The experimental data are represented by symbols, and the solid and dashed lines depict the $\mathcal{R}$ values calculated using Equation 4.46. The theoretical and experimental $\mathcal{R}$ values are in excellent agreement far from the critical point. For instance, at T = 293.13 K and p = 12.000 MPa, the experimental $\mathcal{R}$ = (6.1 ± 0.6), and the GERG-2008 EoS [277] and volume translated Peng–Robinson (VT-PR) EoS [278] predict values of 5.9 and 5.8. Approaching the plait critical point, large discrepancies between the experimental and theoretical $\mathcal{R}$ were observable. These discrepancies are most likely not related to an under- or over-estimation of $\alpha_{e,i}$ of CH_4 and C_3H_8, but rather due to a misevaluation of the osmotic compressibility in the near-critical region [255]. The largest value of $\mathcal{R} \approx 75$ where two modes are resolvable occurred at $T \approx 308$ K and $p \approx 9$ MPa. For this condition, Le was approximately 17. For a larger p, where the experimentally observed Le was smaller, the maximum value of $\mathcal{R}$ at which two modes could be distinguished was also smaller. This demonstrates the relationship between Le and $\mathcal{R}$ in connection with the simultaneous determination of two contributions. For the CH_4–C_3H_8 mixtures, two hydrodynamic modes could be resolved for T and p corresponding to a relative density $\rho \cdot \rho_c^{-1}$ larger than 1.15. The experimental $\mathcal{R}$ varied by nearly two orders of magnitude and exhibited expanded uncertainties (k = 2) between (3.9 and 77.5)%. The average expanded uncertainty (k = 2) was 27.1%. Large uncertainty for $\mathcal{R}$ could be specifically found in the vicinity of the two-phase boundary line. Based on the calculated values of $\mathcal{R}$, c fluctuations dominate the scattered light intensity over the entire range of T investigated in the one-phase region for $p > p_c$. This conclusion confirms that the single mode detected in the supercritical state can also be attributed to c fluctuations. Furthermore, for T below 280 K and above

350 K, D_1 follows the T and p dependence commonly reported for D_{11} in the literature. D_1 increases with rising T [282,296,297], whereas it decreases with increasing p [296–298]. For T between (280 and 350) K, D_1 assigned to D_{11} decreases with decreasing p due to the vicinity of the plait critical point [170,299]. The closer T and p are to the plait critical point, the more critical slowing down is reflected by D_{11}.

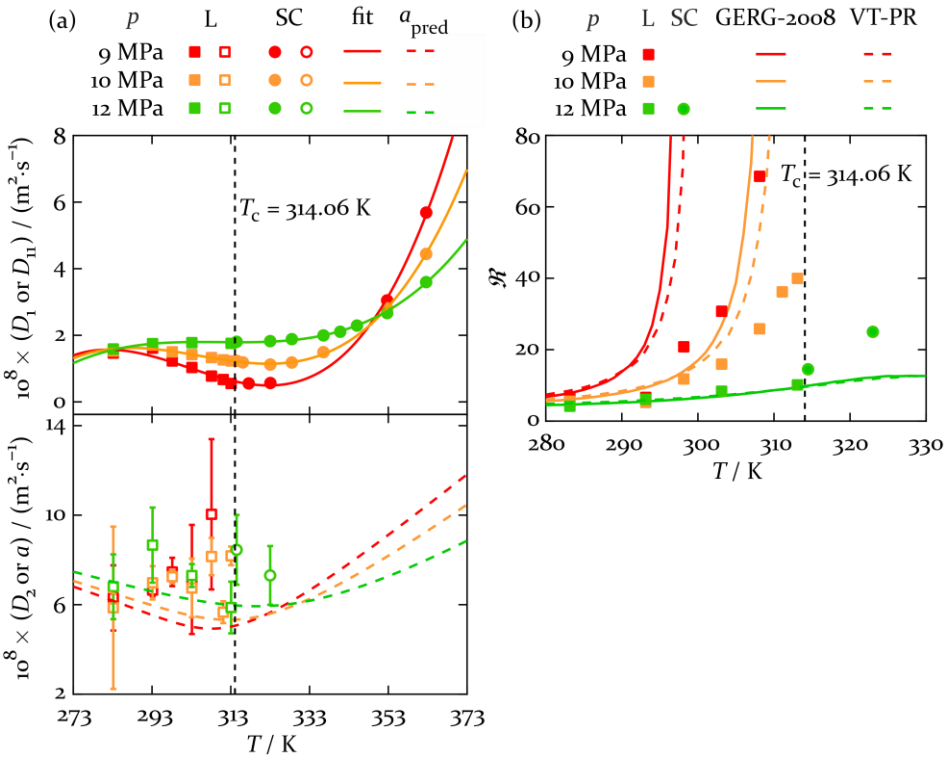

Figure 5.2: (a) Slow diffusivity or D_{11} (upper part) and fast diffusivity or a (lower part) as a function of T along three isobars. (b) Experimental (symbols) and theoretical (lines) $\mathcal{H}$ as a function of T at different p. The solid lines illustrate the results obtained using Equation 4.46 with the GERG-2008 EoS [277], and the dashed lines illustrate the predictions using the VT-PR EoS [278]. The figure was adapted from the respective publication [265].

However, until now, whether or not the diffusivities D_1 and D_2 could be attributed to pure a and D_{11}, as previously claimed, has remained unclear. Calculating the mode coupling parameter was not possible due to a lack of knowledge on the Soret coefficient and the inability of the GERG-2008 EoS [277] to produce osmotic compressibility data in the near-critical region.

Yet, the potential impact of heat and mass transfer coupling was qualitatively assessed based on the findings of Anisimov et al. [124] for CH_4–C_2H_6 mixtures near the vapor-liquid critical line. This assessment was conducted by analyzing the crossover between the two diffusivities and determining T at which $Le = 1$ for the three isobars studied. The study concluded that mode coupling could be disregarded across the entire range of T and p investigated. This finding is supported by a data obtained from the REFPROP database [279], depicted by dashed lines in the lower part of Figure 5.2(a), showing qualitative agreement with the experimental D_2 data. Further direct comparison of data was not possible due to the absence of experimental diffusivity data in the literature.

Diffusivities in the Supercritical State Along Isochores

In the supercritical state, the accessibility of diffusivities via DLS were analyzed along five isochores, including the critical isochore predicted by the GERG-2008 EoS [277]. The diffusivities are shown in Figure 5.3 as a function of the temperature difference $(T - T_c)$.

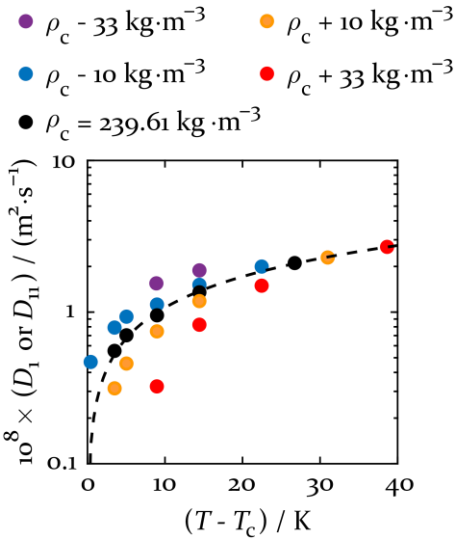

Figure 5.3: Slow diffusivity or D_{11} as a function of the distance away from T_c along five isochores. The dashed line indicates a fit of the data along the critical isochore by a power law. The figure was adapted from the respective publication [265].

In most cases, only one hydrodynamic mode could be resolved in the CFs. According to the previous discussion, the single diffusivity can be associated with $D_{\shortparallel}$. This is confirmed by its behavior, which follows the trend expected for $D_{\shortparallel}$ of slowing down when approaching T_c, as shown in Figure 5.3. This critical slowing down of $D_{\shortparallel}$ reflects the divergence of the correlation length of the fluctuations asymptotically close to the plait critical point of a binary mixture. In the near-critical region, along the critical isochore, $D_{\shortparallel}$ vanishes similar to the inverse of the correlation length to the power of 0.67 [170], and its behavior is the sum of a background and vanishing contribution [123]. For the diffusivities obtained along the predicted critical isochore, a fit in the form of a power law is indicated by the dashed line in Figure 5.3. Here, the exponent was found to be 0.68 ± 0.06, which agrees with the literature [300].

Diffusivities in the Gas State Along Isotherms

To explore the accessibility of diffusivities via DLS in the gas state, experiments were performed at different p for isotherms at T = (293, 303, 323, and 353) K. Among these states, only one hydrodynamic mode was resolvable in the CFs, from which a mixed diffusivity D_m was derived. D_m was found to decrease with increasing p and decreasing T. The uncertainty of D_m was considerably larger at low ρ than in the high-ρ region owing to a weaker amplitude of signals associated with T and c fluctuations in the low-ρ region, where the optical contrast factors and other thermophysical properties are relatively small. This may also be partially attributed to the small RID of the pure gaseous components. Figure 5.4(a) shows the p dependence of the D_m obtained along these isotherms. Figure 5.4(b) depicts the predicted $\mathcal{R}$ behavior in the gas state for p up to 8 MPa. The value of $\mathcal{R}$ is slightly larger than unity far from the dew point line and increased with increasing p and decreasing T. In this region, Le was expected to be close to unity, and the trend of the mixed diffusivity D_m agreed with the behavior of a and $D_{\shortparallel}$ [297]. Note that the theoretical $\mathcal{R}$ values have a large uncertainty in the gas phase. Thus, the single mode resolved in the CFs determined in this region cannot be associated only with T nor c fluctuations. This supports that the single diffusivity should be interpreted as D_m. The interpretation was further verified by a comparison with $D_{\shortparallel}$ data from the literature. D_m was 27% smaller than the $D_{\shortparallel}$ measured by Zangi et al. [301] at T = 293.10 K and p = 0.500 MPa using a Loschmidt cell combined with holographic interferometry. In accordance with the trend of the predicted

$\mathcal{R}$ values in the gas state, D_m obtained at $p < 1$ MPa were closer to a, whereas those obtained at $p > 7$ MPa were closer to or matched D_{11}.

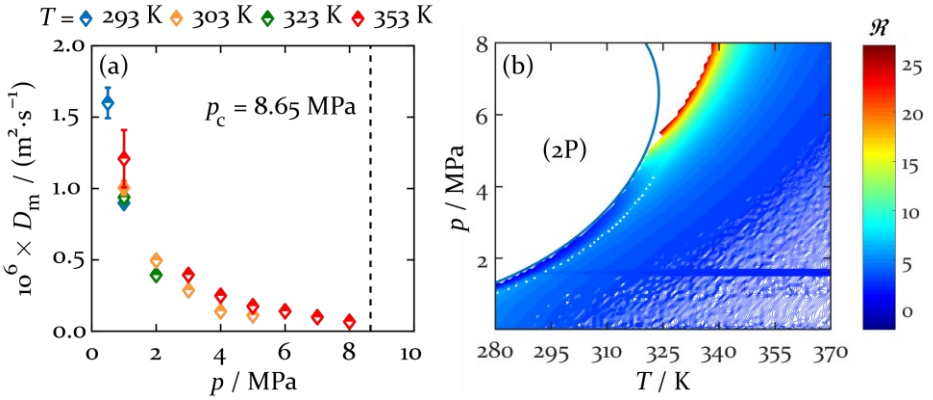

Figure 5.4: (a) D_m obtained along different isotherms in the gas state. (b) Isolines of $\mathcal{R}$ in the gas state predicted by the GERG-2008 EoS [277] and Equation 4.46. The figure was adapted from the respective publication [265].

Diffusivities in the Two-Phase Region Along Isotherms

Depending on the volume fraction of liquid to vapor, the diffusivities in the two-phase region were determined either in both the saturated liquid and vapor phases or only in one of them. Two hydrodynamic modes were generally resolvable in the experimental CFs obtained in the saturated liquid phase, allowing the simultaneous determination of a and D_{11}. In the saturated vapor phase, only one mode was accessible for all T and p studied. Owing to the methodology employed, a theoretical determination of $\mathcal{R}$ within the two-phase region was not possible. Figure 5.5(a) shows the diffusivities and $\mathcal{R}$ as a function of p measured via DLS in the saturated liquid phase (2P-L) at T = (293, 323, and 353) K. The results obtained in the liquid (L) and supercritical (SC) states at the same T are also shown in Figure 5.5(a). The larger uncertainties for a resulted from the smaller amplitude of the corresponding mode ($\mathcal{R} > 1$), as shown in the lower part of Figure 5.5(a). $\mathcal{R}$ increased between the dew and bubble points in the saturated liquid phase, but decreased with increasing p in the liquid state. Furthermore, the closer T was to T_c, the more pronounced was the change in $\mathcal{R}$ owing to a variation in p around the bubble point. Figure 5.5(b) shows the p dependence of the single diffusivity obtained via DLS in the saturated vapor phase (2P-V) along the aforementioned isotherms. The figure also includes data

for the gas state (G) for comparison purposes. For all $T \geq 303$ K, an increase in p results in a decrease in D_m, whereas at $T = 293$ K an increase in D_m can be observed. D_m exhibits a continuous behavior when crossing the dew point line.

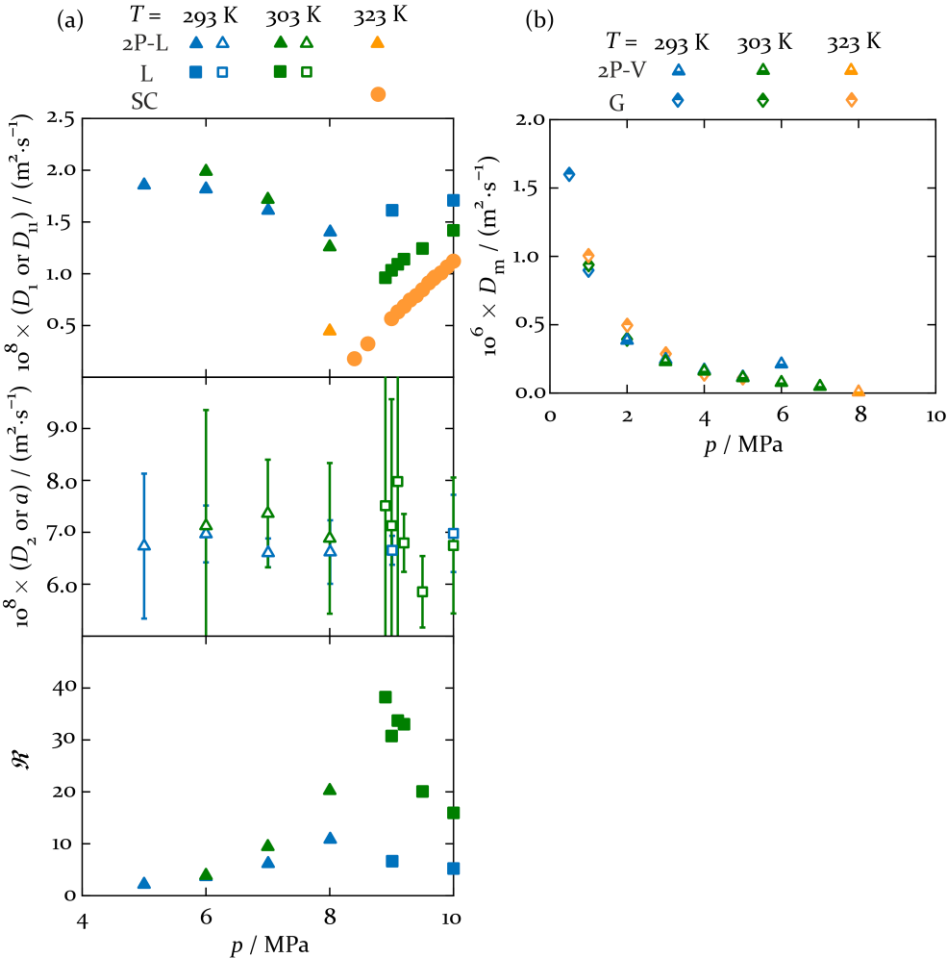

Figure 5.5: (a) p dependence of the slow diffusivity or D_{11} (top) and the fast diffusivity or a (middle) in the saturated liquid phase at vapor–liquid equilibrium (2P-L), as well as in the liquid (L) or supercritical (SC) state for T = (293, 303, and 323) K. Evolution of the corresponding $\mathcal{H}$ as a function of p (bottom). (b) p dependence of D_m in the saturated vapor phase at vapor– liquid equilibrium (2P-V) and in the gas state (G) for T = (293, 303, and 323) K. The figure was adapted from the respective publication [265].

5.1.2 Liquids with Dissolved Gases

Systems consisting of liquids with dissolved gases are important working fluids in many areas of chemical and energy engineering and technology [16,21,23,24,302–305]. The purpose of a research project at AOT-TP was to develop a simple prediction model for D_{11} in such systems. To achieve this, 82 unique binary systems of a liquid solvent with a dissolved gas close to infinite dilution [47,48,285,286,288,291,292,306] and 15 binary systems as a function of composition [243,244,283,284,286,290] were investigated using DLS, Raman spectroscopy, and equilibrium molecular dynamics simulations over a wide range of thermodynamic states. The solvents included *n*-alkanes and 1-alcohols with different chain lengths, cyclic and branched alkanes, an acid, an ether, and ILs. The solutes varied in terms of molar mass, shape, mass, and polarity. All related DLS investigations were performed in the saturated liquid phase. In addition to their practical importance, mixtures consisting of liquids with dissolved gases facilitate the simultaneous determination of a and D_{11} because, for many related systems, the light-scattering signals originating from T and c fluctuations appear at similar time scales. A further advantage of such mixtures is that their composition can be modified by the amount and p of gas, thus taking advantage of the solubility of the respective gas without altering the entire sample. This helps limit errors that may arise from incorrect experimental preparation, including cell cleaning and sample handling. However, c and p effects on the diffusivities cannot be analyzed separately. Investigations of systems close to infinite dilution of the dissolved gas enable the study of the influence of molecular properties and, to some extent, that of SNR on the magnitudes and resolvability of diffusivities. However, studying the influence of the RID of pure components is only partially possible because liquid phase refractive indices of the dissolved gases are often unavailable under the study conditions. Studies focusing on composition evaluate the evolution of $\mathcal{R}$, which, along with Le, is a crucial factor in determining whether both a and D_{11} are simultaneously accessible. Selected results presented below show the associated behavior of signal amplitudes and temporal spacing as a function of T and the mole fraction of the dissolved gas x_{gas} for various systems. The presentation and interpretation of the diffusivity data and further details can be found in the respective publications, which are part of this thesis.

Systems Close to Infinite Dilution

For the systems within the limit of infinite dilution [63–65], x_{gas} was assumed to be below or equal to 0.05. In most of the studied systems and thermodynamic states, the CFs of the binary mixtures showed two contributions, which were confirmed to be related to a and D_{11} by comparing the results with literature data. Mode coupling could be excluded. Figures 5.6(a) and 5.6(b) show $\mathcal{R}$ as a function of T for systems of helium (He) and krypton (Kr) dissolved in various liquids. Typical values of $\mathcal{R}$ were 0.2 close to infinite dilution; this was also observed for other mixtures studied. No clear trends of $\mathcal{R}$ as a function of T or mixture constituents were observable. The slight increase of $\mathcal{R}$ for He and decrease for Kr with increasing T might be related to the solubility of the gases. The solubility of He increases with rising T, whereas for Kr, a decrease has been observed [307–310]. For most measurement series, gas was initially injected at a specific p to obtain a signal amplitude related to c fluctuations large enough to facilitate the accurate determination of D_{11}, while remaining within close to infinite dilution. Increasing T of the closed volume will also increase p. Therefore, an increase in x_{gas} could be expected in mixtures with He because of the T dependence of solubility. This was confirmed by the related mixture compositions reported in the corresponding publication [288]. The increase in x_{gas} resulted in an increase in I_c. Figures 5.6(c) and 5.6(d) illustrate the typical decrease in Le with increasing T. Larger Le values were exhibited by systems with hindered molecular diffusion, that is, where D_{11} was comparatively small. This relationship usually holds true for large, heavy, and bulky solvents and solutes. To understand the factors that affect the relative magnitude of a and D_{11} in these systems, refer to the respective publications [47,48,285,286,288,291,292,306].

Assuming a sufficient SNR, the simultaneous accessibility of both a and D_{11} in mixtures of liquids with dissolved gases close to infinite dilution was influenced by three main factors. First, the solute concentration must be sufficient to give rise to a resolvable signal in the CF related to c fluctuations. The corresponding $\mathcal{R}$ should be at least approximately 0.05, depending on SNR. For the studied systems, the smallest related composition at which a simultaneous determination of a and D_{11} was reliably possible was $x_{gas} \approx 0.0015$. Second, because Le decreases with T, there might be a range where Le is close to unity, and only D_m can be obtained due to the limited SNR. This scenario was observed, for example, for mixtures of He with C_6H_{12}, 2,2-dimethylbutane, 2-methylpentane, or ethyl butanoate at T above 348 K. The exact T varied for each mixture. Notably, after the region where both the T-dependent trend of a and D_{11} intersect, that is, $Le = 1$, the attribution

of fluctuations in T and c to the faster and slower decaying exponentials was reversed. With regards to Le approaching 1, increased uncertainties in $\mathcal{H}$ often exist owing the difficulty in fitting CF data.

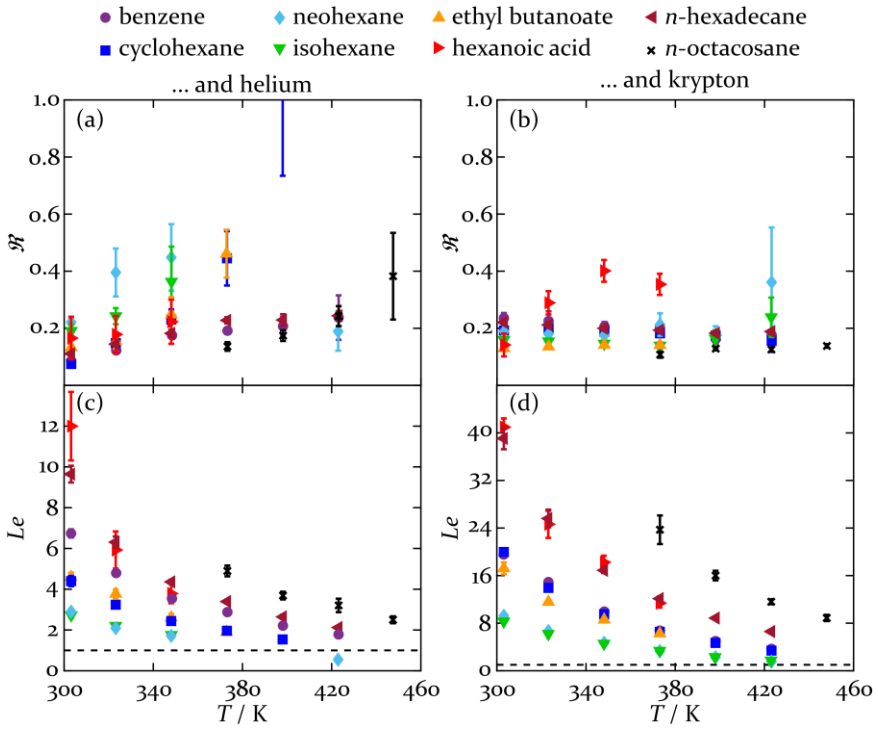

Figure 5.6: Experimental $\mathcal{H}$ and Le for various mixtures of liquids with dissolved helium, (a) and (c), or krypton, (b) and (d), close to infinite dilution of the dissolved gas. The dashed lines represent $Le = 1$.

Additionally, in some systems, the accurate determination of D_{11} and a could not be performed at elevated T due to the formation of particle-like impurities or sample discoloration. The formation of particles at elevated T was most likely due to interactions between the solvents and the cell and sealing materials. Sample discoloration may indicate degradation or oxidation. Both factors may result in a significant long-term disturbance in CF, impeding the accurate determination of a and D_{11}. However, due to the significantly larger amplitude of the signal associated with T fluctuations, it may still be possible to determine a in some cases. Determining D_{11}, on the other hand, was not possible. The typical relative expanded uncertainties

(k = 2) for both a and D_{11}, simultaneously determined within the region of infinite dilution, were between about (2 and 15)%.

Systems as a Function of Composition

Figures 5.7(a) and 5.7(b) show exemplary values of $\mathcal{R}$ and *Le* in the systems of *n*-C_6H_{14} with R143a or SF_6 and *n*-$C_{16}H_{34}$ with CO_2 at different T as a function of x_{gas}. The corresponding x_{gas} values were obtained using the isochoric saturation method and/or Raman spectroscopy [290,311]. As observed for the investigations in the limit of infinite dilution, the system and T had only a negligible influence on $\mathcal{R}$ for x_{gas} up to approximately 0.05. However, as shown in Figure 5.7(a), for x_{gas} > 0.5, slight behaviors of $\mathcal{R}$ can be observed. $\mathcal{R}$ generally increases as it approaches equimolar composition, but the position of the maximum depends strongly on the investigated system. For x_{gas} > 0.10, the various systems begin to exhibit distinct behaviors of $\mathcal{R}$. However, for values of approximately x_{gas} < 0.20, T had only a minor influence. Distinct T-dependent trends were only observable within the range of x_{gas} ≈ (0.25 and 0.75), where the higher T, the smaller the value of $\mathcal{R}$. This can be explained by considering the definition of the $\mathcal{R}$ given by Equation 4.46, where T is in the denominator. Figure 5.7(b) illustrates the relationship between *Le* and x_{gas} for the studied systems. *Le* was strongly dependent on the behavior of a and D_{11} with respect to the thermodynamic state, as per the definition. This dependence can be attributed to the various composition-dependent trends of D_{11}, which have been discussed in the respective publications [243,244,283,284,286,290]. For the systems shown in Figure 5.7(b), *Le* generally increased as the composition approached equimolarity. Owing to the similar behaviors of *Le* and $\mathcal{R}$, approaching equimolar composition, the signal related to T fluctuations was represented by only a few data points in the experimental CF, and the related amplitude was considerably smaller than that related to concentration fluctuations. Thus, larger uncertainties were generally obtained in this region for a than for D_{11}. As a result, for some state points and systems, such as *n*-hexane and SF_6, only D_{11} could be obtained in the equimolar region. In concentrated mixtures, the relative expanded uncertainties (k = 2) of D_{11} were as low as 0.6%, whereas the uncertainties of a were as high as 100% due to the described circumstances.

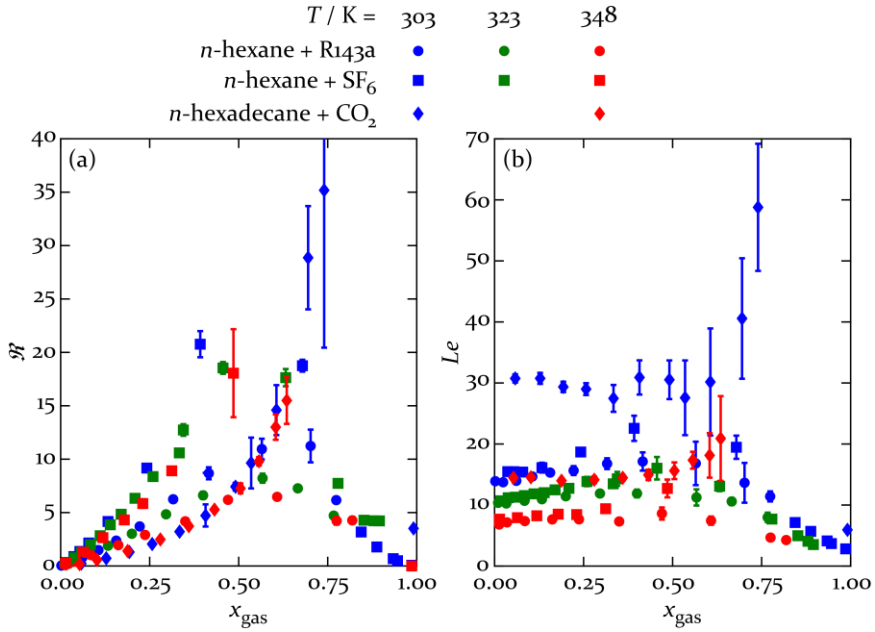

Figure 5.7: Experimental $\mathfrak{N}$ (a) and *Le* (b) as a function of x_{gas} for different systems at three *T*.

5.2 Systems Relevant to Process and Energy Technology

This section focuses on the applicability of DLS to more technical systems across a broad range of thermodynamic states and is structured as follows: first, the diffusivities accessible in different types of liquid–liquid mixtures will be discussed, followed by mixtures of liquids with dissolved gases, and finally gaseous and supercritical mixtures. The different thermodynamic regimes are closely linked, and the separation into three sections is mainly for structure and readability. For each type of system, motivation for its applicability, respective experimental and scientific challenges, and technical aspects related to the measurement equipment and the conduction of the experiment are provided. These aspects are discussed in relation to the simultaneous determination of a and D_{11} and diffusivities accessible via DLS. Typical uncertainties will be reported, and the main outcomes related to the thermophysical properties will be discussed briefly.

5.2.1 Liquid Mixtures

Biofuel-Related Mixtures Under Pre-Combustion Conditions

Until a successful transition to a hydrogen economy can be achieved, researchers will focus on the development of new generations of fuels for increased engine efficiency and reduced emissions. Considerable effort is being devoted to the development and characterization of biogenic surrogate fuels that match the distillation curves of the target fuels. Owing to the multicomponent nature of fuels, intra-droplet heat and mass transfer must be considered to correctly model the dynamics of the evaporation process in gasoline direct injection engines [25]. However, such research activities are mostly based on theoretical diffusivity data due to the lack of reliable experimental data including specifications related to their uncertainties. In this context, nine model binary mixtures composed of isopentane, isooctane, $C_6H_5CH_3$, *n*-$C_{10}H_{22}$, and C_2H_5OH were investigated at T up to 523 K and close to their bubble point line via DLS [282]. Here, the challenge encountered was the large T difference between the p control circuit including SaCe and ambient. Thus, special precautions had to be taken to avoid disturbing the macroscopic thermodynamic equilibrium in the compressed liquid phase at elevated T. For this purpose, a multi-stage T and p control loop was developed that allowed advection-free measurements to be taken.

For most of the investigated systems and thermodynamic states, a and D_{11} were simultaneously accessible via DLS at small Θ_S. This was confirmed by comparing them with literature values, leading to the conclusion that mode coupling could be excluded. The a of equimolar binary mixtures typically showed larger uncertainties than the other compositions owing to the high value of $\mathcal{R}$, as shown in Figure 5.8(a) for the mixtures of isooctane and $C_6H_5CH_3$. However, for certain systems and thermodynamic states, $\mathcal{R} < 1$ and an Le close to unity was observed. In these cases, the CF could be accurately represented by a single exponential related only to the T fluctuations. This was further supported by the variation of diffusivities as a function of T. Figure 5.8(a) shows $\mathcal{R}$ as a function of the mole fraction of isooctane $x_{\mathrm{isooctane}}$. Consistent with the behavior of $\mathcal{R}$ in mixtures of liquids with dissolved gases, as shown in Figure 5.7(a), higher T resulted in a decrease in $\mathcal{R}$. However, in contrast, the maximum $\mathcal{R}$ achieved was significantly smaller, and the T dependence was evident at low and high $x_{\mathrm{isooctane}}$ values, suggesting that simultaneously determining both a and D_{11} is generally more realistic in concentrated liquid mixtures rather than in concentrated mixtures of liquids with dissolved gases. However, Figure 5.8(b) reveals that, especially at low T, Le is generally relatively large in binary liquid

mixtures, which is counterproductive for the simultaneous determination of a and D_{11}.

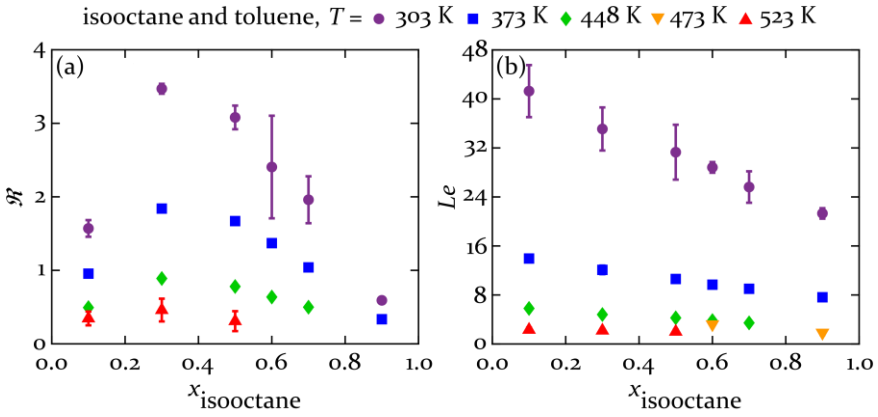

Figure 5.8: (a) Experimental $\mathcal{R}$ and (b) Le as a function of composition for mixtures of isooctane and $C_6H_5CH_3$ at five T.

For all systems, compositions, and T studied, a changed only slightly. In contrast, D_{11} (see Figure 5.9) varied by more than two orders of magnitude from about (10^{-10}–10^{-8}) $m^2 \cdot s^{-1}$. The average expanded relative uncertainties ($k = 2$) of (8 and 6)% were obtained for a and D_{11}. One of the main outcomes was that the presence of the biofuel C_2H_5OH in alkane-based surrogate-fuels causes a significant slowing down of D_{11} at low T, but not at elevated T, which are relevant for combustion. In addition to the binary mixtures, a quaternary mixture consisting of isopentane, isooctane, $C_6H_5CH_3$, and n-$C_{10}H_{22}$ as well as a quinary surrogate fuel mixture consisting of the same components as the quaternary mixture and C_2H_5OH as the biogenic component were investigated via DLS. At a given thermodynamic state, a and one apparent diffusion coefficient D_{app} were obtained for the quaternary and quinary mixtures. This contradicts the theory of DLS, since for multi-component mixtures with n_c components a as well as n_c–1 individual eigenvalues of the Fick diffusion matrix should be observable. The observation of a single D_{app} could be explained by the refractive indices of the mixture components, which were relatively similar.

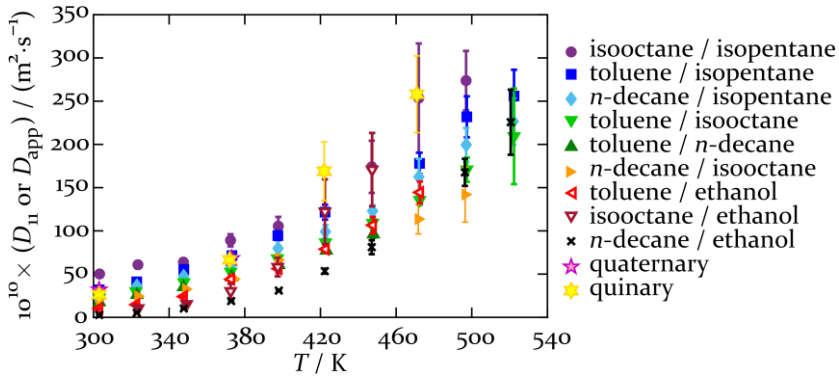

Figure 5.9: D_{11} or D_{app} of different equimolar binary mixtures or a quaternary and a quinary mixture related to a surrogate fuel as a function of T. The volume fractions were 0.323 isopentane–0.323 isooctane–0.097 $C_6H_5CH_3$–0.257 *n*-$C_{10}H_{22}$ for the quaternary mixture and 0.291 isopentane–0.291 isooctane–0.087 $C_6H_5CH_3$–0.231 *n*-$C_{10}H_{22}$–0.100 C_2H_6O for the quinary mixture. The figure was adapted from the respective publication [282].

Electrolyte Systems Consisting Entirely of Ions

Electrolytes are an important fluid class for numerous applications, including energy storage [26–28] and conversion techniques [29,30]. The efficiency of these processes relies heavily on ion mobility and molecular mass transport within the electrolyte [31,32], which can be described by D_{11}. Although electrolytes composed solely of ions are of great interest, there are few studies available in the literature that focus on determining D_{11} in these mixtures because of the limitations of conventionally applied techniques. This thesis demonstrated, for the first time, the applicability of DLS for investigating molecular diffusive mass transport in total ionic electrolyte systems [281].

Four binary model mixtures composed entirely of ions were used to prove that the experimental signals obtained were associated with hydrodynamic modes. Mode coupling could be neglected. The systems were based on three different ILs and a salt, always sharing a common ion in the mixture. In terms of Fickian formalism, consider that each electrolyte system studied herein was produced by mixing two substances consisting of three different ions. In such cases, owing to the electroneutrality of the system which led to a coupling between the mass fluxes of the ions involved, the diffusive mass transport could be described by a single mutual diffusion coefficient D_{11} [31,312]. For the present mixtures, D_{11} was predicted to be approximately three orders of magnitude smaller than the corresponding a. Because scattering geometry was chosen to resolve D_{11} with the lowest

uncertainties, that is, a $\Theta_S = 90°$ was used, a could not be obtained simultaneously due to the large temporal spacing. Owing to the hygroscopic nature of the samples, one major challenge was to isolate the signals related to molecular ion mass transport. Figure 5.10(a) shows the results for D_{11} for virtually equimolar binary mixtures of 1-ethyl-3-methylimidazolium bis(trifluoromethylsulfonyl)imid ([EMIM][NTf_2]), 1-ethyl-3-methyli-midazolium ethylsulfate ([EMIM][$EtSO_4$]), 1-decyl-3-methylimidazolium bis(trifluoromethylsulfonyl) imide ([DcMIM][NTf_2]), 1-butyl-3-methylimidazolium hexafluorophosphate ([BMIM][PF_6]), 3-methyl-1-(3,3,4,4,4-pentafluorobutyl)imidazolium hexafluorophosphate ([PFBMIM][PF_6]), and lithium bis(trifluoromethylsulfonyl)imide ([Li][NTf_2]) as a function of T. Figure 5.10(b) shows the results of D_{11} for mixtures [EMIM][NTf_2] and [EMIM][$EtSO_4$] as a function of the [EMIM][NTf_2] mole fraction $x_{[EMIM][NTf_2]}$. The main outcome was that the constituent ions had a significant influence on D_{11} and that D_{11} exhibited a non-ideal concentration dependence in such systems. The expanded mean relative uncertainty of D_{11} was 8.0%.

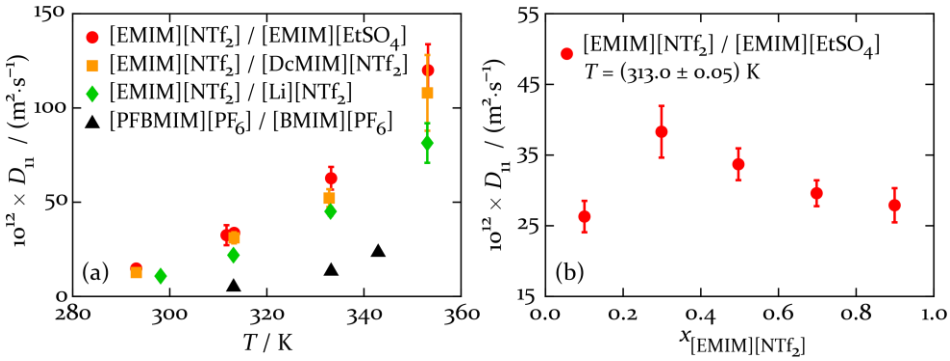

Figure 5.10: (a) D_{11} as a function of T for the investigated mixtures consisting of $x_{[EMIM][NTf2]} = 0.4968/x_{[EMIM][EtSO4]} = 0.5032$ (red circles), $x_{[EMIM][NTf2]} = 0.5678/x_{[DcMIM][NTf2]} = 0.4322$ (orange squares), $x_{[EMIM][NTf2]} = 0.9271/x_{[Li][NTf2]} = 0.0729$ (green diamonds), and $x_{[PFBMIM][PF6]} = 0.4993/x_{[BMIM][PF6]} = 0.5007$ (black triangles). (b) D_{11} in mixtures consisting of [EMIM][NTf_2] and [EMIM][$EtSO_4$] (red circles) as a function of $x_{[EMIM][NTf2]}$ at a mean T of 313.0 K. The figures were adapted from the respective publication [281].

Binary Mixtures of LOHCs

H_2 as a working fluid for energy storage and transport is currently being evaluated with regard to the expansion of renewable energies [313–315]. The large-scale use of H_2 requires the development of technologies for H_2 production [316–319], distribution [320], and storage [35,321]. In addition to

compression [322], liquefaction [323], and absorption [324], the chemical storage using LOHCs [33,325] is considered as promising alternative. In this context, precise knowledge on transport properties is key for the optimized design of catalyst materials for hydrogenation and dehydrogenation processes [33]. A binary mixture consisting of equal masses of diphenylmethane (DPM) and its fully hydrogenated derivative dicyclohexylmethane (DCM) was studied at T between (298 and 473) K and p of about (0.5 and 7) MPa via DLS [80]. Mode coupling could be excluded. Both a and D_{11} were accessible, but not always simultaneously owing to $\mathcal{R}$ and Le, shown in Figures 5.11(a) and 5.11(b) as a function of T at different p. $\mathcal{R}$ was in the same order of magnitude as observed for the biofuel-related mixtures and exhibited a similar decrease with increasing T. Furthermore, a slight increase in $\mathcal{R}$ with increasing p was observable. This corresponds with the observations made for the equimolar CH_4–C_3H_8 model mixture. As shown in Figure 5.11(b), the equimass DPM–DCM mixture exhibits considerably large Le values at low T because of the bulky structures and large M, resulting in relatively small values for D_{11}. Thus, and considering that $\mathcal{R} > 4$ according to the trend shown in Figure 5.11(a), at $T \leq 385$ K, a and D_{11} could be determined in individual measurements at $\Theta_1 \leq 5°$ and $\Theta_3 \leq 90°$, respectively. At $T \geq 385$ K, both a and D_{11} were simultaneously determined from one CF. The expanded mean relative uncertainty ($k = 2$) in both a and D_{11} was approximately 10%.

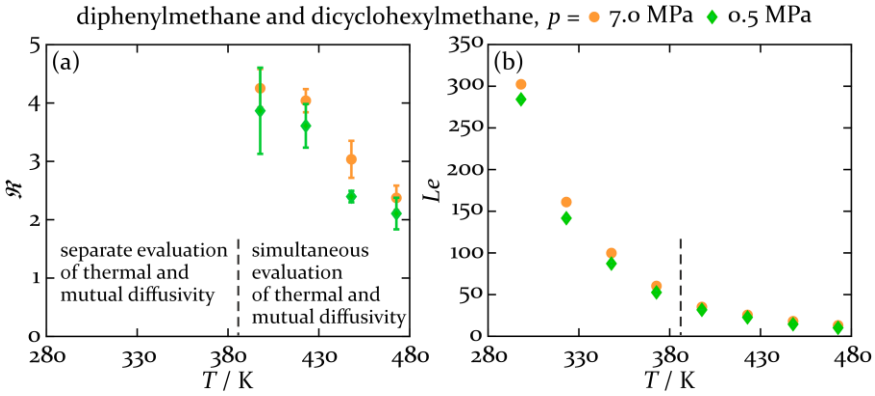

Figure 5.11: Experimental $\mathcal{R}$ (a) and Le (b) as a function of T for mixtures of DPM with its fully hydrogenated derivative DCM at two p. The dashed lines represent the border where a and D_{11} were determined in either single or two separate measurements.

5.2.2 Liquids with Dissolved Gases

Binary mixtures of DCM with Dissolved Hydrogen

With respect to LOHC systems, the saturated liquid phase of binary mixtures of DCM with dissolved H_2 near infinite dilution was also investigated via DLS at T between (323 and 573) K and p between (2.7 and 6.2) MPa. The measured data for a and D_{11} shown in Figure 5.12(a) demonstrate the typical decreasing and increasing trends with increasing T. The solid lines in Figure 5.12(a) represent weighted fits to the diffusivity data and are intended as a visual guide. Similar to some of the model systems consisting of liquids with dissolved gases, an intersection of the T-dependent trends of a and D_{11} was observed. For this system, the crossing was between approximately T = (450 and 530) K. In this range, only D_m was accessible. Figure 5.12(b) presents the corresponding $\mathcal{R}$ values obtained in the case where two contributions could be resolved. Similar to other systems close to infinite gas dilution (see Figures 5.6(a) and 5.6(b)), $\mathcal{R}$ is between (0.2 and 0.4). The increase in $\mathcal{R}$ with increasing T was most likely related to the increasing solubility of H_2 with T [326]. Owing to the small $\mathcal{R}$, the obtained D_m data could be treated as a. This was confirmed by the comparison between D_m and the T-dependent trend of a. At T above 530 K, where both diffusivities were resolved, large uncertainties were observed for a, D_{11}, and $\mathcal{R}$ because of the large fit uncertainties resulting from the difficulty in separating the individual contributions, considering SNR.

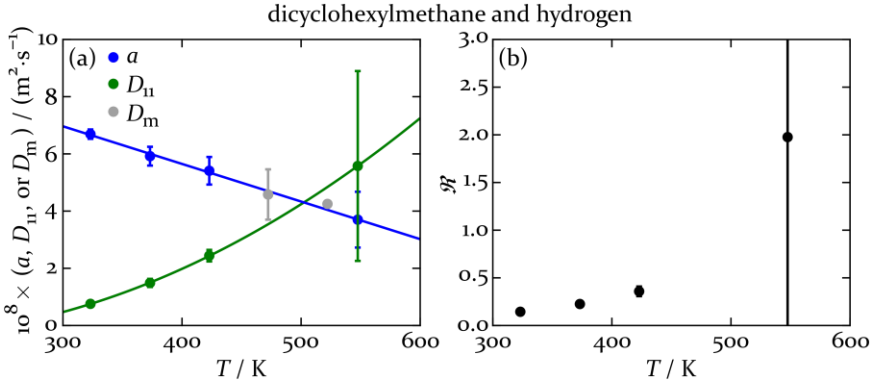

Figure 5.12: (a) a, D_{11}, or D_m and (b) experimental $\mathcal{R}$ as a function of T for mixtures of DCM with dissolved H_2 close to infinite dilution of the gas. The solid lines represent weighted fits to the experimental data and serve as a visual guide. The figure (a) was adapted from the respective publication [327].

Aqueous Solutions of NaCl with Dissolved H_2 and CH_4

Another promising solution for efficient and safe large-scale H_2 storage is geological or subsurface storage [328–330]. This includes storage of H_2 in salt caverns [331], (saline) aquifers [332], or depleted gas or oil reservoirs [333,334], where CH_4 might be a pre-existing residual or intentionally used as cushion gas [333,335,336]. Knowledge on diffusion in H_2O or aqueous solutions of NaCl with dissolved H_2 and CH_4 is crucial for modeling, designing, and optimizing the related processes, e.g., for estimating the leak rate of the storage facility [34–37]. However, corresponding experimental diffusivity data under process- or storage-relevant conditions are scarce. To overcome the lack of data, related mixtures were investigated in a cooperative project with Shell Global Solutions International BV. In the related publication, the applicability and limitations of DLS for the measurement of diffusivities in mixtures relevant for geological or subsurface H_2 storage were demonstrated for the first time [287]. Mixtures of H_2O or aqueous solutions of NaCl (also known as brine) with c_{NaCl} up to 0.34, containing dissolved H_2 or dissolved mixtures of H_2 + CH_4, were investigated at saturation conditions at T between (293 and 393) K and p up to 20 MPa. The salt concentration c_{NaCl} was defined as kilogram of NaCl per kilogram of H_2O. A major challenge was the corrosive nature of brine, which resulted in a turbid sample contaminated with particles when using the standard and further SaCes. Different polymer coatings were considered as potential solutions for obtaining a brine-resistant SaCe. The final solution used a coating composed of a polytetrafluoroethylene + perfluoroalkoxy alkane (PFA) primer with a PFA top coating. The study was complex, and only key results will be presented below. For more information, please refer to the publication [287].

In binary mixtures of H_2O and H_2, both a and D_{11} were simultaneously accessible at small Θ_S. Their mean relative expanded experimental uncertainties (k = 2) were (18 and 12)%. Figures 5.13(a) and 5.13(c) show the corresponding results, which agree with available literature data [72,279,337–343]. The $\mathcal{R}$ in mixtures of H_2O and H_2 exhibits similar p- and T-dependent trends observed for other gas–liquid mixtures. However, owing to the relatively large noise level in the experimental CFs, resulting in significant uncertainties in the decay times and $\mathcal{R}$, definitive conclusions could not be drawn. Note that H_2 and CH_4 are poorly soluble in H_2O [344,345]. Therefore, at p = 20 MPa, only a maximum x_{gas} of about 0.0035 could be achieved within the studied T range. This demonstrates that even at such low concentrations, DLS is capable of resolving the contribution related to c fluctuations under certain conditions.

For ternary mixtures of H_2O and CH_4 + H_2 with varying x_{CH_4}, a and D_{app}, which is related to the diffusion of the gas mixture in the liquid, were resolvable at small Θ_S via DLS. Figure 5.13(b) exemplarily shows the corresponding D_{app} results as a function of CH_4 mole fraction x_{CH_4} for p = 10 MPa and T = (293, 333, 363, and 393) K. In addition, D_{11} in the mixtures of H_2O and H_2 obtained via DLS, as well as D_{11} data from a correlation proposed by Guo et al. [346] for mixtures of H_2O and CH_4 are shown at x_{CH_4} = (0 and 1). D_{app} exhibited a slight composition-dependent trend with maxima at x_{CH_4} ≈ 0.4, considering the uncertainties. The relative expanded experimental uncertainties (k = 2) of a and D_{app} were on average (43 and 29)%. The relatively large uncertainties could be partly related to a long-term disturbance apparent in the experimental CFs, which must be considered during fitting. The origin of the disturbance appeared to be related to the presence of CH_4.

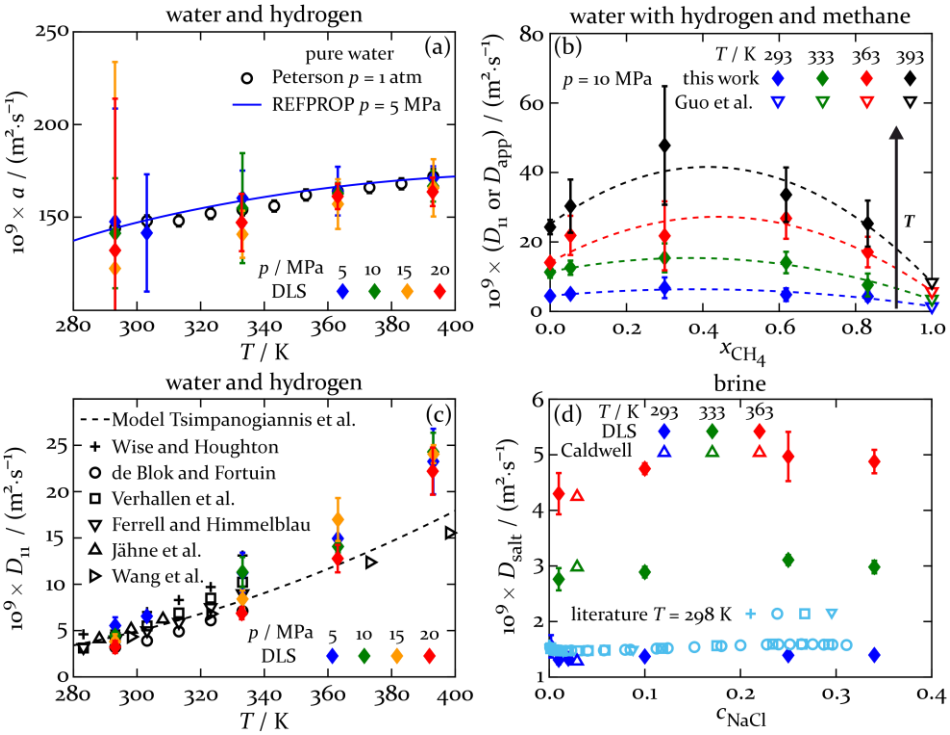

Figure 5.13: Liquid phase a (a) and D_{11} (c) in binary mixtures of H_2O with dissolved H_2 under saturation conditions obtained via DLS as a function of T at different p. For comparison, a data of pure H_2O from Peterson [337] and estimated values taken from REFPROP [279] are also shown in (a). D_{11} data at about p = 1 atm from Wise and Houghton [72], de Blok and Fortuin [338], Verhallen et al. [339], Ferrell and Himmelblau [340], and Jähne et al. [341] are also shown in (c) for comparison. Additionally, D_{11} from Wang et al. [342] at p ≈ 28 MPa and

D_{11} calculated with the engineering model from Tsimpanogiannis et al. [343] for p = 10 MPa are shown. (b) D_{app} in the saturated liquid phase of ternary mixtures of H_2O and H_2 + CH_4 obtained via DLS as a function of x_{CH_4} at T = (293, 333, 363, and 393) K) and p = 10 MPa. D_{11} in mixtures of H_2O and H_2 obtained by DLS and D_{11} data from a correlation proposed by Guo et al. [346] for mixtures of H_2O and CH_4 are shown at x_{CH_4} = 0 and 1. The dashed lines represent fits weighted by the inverse uncertainties of the diffusivity data and are meant to be visual guides. (d) D_{salt} in the liquid phase of brine at 0.1 MPa H_2 atmosphere or ambient p obtained via DLS at small Θ_S or Θ_S = 90° as a function of c_{NaCl} at T = (293, 333, and 363) K. The open triangles correspond to D_{salt} obtained by using a correlation given by Caldwell [347]. The light blue open symbols indicate selected literature data for D_{salt} at T = 298 K [348–351]. The figures were adapted from the respective publication [287].

The diffusion coefficient of salt D_{salt} could be determined as a function of T and c_{NaCl} in aqueous solutions of NaCl. However, the H_2-related diffusion coefficient was only accessible at small c_{NaCl} and T = 293 K in ternary mixtures of brine with dissolved H_2 owing to the rapidly increasing signal amplitude in the CF related to D_{salt} with increasing c_{NaCl} and a strong molecular association leading to a quasi-static light scattering pattern in the liquid sample for T > 300 K that hindered the determination of molecular gas diffusivities. The structuring of the liquid phase represented a physical limitation given by the studied system and hindered furthermore the determination of a and/or D_{salt} at about T > 300 K at small Θ_S via DLS. However, by applying a Θ_S = 90° and adjusting the correlators' temporal resolution, the signal related to D_{salt} could be isolated from the long-term disturbances caused by the structuring. This enabled the determination of D_{salt} over the entire T range investigated in the study. Owing to the temporal spacing, a simultaneous determination of a was not possible. The corresponding D_{salt} results shown in Figure 5.13(d) demonstrate a relatively weak composition-dependent trend. This is in agreement with literature. Considering the mean relative expanded experimental uncertainties of (64 and 44)%, no dependency of a or quasi binary diffusion coefficient $D_{11,q}$ related to the diffusion of H_2 in the mixture on c_{NaCl} was observable within the investigated range of c_{NaCl} up to 0.02. For quaternary mixtures of brine with dissolved H_2 + CH_4, a, D_{app}, and the salt diffusion coefficient in the quaternary mixture $D_{salt,quad}$ could be simultaneously accessed via DLS at T = 293 K with average relative expanded experimental uncertainties of (80 and 73)%.

Polymer Melts with Dissolved Blowing Agents

Thermoplastic foams are used in a wide range of technical applications and are produced by injection molding or extrusion with physical or chemical

blowing agents. In such processes, the resulting foam properties are governed by nucleation and bubble growth kinetics [352,353], both of which are significantly affected by D_{11}. Therefore, knowledge of D_{11} is necessary to understand nucleation and bubble growth processes and develop prediction approaches for the resulting foam properties [354,355]. However, owing to certain limitations of the conventionally applied techniques, there is currently a lack of D_{11} data under process-relevant conditions. In collaboration with Prof. Christian Bonten from the University of Stuttgart, a mixture of technical-grade polystyrene (PS) melt and dissolved nitrogen (N_2) as a blowing agent was selected as a model system and investigated via DLS. DLS was used, for the first time, to characterize a and D_{11} of binary mixtures consisting of a macromolecular polymer melt and a dissolved gas [264]. Figures 5.14(a) and 5.14(b) show the diffusivity results obtained at small Θ_S, which exhibit the typical behavior observed in liquids with dissolved gases.

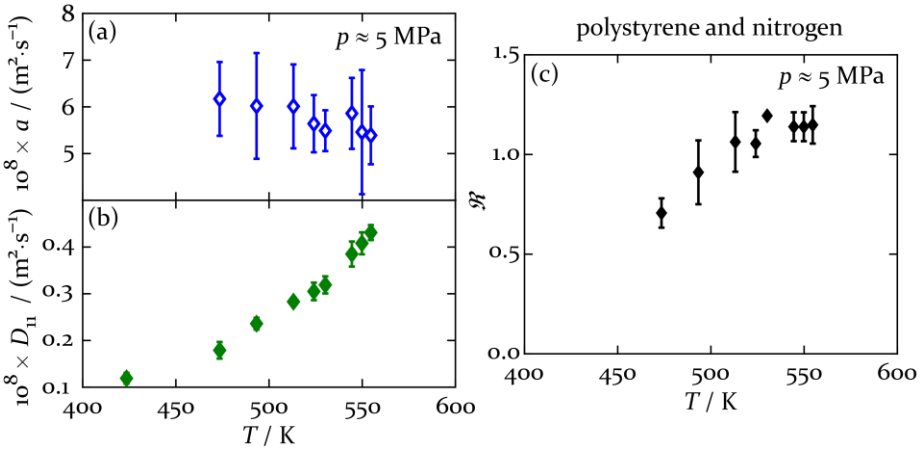

Figure 5.14: a (a) and D_{11} (b) in mixtures of PS with dissolved N_2 as a function of T for $p \approx 5$ MPa. The corresponding $\mathcal{H}$ values are shown in (c). Figures (a) and (b) were adapted from the respective publication [264].

At $\Theta_S = 90°$, an additional signal related to c fluctuations of polymer chains with different molecular weights was observed. The corresponding results for $\mathcal{H}$ are shown in Figure 5.14(c) and range from approximately (0.6 to 1.2). However, interpreting the magnitude of $\mathcal{H}$ is challenging. N_2 might not have been dissolved at c close to infinite dilution. Owing to the large difference in molar mass between N_2 ($M \approx 28$ g·mol^{-1}) and PS (weight average molar mass $M_w = 306\,000$ Da), as well as the chain-length distribution of

PS, definitive statements are difficult. The increase in $\mathcal{R}$ with increasing T at approximately constant p is likely due to the increasing solubility of N_2 in PS with increasing T [356]. Identifying signals related to D_{11} and a in the obtained CFs at conditions relevant to foaming processes, including T up to 555 K, was a major challenge due to distortions related to the technical grade of the polymer. However, a thorough evaluation of the obtained signals allowed for a discussion of the influence of p and T on a and D_{11}. The expanded mean relative uncertainties (k = 2) in a and D_{11} were (13 and 7.4)%.

5.2.3 Gaseous and Supercritical Mixtures

Binary Mixtures Consisting of CO_2, CH_4, and C_3H_8

To further test the mode allocations strategy developed in connection with the investigations of the equimolar CH_4–C_3H_8 mixture, binary mixtures of CO_2, CH_4, and C_3H_8, which are constituents of natural gas, were investigated between T = (293 and 353) K, p = (0.5 and 12) MPa, and x between (0.0833 and 0.917) via DLS. Which diffusivities were accessible depended on the location of the thermodynamic state points studied relative to the mixture phase envelopes, mixture ρ, optical contrast factors, and osmotic compressibility. Similar to the equimolar CH_4–C_3H_8 mixture (see Section 5.5.1), the obtained diffusivities were attributed to a, D_{11}, or D_m using the experimental and calculated $\mathcal{R}$, as well as T-, p- and c-dependent behaviors. Although the experimental $\mathcal{R}$ exhibited relatively large uncertainties, they agreed well with the calculated ratios far from the critical plait point. In some cases, literature data supported the attribution of the obtained diffusivities to a or D_{11}. In the compressed liquid phase and in some cases in the supercritical state, a and D_{11} could be determined simultaneously, whereas in the gaseous phase either a or D_m was obtained. A qualitative analysis was performed and showed that mode coupling should not have an impact on the diffusivity results. The average expanded uncertainty (k = 2) for all determined D_{11} was 5.8%. For the a, these uncertainties were 22% for the cases where it was determined simultaneously with the D_{11} and 3.0% where it was determined alone.

Figures 5.15(a) and 5.15(b) exemplarily show the concentration dependency of the experimental diffusivities for the CO_2–CH_4 system obtained along two isobars with p = (9 and 12) MPa for x_{CO_2} = (0.0833, 0.333, 0.500, 0.667, and 0.917) and T = (293, 303, 323, 338, and 353) K. The a values for the pure components calculated using REFPROP [279] are shown for comparison. To ensure legibility, the respective experimental expanded uncertainties (k = 2) were not included but can be found together with the diffusivity data

and experimentally accessible $\mathcal{R}$ in the tables in the publication [289]. For x_{CO_2} = 0.917 and T = 293 K, the fluid was in the compressed liquid phase where two exponentials could be resolved in the CFs for all investigated p. Here, the average experimental expanded uncertainties for a and D_{11} were (24 and 9)%. The experimental $\mathcal{R}$ values were between 1.2 and 6.4, indicating that the signal contribution related to c fluctuations exhibited a larger amplitude. This explains why the uncertainties for a were larger than those for D_{11}.

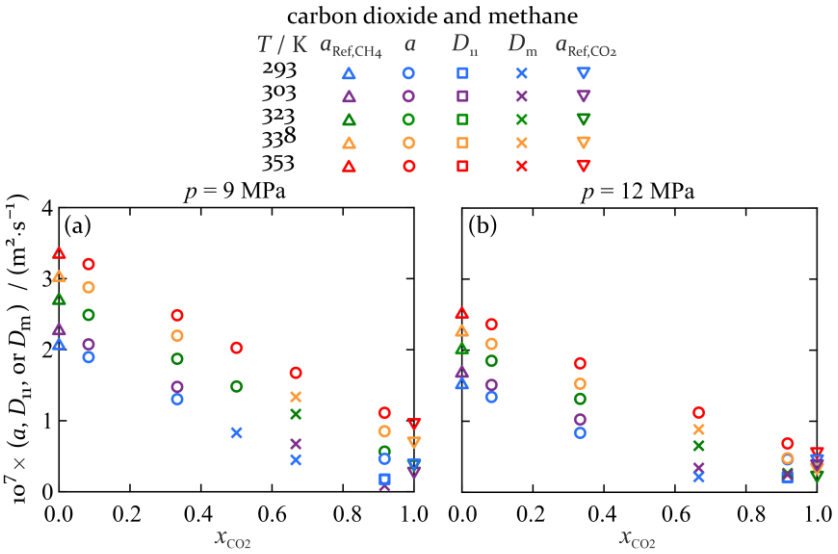

Figure 5.15: a (circles), D_{11} (squares), and D_m (crosses) measured via DLS for the CO_2–CH_4 system at different p and T as a function of the mole fraction of CO_2 x_{CO_2}. The T = (293, 303, 323, 338 and 353) K are represented by the blue, purple, green, orange, and red symbols, respectively. Furthermore, a data for pure CH_4 and pure CO_2 (triangles pointing upwards and downwards) obtained from the REFPROP database [279] are shown at x_{CO_2} = (0 and 1). Error bars are not given to ensure legibility. In virtually all cases, the measured diffusivities increase with increasing T for a given p and mixture composition. The figures were adapted from the respective publication [289].

Only a single exponential was found in the CFs for mixtures in the supercritical state. Considering all the supercritical state points, the experimental expanded uncertainties for the diffusivities obtained ranged from (0.5 to 5.0)% with an average of 2.2%. To judge which diffusivity was obtained via DLS in these cases, the mode attribution strategy based on the calculated $\mathcal{R}$ values described above was followed. Examples of the

calculated $\mathcal{R}$ values are shown in Figure 5.16 for x_{CO_2} = (0.500 and 0.917). In accordance with $\mathcal{R}$, for x_{CO_2} = (0.0833 and 0.333), a was obtained via DLS for all investigated p and T. This was confirmed by the fact that extrapolation of the c-dependent data for a given T and p to x_{CO_2} = 0 resulted in values matching the a data for pure CH_4 as calculated using REFPROP [279]. For x_{CO_2} = (0.500 and 0.667) and all p investigated, the obtained diffusivities could be related to a only at the higher T, whereas they represented D_m at the lower T. For the mixture with x_{CO_2} = 0.917, D_m was obtained at T = 303 K for all p according to the calculated $\mathcal{R}$ values. This is confirmed by the smaller values of D_m compared to a for pure CO_2. Furthermore, D_m increases with increasing p and, thus, increasing distance from the critical point. This behavior may be related to the critical slowing down of D_{11} when the critical point is approached [170,299]. At $T \geq 323$ K and x_{CO_2} = 0.917, the calculated $\mathcal{R}$ values indicate that the measured diffusivities represent a. This is supported by the good agreement of the c-dependent trend of the experimental diffusivities for the mixtures with the a values calculated for pure CO_2 using REFPROP [279]. A comparison with additional literature values for both a and D_{11} at x_{CO_2} different from 0.500 was not possible owing to the lack of respective literature data.

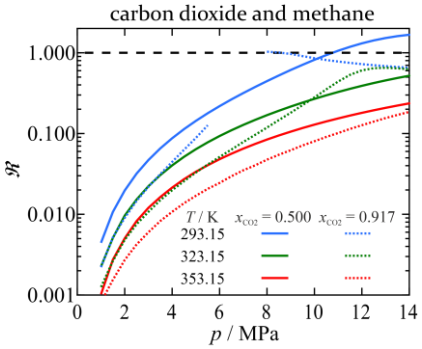

Figure 5.16: p dependency of the calculated $\mathcal{R}$ for the CO_2–CH_4 system for two different x_{CO_2} and three different T. The solid and dotted lines represent x_{CO_2} = (0.500 and 0.917). The T = (293, 323, and 353) K are represented by blue, green, and red lines, respectively, where higher $\mathcal{R}$ are always found for larger T at a given p and x_{CO_2}. The figure was adapted from the respective publication [289].

Binary Mixtures of H_2 and CH_4

Mixtures of H_2 and CH_4 are involved in numerous conventional technical processes, such as the production of H_2 from natural gas via steam reforming [357] or pyrolysis [358], as well as the photocatalytic production of H_2 and CH_4 from glycerol reforming [359]. For energy transition, the utilization of H_2-natural gas blends appears to be a promising solution because the blended H_2 can be transported through existing natural gas pipelines that are not suitable for pure H_2 [360]. Furthermore, for the large-scale storage of produced H_2 from offshore wind energy, the use of depleted reservoirs or subsurface caverns is currently under discussion [329]. In such reservoirs, CH_4 might be a pre-existing residual or intentionally used as cushion gas [333,335,336]. The accessibility of a and D_{11} in gaseous binary mixtures of H_2 and CH_4 via DLS was evaluated in cooperation with Shell Global Solutions International BV, as previously mentioned [280]. The investigations were performed at T = (293, 333, 363, and 393) K and p = (5, 10, and 15) MPa with varying x_{CH_4} of (0.05, 0.3, 0.6, and 0.8). For all thermodynamic states investigated, only one hydrodynamic mode was observable via DLS; the corresponding results are shown in Figure 5.17.

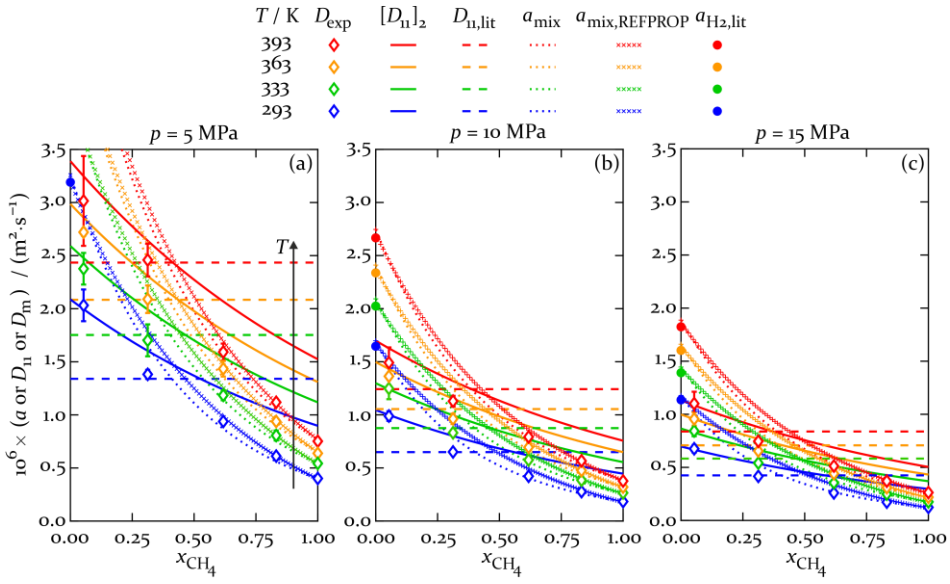

Figure 5.17: a, D_{11}, or D_m in the gaseous phase of mixtures of H_2 and CH_4 or pure CH_4 obtained via DLS (D_{exp}, diamonds) as a function of the CH_4 mole fraction x_{CH_4} at T = 293 K (blue), T = 333 K (green), T = 363 K (orange), and T = 393 K (red). (a), (b), and (c) show the results for p = 5, 10, and 15 MPa, respectively. Expanded uncertainties (k = 2) of the present experimental data are shown as error bars if they are larger than the symbol size. The solid and

dotted lines represent predicted D11 or a data using the Chapman–Enskog theory [361], $[D_{11}]_2$, or the model proposed by Lima et al. [362], a_{mix}. Data for the composition-independent integral diffusion coefficient ($D_{11,lit}$) from Bogatyrev and Nezovitina [74] interpolated to the present T and p is indicated by dashed lines. The a data for the mixtures using Equation 4.6 and literature data [277,363–367], $a_{mix,REFPROP}$, or for pure H_2 obtained via Equation 4.6 using data reported in a data compilation [368] is indicated by lines composed of x symbols or filled circles. The figure was adapted from the respective publication [280].

The related diffusivity exhibited a decreasing trend with decreasing T and increasing p and x_{CH_4}. Corresponding expanded (k = 2) experimental uncertainties ranged from (0.91 to 14)% and were on average 3.8%. The assignment of the single related diffusivity to either a, D_{11}, or D_m could be performed by considering D_{11} calculated using the Chapman–Enskog kinetic theory [361], experimental D_{11} literature data [74], predicted a using two different approaches [279,362], and calculations of $\mathcal{H}$. The obtained diffusivities were assigned to D_{11} at x_{CH_4} = 0.0533, D_m at x_{CH_4} = 0.3125, and a at x_{CH_4} = (0.6180 and 0.8319) by comparing them with the predicted and literature.

6 Conclusions and Prospect

This thesis highlights limits and capabilities of DLS for the simultaneous determination of thermal and mutual diffusivities in homogeneous molecular fluid mixtures. Although the focus is on binary fluid mixtures, some aspects related to multicomponent mixtures are also discussed. The evaluation is based on two main pillars: theory and experimental implementation of DLS. Theory provided a general understanding of the various contributions to the observed signals including the expected signal amplitudes of the studied fluctuations, their interrelationships, and possible coupling of heat and mass transfer. Experiments were performed for selected model systems facilitating fundamental investigations into different influencing factors, but also for systems relevant to process and energy engineering, encompassing T between (280 and 560) K, p between (0.030 and 20) MPa, and x between about (0.002 and 0.995). This allowed for bridging theoretical considerations with practical conditions and the aspects related to the experimental implementation of DLS. In addition to evaluating the applicability of DLS, this thesis significantly expanded the database of reliable diffusivity data for the systems studied. The studies referenced often demonstrated, for the first time, the applicability of DLS to the respective fluid class, system, or thermodynamic region.

For binary mixtures, the thermal diffusivity a and the Fick or mutual diffusion coefficient D_{11} can only be obtained by DLS if a coupling of heat and mass transfer can be excluded or, more precisely, is sufficiently small. In the presence of mode coupling, only two effective diffusivities $D_{\mathrm{eff},\{1,2\}}$ can be accessed, which are neither a nor D_{11}. While there is general knowledge available on the parameters that affect mode coupling in various thermodynamic states, detailed assessments of the impact of mode coupling on diffusivities are only available in the literature for a few specific systems. A thorough evaluation of mode coupling is often not possible due to the lack of accurate input data necessary for calculating the coupling parameter. To date, no study exists that evaluates the type of error that arises in the obtained diffusivities when only limited coupling is present. Further research is necessary to evaluate the influence of varying strengths of mode coupling on diffusivities and clarify this topic.

Although mode coupling can be excluded, there are experimental situations where it is unclear which signal is related to which type of fluctuations, or where only a single exponential signal can be resolved in the experimental CFs obtained for binary mixtures. Whether two contributions

related to T and c fluctuations can be simultaneously resolved depends primarily on four factors: the temporal spacing in terms of the Lewis number $Le = a \cdot D_{11}^{-1}$, relative signal amplitudes in terms of the Rayleigh ratio $\mathcal{R}$, SNR, and, to a certain extent, strength of possible disturbances in the CFs. In real experimental conditions, the difficulty lies in the fact that all of these influencing factors are superimposed, and that magnitudes of these parameters are initially unknown. Based on the results obtained in this thesis, for binary mixtures the following general statements can be made. A first indication of whether two contributions can be resolved is *Le*, which should be either greater than 1.5 or less than 0.5 to ensure a sufficient temporal separation of the two modes is given. For *Le* very close to unity, only a mixed diffusivity D_m related to both transport properties, that is, a and D_{11}, can be accessed. In addition, none of the signal amplitudes associated with the fluctuations in T, b_t, and in c, b_c, should be considerably large or considerably small. In general, the closer $\mathcal{R} = b_c \cdot b_t^{-1}$ is to unity, the larger the deviation of *Le* from unity should be to allow both contributions to be detected. When *Le* is not very close to unity, for instance, when $0.4 < Le < 0.9$ or $1.1 < Le < 1.6$, either two modes and, thus, a and D_{11} or only a single mode and, thus, D_m can be accessed. Here, the decision is mainly based on the signal quality and, thus, on SNR. For the latter case, D_m represents a if $b_t >> b_c$ or D_{11} when $b_c >> b_t$. Here, the greater the differences in b_t and b_c, the better the agreement between D_m and a or D_{11}. Furthermore, even if *Le* is far from unity, only a single mode may be accessible if either b_t or b_c tends to zero. The presence of a long-term disturbance in the CF has little effect on determining a and D_{11} simultaneously, as long as it can be accurately described. However, accurately describing the long-term disturbance can be challenging and only partly possible. This is clearly a weak point in the DLS technique. In most situations, SNR is the decisive factor that determines whether both a and D_{11} can simultaneously be successfully determined. However, how large the SNR must be depends on the individual conditions. The smaller SNR is, the larger the deviation of *Le* from unity and the closer $\mathcal{R} = 1$ should be to allow for a simultaneous determination of a and D_{11}. Furthermore, given the technical limitations of the measurement equipment, if $Le >> 1$ or $Le << 1$, the temporal spacing between the two signal contributions may be too large to be obtained in a single CF.

Drawing on insights gained from the studies related to this thesis, a mode attribution strategy was developed, which is universally applicable to any binary fluid mixture. A key element is the theoretical calculation of $\mathcal{R}$, which reveals that not only the optical contrast factors but also other properties, particularly the osmotic compressibility, are significant. However,

obtaining accurate values for osmotic compressibility has proven challenging. For a comprehensive assessment of various factors that affect $\mathcal{R}$, performing research on systems with a known osmotic compressibility would be beneficial. Despite the relatively large uncertainties in the calculated $\mathcal{R}$ due to the individual uncertainty contributions from the input parameters, generally excellent agreement between the calculated and experimental $\mathcal{R}$ values were found for the investigated systems. Thus, rewriting and iteratively solving the equations related to the calculation of $\mathcal{R}$ might allow estimating the mixture composition based on the experimental $\mathcal{R}$ values in DLS experiments.

The accessibility of specific diffusivities is strongly related to the location of the investigated thermodynamic state point relative to the phase envelope of the mixture, mixture density, optical contrast factors, and osmotic compressibility. Obtainable relative experimental uncertainties of the diffusivities typically range between (0.6 and 15)%, but can also be as high as 100% under certain conditions. Generally, molecular diffusivities in the range between about (10^{-14} and 10^{-6}) $m^2 \cdot s^{-1}$ can be accurately accessed by DLS if the analysis is performed in the time domain. A simultaneous determination of a and D_{11} was possible in the liquid phases and at some higher-density states in the supercritical phase. For the gaseous and most of the supercritical state points, only a single diffusivity, namely a, D_{11}, or D_m could be obtained and was identified with the help of the developed mode allocation strategy. In addition to the diffusivity data, a large pool of experimental $\mathcal{R}$ for various systems and thermodynamic states was determined. Further analysis of this data may allow for the establishment of fundamental relationships between molecular properties of the mixture constituents and $\mathcal{R}$. This could allow for the establishment of a simple model for $\mathcal{R}$.

For the multicomponent mixtures studied herein, mostly a and an apparent diffusivity D_{app} could be determined rather than the individual eigenvalues of the Fick diffusion matrix. Only in cases where a large temporal spacing between individual decay times can be expected, such as in aqueous solutions of sodium chloride with dissolved H_2, individual mass diffusive contributions were resolvable. Given the interest in obtaining accurate diffusivity data for multicomponent mixtures, further analysis of the applicability of DLS for such fluid mixtures would be desirable.

7 References

[1] Annual energy Outlook 2018 with projections to 2050, U.S. Energy Information Administration Office of Energy Analysis (EIA), Washington, 2018.

[2] Ammonia Technology Roadmap, International Energy Agency (IEA), Paris, 2021.

[3] T. Mang, Rheology of Lubricants, in: In Lubricants and Lubrication, eds W. Dresel and T. Mang, Wiley Online Library, pp. 31–50, 2017.

[4] J.H. Rushton, Mixing of Liquids in Chemical Processing, Ind. Eng. Chem. 44 (1952) 2931–2936.

[5] K. Palazoglu, Influence of convective heat transfer coefficient on the heating rate of materials with different thermal diffusivities, J. Food Eng. 73 (2006) 290–296.

[6] T.R. Waite, Theoretical Treatment of the Kinetics of Diffusion-Limited Reactions, Phys. Rev. 107 (1957) 463–470.

[7] T.N.P. Bosma, P.J.M. Middeldorp, G. Schraa, A.J.B. Zehnder, Mass Transfer Limitation of Biotransformation: Quantifying Bioavailability, Environ. Sci. Technol. 31 (1997) 248–252.

[8] R. Klaewkla, M. Arend, W.F. Hoelderich, A Review of Mass Transfer Controlling the Reaction Rate in Heterogeneous Catalytic Systems, INTECH Open Access Publisher, 2011.

[9] N. Kantarci, F. Borak, K.O. Ulgen, Bubble column reactors, Process Biochem. 40 (2005) 2263–2283.

[10] G. Ozel-Erol, M. Klein, N. Chakraborty, Lewis Number Effects on Flame Speed Statistics in Spherical Turbulent Premixed Flames, Flow, Turbul. Combust. 106 (2021) 1043–1063.

[11] L.-Y. Jiang, I. Campbell, Prandtl/Schmidt number effect on temperature distribution in a generic combustor, Int. J. Therm. Sci. 48 (2009) 322–330.

[12] B.E. Rapp, Chapter 9 - Fluids, in: Micro and Nano Technologies, Microfluidics: Modelling, Mechanics and Mathematics, Elsevier, Oxford, pp. 243–263, 2017.

[13] G. Yakar, R. Karabacak, Effects of Different Fin Spacings on the Nusselt Number and Reynolds Number in Perforated Finned Heat Exchangers, Heat Transf. Eng. 32 (2011) 399–407.

[14] H. Ganapathy, A. Shooshtari, S. Dessiatoun, M.M. Ohadi, M. Alshehhi, Hydrodynamics and Mass Transfer Performance of a Microreactor for Enhanced Gas Separation Processes, Chem. Eng. J. 266 (2015) 258–270.

[15] S. Ahuja, 5 Mass transport and separation, in: Separation Science and Technology, Academic Press, pp. 69–79, 2003.

[16] M. Hasib-ur-Rahman, M. Siaj, F. Larachi, Ionic liquids for CO_2 capture — Development and progress, Chem. Eng. Process. 49 (2010) 313–322.

[17] R. Baur, R. Krishna, R. Taylor, Influence of mass transfer in distillation: Feasibility and design, AIChE J. 51 (2005) 854–866.

[18] S.O. Olatunji, L.M. Camacho, Heat and Mass Transport in Modeling Membrane Distillation Configurations: A Review, Front. Energy Res. 6 (2018).

[19] J.J. Carberry, D. White, On the role of transport phenomena in catalytic reactor behavior, Ind. Eng. Chem. 61 (1969) 27–35.

[20] D.Y. Murzin, T. Salmi, Chapter 10 - Mass Transfer and Catalytic Reactions, in: Catalytic Kinetics (Second Edition), Elsevier, Amsterdam, pp. 589–664, 2016.

[21] P.M. Maitlis, A. de Klerk, Greener Fischer-Tropsch Processes for Fuels and Feedstocks, John Wiley & Sons, Weinheim, 2013.

[22] H. Becker, R. Güttel, T. Turek, Performance of diffusion-optimised Fischer–Tropsch catalyst layers in microchannel reactors at integral operation, Catal. Sci. Technol. 9 (2019) 2180–2195.

[23] L.W. Lake, R. Johns, B. Rossen, G.A. Pope, Fundamentals of enhanced oil recovery, Society of Petroleum Engineers, 2014.

[24] O. Massarweh, A.S. Abushaikha, A review of recent developments in CO_2 mobility control in enhanced oil recovery, Petroleum. 8 (2022) 291–317.

[25] P. Keller, A. Bader, C. Hasse, The influence of intra-droplet heat and mass transfer limitations in evaporation of binary hydrocarbon mixtures, Int. J. Heat Mass Transf. 67 (2013) 1191–1207.

[26] T. Rüther, A.I. Bhatt, A.S. Best, K.R. Harris, A.F. Hollenkamp, Electrolytes for Lithium (Sodium) Batteries Based on Ionic Liquids: Highlighting the Key Role Played by the Anion, Batter. Supercaps. 3 (2020) 1–36.

[27] R. Ye, D. Henkensmeier, S.J. Yoon, Z. Huang, D.K. Kim, Z. Chang, S. Kim, R. Chen, Redox Flow Batteries for Energy Storage: A Technology Review, J. Electrochem. Energy Convers. Storage. 15 (2018) 1–21.

[28] R. Lin, P.-L. Taberna, S. Fantini, V. Presser, C.R. Pérez, F. Malbosc, N.L. Rupesinghe, K.B.K. Teo, Y. Gogotsi, P. Simon, Capacitive Energy Storage from –50 to 100 °C Using an Ionic Liquid Electrolyte, J. Phys. Chem. Lett. 2 (2011) 2396–2401.

[29] M. Grätzel, Recent advances in sensitized mesoscopic solar cells, Acc. Chem. Res. 42 (2009) 1788–1798.

[30] T.J. Abraham, D.R. Macfarlane, R.H. Baughman, L. Jin, N. Li, J.M. Pringle, Towards ionic liquid-based thermoelectrochemical cells for the harvesting of thermal energy, Electrochim. Acta. 113 (2013) 87–93.

[31] R. Pollard, J. Newman, Transport Equations for a Mixture of Two Binary Molten Salts in a Porous Electrode, J. Electrochem. Soc. 126 (1979) 1713.

[32] H. Lundgren, J. Scheers, M. Behm, G. Lindbergh, Characterization of the Mass-Transport Phenomena in a Superconcentrated LiTFSI:Acetonitrile Electrolyte, J. Electrochem. Soc. 162 (2015) A1334–A1340.

[33] P. Preuster, C. Papp, P. Wasserscheid, Liquid Organic Hydrogen Carriers (LOHCs): Toward a Hydrogen-free Hydrogen Economy, Acc. Chem. Res. 50 (2017) 74–85.

[34] V. Arekhov, T. Clemens, J. Wegner, M. Abdelmoula, T. Manai, The Role of Diffusion on the Reservoir Performance in Underground Hydrogen Storage, Paper presented at the SPE EuropEC - Europe Energy Conference featured at the 84th EAGE Annual Conference & Exhibition, Vienna, Austria. (2023).

[35] D. Zivar, S. Kumar, J. Foroozesh, Underground hydrogen storage: A comprehensive review, Int. J. Hydrogen Energy. 46 (2021) 23436–23462.

[36] M. Ghasemi, S. Omrani, S. Mahmoodpour, T. Zhou, Molecular dynamics simulation of hydrogen diffusion in water-saturated clay minerals; implications for Underground Hydrogen Storage (UHS), Int. J. Hydrogen Energy. 47 (2022) 24871–24885.

[37] J. Liu, S. Wang, F. Javadpour, Q. Feng, L. Cha, Hydrogen Diffusion in Clay Slit: Implications for the Geological Storage, Energy & Fuels. 36 (2022) 7651–7660.

[38] E. Hendriks, G.M. Kontogeorgis, R. Dohrn, J.C. De Hemptinne, I.G. Economou, L.F. Žilnik, V. Vesovic, Industrial requirements for thermodynamics and transport properties, Ind. Eng. Chem. Res. 49 (2010) 11131–11141.

[39] G.M. Kontogeorgis, R. Dohrn, I.G. Economou, J.C. De Hemptinne, A. Kate, S. Kuitunen, M. Mooijer, L.F. Žilnik, V. Vesovic, Industrial requirements for thermodynamic and transport properties: 2020, Ind. Eng. Chem. Res. 60 (2021) 4987–5013.

[40] J.M.P. França, C.A. Nieto de Castro, M.M. Lopes, V.M.B. Nunes, Influence of Thermophysical Properties of Ionic Liquids in Chemical Process Design, J. Chem. Eng. Data. 54 (2009) 2569–2575.

[41] J. Millat, J.H. Dymond, C.A.N. de Castro, W.A. Wakeham, Transport properties of fluids, Cambridge University Press, Cambridge, 1996.

[42] D.M. Himmelblau, Diffusion of dissolved gases in liquids, Chem. Rev. 64 (1964) 527–550.

[43] C.R. Wilke, P. Chang, Correlation of diffusion coefficients in dilute solutions, AIChE J. (1955) 1:264–270.

[44] M.T. Tyn, W.F. Calus, Diffusion Coefficients in Dilute Binary Liquid Mixtures, J. Chem. Eng. Data. 20 (1975) 106–109.

[45] T. Sridhar, O.E. Potter, Quantum Effects in the Diffusion of Gases in Liquids, AlChE J. 23 (1977) 946–948.

[46] N. Umesi, R.P. Danner, Predicting Diffusion Coefficients in Nonpolar Solvents, Ind. Eng. Chem. Process Des. Dev. 20 (1981) 662–665.

[47] C. Giraudet, T. Klein, G. Zhao, M.H. Rausch, T.M. Koller, A.P. Fröba, Thermal, Mutual, and Self-Diffusivities of Binary Liquid Mixtures Consisting of Gases Dissolved in *n*-Alkanes at Infinite Dilution, J. Phys. Chem. B. 122 (2018) 3163–3175.

[48] W. Wu, T. Klein, M. Kerscher, M.H. Rausch, T.M. Koller, C. Giraudet, A.P. Fröba, Diffusivities in 1-Alcohols Containing Dissolved H_2, He, N_2, CO, or CO_2 Close to Infinite Dilution, J. Phys. Chem. B. 123 (2019) 8777–8790.

[49] D.C. Rapaport, D.C.R. Rapaport, The Art of Molecular Dynamics Simulation, Cambridge University Press, Cambridge, 2004.

[50] M.P. Allen, D.J. Tildesley, Computer Simulation of Liquids, Oxford University Press, New York, 1987.

[51] D. Frenkel, B. Smit, Understanding Molecular Simulation: from Algorithms to Applications, Academic Press, San Diego, 2002.

[52] L. Vozár, W. Hohenauer, Flash method of measuring the thermal diffusivity. A review, High Temp. Press. 36 (2004) 253–264.

[53] Y. Nagasaka, T. Hatakeyama, M. Okuda, A. Nagashima, Measurement of the thermal diffusivity of liquids by the forced Rayleigh scattering method: Theory and experiment, Rev. Sci. Instrum. 59 (1988) 1156–1168.

[54] G. Wu, M. Fiebig, J. Wang, Determination of the thermal diffusivity of liquids by laser induced thermal grating, Fluid Phase Equilib. 88 (1993) 239–249.

[55] S.E. Gustafsson, E Karawacki, M.N. Khan, Transient hot-strip method for simultaneously measuring thermal conductivity and thermal diffusivity of solids and fluids, J. Phys. D. Appl. Phys. 12 (1979) 1411.

[56] S.E. Gustafsson, On the development of the hot strip, hot disc, and pulse hot strip methods for measuring thermal transport properties, 20th Int. Therm. Expans. Symp., 2015.

[57] Y. Nagasaka, A. Nagashima, Simultaneous measurement of the thermal conductivity and the thermal diffusivity of liquids by the transient hot-wire method, Rev. Sci. Instrum. 52 (1981) 229–232.

[58] M.J. Assael, K.D. Antoniadis, D. Velliadou, W.A. Wakeham, Correct Use of the Transient Hot-Wire Technique for Thermal Conductivity Measurements on Fluids, Int. J. Thermophys. 44 (2023) 85.

[59] J.A.P. Lima, E. Marín, O. Correa, M.G. da Silva, S.L. Cardoso, C. Gatts, C.E. Rezende, H. Vargas, L.C.M. Miranda, Measurement of the thermal properties of liquids using a thermal wave interferometer, Meas. Sci. Technol. 11 (2000) 1522.

[60] E. Marín, E. Hernández-Rosales, A.M. Mansanares, R. Ivanov, J.B. Rojas-Trigos, A. Calderón, A method for thermal diffusivity measurement in fluids, Rev. Sci. Instrum. 84 (2013) 104903.

[61] D.E. Wetzler, P.F. Aramendía, M.L. Japas, R. Fernández-Prini, Thermal Diffusivity in Supercritical Fluids Measured by Thermal Lensing, Int. J. Thermophys. 19 (1998) 27–42.

[62] F. Cernuschi, P.G. Bison, A. Figari, S. Marinetti, E. Grinzato, Thermal Diffusivity Measurements by Photothermal and Thermographic Techniques, Int. J. Thermophys. 25 (2004) 439–457.

[63] M.J. Assael, A.R.H. Goodwin, V. Vesovic, W.A. Wakeham, Experimental Thermodynamics Volume IX: Advances in Transport Properties of Fluids, The Royal Society of Chemistry, 2014.

[64] J.G. Albright, R. Mills, A Study of Diffusion in the Ternary System, Labeled Urea-Urea-Water, at 25° by Measurements of the Intradiffusion Coefficients of Urea, J. Phys. Chem. 69 (1965) 3120–3126.

[65] J. Wu, M.J. Assael, K.D. Antoniadis, C. Wang, A. Mandelis, J. Hu, R. Tai, R.M. Banish, J.I.D. Alexander, K.R. Harris, Thermal Conductivity and Diffusivity, in: M.J. Assael, A.R.H. Goodwin, V. Vesovic, W.A. Wakeham (Eds.), Exp. Thermodyn. Vol. IX Adv. Transp. Prop. Fluids, The Royal Society of Chemistry, 2014.

[66] S.P. Cadogan, B. Mistry, Y. Wong, G.C. Maitland, J.P.M. Trusler, Diffusion Coefficients of Carbon Dioxide in Eight Hydrocarbon Liquids at Temperatures between (298.15 and 423.15) K at Pressures up to 69 MPa, J. Chem. Eng. Data. 61 (2016) 3922–3932.

[67] A. Bardow, V. Göke, H.-J. Koß, K. Lucas, W. Marquardt, Concentration-dependent diffusion coefficients from a single experiment using model-based Raman spectroscopy, Fluid Phase Equilib. 228–229 (2005) 357–366.

[68] A. Mialdun, V. Shevtsova, Measurement of the Soret and diffusion coefficients for benchmark binary mixtures by means of digital interferometry, J. Chem. Phys. 134 (2011) 44524.

[69] S.P. Cadogan, J.P. Hallett, G.C. Maitland, J.P.M. Trusler, Diffusion Coefficients of Carbon Dioxide in Brines Measured Using ^{13}C Pulsed-Field Gradient Nuclear Magnetic Resonance, J. Chem. Eng. Data. 60 (2015) 181–184.

[70] D. Bellaire, O. Großmann, K. Münnemann, H. Hasse, Diffusion coefficients at infinite dilution of carbon dioxide and methane in water, ethanol, cyclohexane, toluene, methanol, and acetone: A PFG-NMR and MD simulation study, J. Chem. Thermodyn. 166 (2022) 106691.

[71] V. Loianno, On the measurement of the mutual diffusivity of binary gas mixtures with FTIR Spectroscopy, Chem. Eng. Sci. 270 (2023) 118546.

[72] D.L. Wise, G. Houghton, The diffusion coefficients of ten slightly soluble gases in water at 10–60°C, Chem. Eng. Sci. 21 (1966) 999–1010.

[73] W.A. Wakeham, Diffusion coefficient measurements by the chromatographic method, Faraday Symp. Chem. Soc. 15 (1980) 145–154.

[74] A.F. Bogatyrev, M.A. Nezovitina, The Experimental Study of Temperature Dependence of Binary Diffusion Coefficients of Gases at Different Pressures, Int. J. Thermophys. 34 (2013) 2065–2075.

[75] T. Hou, C.W. Monroe, Composition-dependent thermodynamic and mass-transport characterization of lithium hexafluorophosphate in propylene carbonate, Electrochim. Acta. 332 (2020) 135085.

[76] A. Ehrl, J. Landesfeind, W.A. Wall, H.A. Gasteiger, Determination of Transport Parameters in Liquid Binary Lithium Ion Battery Electrolytes, J. Electrochem. Soc. 164 (2017) A826–A836.

[77] K. Nishikawa, Y. Fukunaka, T. Sakka, Y.H. Ogata, J.R. Selman, Measurement of $LiClO_4$ Diffusion Coefficient in Propylene Carbonate by Moiré Pattern, J. Electrochem. Soc. 153 (2006) A830.

[78] Y. Sato, K. Fujiwara, T. Takikawa, Sumarno, S. Takishima, H. Masuoka, Solubilities and diffusion coefficients of carbon dioxide and nitrogen in polypropylene, high-density polyethylene, and polystyrene under high pressures and temperatures, Fluid Phase Equilib. 162 (1999) 261–276.

[79] A. Königer, B. Meier, W. Köhler, Measurement of the Soret, diffusion, and thermal diffusion coefficients of three binary organic benchmark mixtures and of ethanol–water mixtures using a beam deflection technique, Philos. Mag. 89 (2009) 907–923.

[80] W. Wu, P.S. Schmidt, M. Piszko, C. Giraudet, M.H. Rausch, A.P. Fröba, Determination of diffusivities in binary fluid mixtures with various Lewis numbers as well as positive and negative Soret coefficients by the shadowgraph method, J. Chem. Phys. 159 (2023) 74502.

[81] F. Cernuschi, P.G. Bison, S. Marinetti, A. Figari, L. Lorenzoni, E. Grinzato, Comparison of thermal diffusivity measurement techniques, Quant. Infrared Thermogr. J. 28 (2002) 211–221.

[82] X. Huang, Comparison of thermal diffusivity measurement techniques, Michigan State University, M.Sc. thesis, 2004.

[83] P.A. Johnson, A.L. Babb, Liquid Diffusion Of Non-Electrolytes, Chem. Rev. 56 (1956) 387–453.

[84] P.J. Dunlop, K.R. Harris, D.J. Young, Experimental methods for studying diffusion in gases, liquids, and solids, in: Rossiter BW; Baetzold RC (ed.), Physical Methods of Chemistry. Vol. 6, Determination of Thermodynamic Properties, edn. 2, Wiley, New York, pp. 175–282, 1992.

[85] J. Winkelmann, Methods for the measurement of diffusion coefficient of fluids, in: Volume 15B2: "Diffusion in Gases, Liquids and Electrolytes", SpringerMaterials, 2018.

[86] L. García-Fernández, H. Bataller, P. Fruton, C. Giraudet, A. Vailati, F. Croccolo, Stabilized convection in a ternary mixture with two Soret coefficients of opposite sign, Eur. Phys. J. E. 45 (2022) 52.

[87] P.N. Segrè, R. Schmitz, J. V Sengers, Fluctuations in inhomogeneous and nonequilibrium fluids under the influence of gravity, Phys. A Stat. Mech. Its Appl. 195 (1993) 31–52.

[88] M.L. V Ramires, C.A. Nieto de Castro, Y. Nagasaka, A. Nagashima, M.J. Assael, W.A. Wakeham, Standard Reference Data for the Thermal Conductivity of Water, J. Phys. Chem. Ref. Data. 24 (1995) 1377–1381.

[89] C.A. Nieto de Castro, S.F.Y. Li, A. Nagashima, R.D. Trengove, W.A. Wakeham, Standard Reference Data for the Thermal Conductivity of Liquids, J. Phys. Chem. Ref. Data. 15 (1986) 1073–1086.

[90] M.J. Assael, A.E. Kalyva, S.A. Monogenidou, M.L. Huber, R.A. Perkins, D.G. Friend, E.F. May, Reference Values and Reference Correlations for the Thermal Conductivity and Viscosity of Fluids, J. Phys. Chem. Ref. Data. 47 (2018) 21501.

[91] F.J. V Santos, C.A. Nieto de Castro, J.H. Dymond, N.K. Dalaouti, M.J. Assael, A. Nagashima, Standard Reference Data for the Viscosity of Toluene, J. Phys. Chem. Ref. Data. 35 (2005) 1–8.

[92] D.G. Miller, Some comments on multicomponent diffusion: negative main term diffusion coefficients, second law constraints, solvent choices, and reference frame transformations, J. Phys. Chem. 90 (1986) 1509–1519.

[93] S. Kozlova, A. Mialdun, I. Ryzhkov, T. Janzen, J. Vrabec, V. Shevtsova, Do ternary liquid mixtures exhibit negative main Fick diffusion coefficients?, Phys. Chem. Chem. Phys. 21 (2019) 2140–2152.

[94] J.V Sengers, Mass Diffusion and Thermodiffusion in Multicomponent Fluid Mixtures, Int. J. Thermophys. 43 (2022) 59.

[95] R. Pecora, Dynamic Light Scattering: Applications of Photon Correlation Spectroscopy, Springer New York, New York, 1985.

[96] B.J. Berne, R. Pecora, Dynamic Light Scattering: With Applications to Chemistry, Biology, and Physics, Dover Publications, Mineola, 2000.

[97] B. Chu, Laser Light Scattering, Second Edi, Dover Publications, Mineola, 2007.

[98] A.P. Fröba, Dynamic Light Scattering (DLS) for the Characterization of Working Fluids in Chemical and Energy Engineering, Friedrich-Alexander-Universität Erlangen-Nürnberg, habil. thesis, 2009.

[99] L. Onsager, Reciprocal relations in irreversible processes. I, Phys. Rev. 37 (1931) 405–426.

[100] L. Onsager, Reciprocal relations in irreversible processes. II., Phys. Rev. 38 (1931) 2265–2279.

[101] R. Zwanzig, Time-Correlation Functions and Transport Coefficients in Statistical Mechanics, Annu. Rev. Phys. Chem. 16 (1965) 67–102.

[102] L. Blum, Light Scattering from Multicomponent Fluids, J. Chem. Phys. 50 (2003) 17–20.

[103] A. Heller, C. Giraudet, Z.A. Makrodimitri, M.S.H. Fleys, J. Chen, G.P. van der Laan, I.G. Economou, M.H. Rausch, A.P. Fröba, Diffusivities of Ternary Mixtures of *n*-Alkanes with Dissolved Gases by Dynamic Light Scattering, J. Phys. Chem. B. 120 (2016) 10808–10823.

[104] W. Krahn, G. Schweiger, K. Lucas, Light scattering measurements of mutual diffusion coefficients in binary liquid mixtures, J. Phys. Chem. 87 (1983) 4515–4519.

[105] K. Kraft, A. Leipertz, Sound velocity and sound attenuation measurements by dynamic light scattering, Int. J. Thermophys. 16 (1995) 445–453.

[106] H.Z. Cummins, R.W. Gammon, Rayleigh and Brillouin Scattering in Liquids: The Landau—Placzek Ratio, J. Chem. Phys. 44 (1966) 2785–2796.

[107] L. Fishman, R.D. Mountain, Activity coefficients of solutions from the intensity ratio of Rayleigh to Brillouin scattering, J. Phys. Chem. 74 (1970) 2178–2182.

[108] G.A. Miller, C.S. Lee, Brillouin spectra of dilute solutions and the Landau-Placzek formula, J. Phys. Chem. 72 (1968) 4644–4650.

[109] A.P. Fröba, A. Leipertz, Viscosity of Diisodecyl Phthalate by Surface Light Scattering (SLS), J. Chem. Eng. Data. 52 (2007) 1803–1810.

[110] A.P. Fröba, S. Will, A. Leipertz, Light scattering by surface waves on a vertical layer of liquid toluene, Appl. Opt. 36 (1997) 7615–7620.

[111] Z. Sun, C.H. Wang, Self-diffusion and interaction of the polystyrene-polyisoprene blend in chloroform probed by quasielastic light scattering, J. Chem. Phys. 112 (2000) 6844–6850.

[112] P. Daivis, I. Snook, W. V. Megen, B.N. Preston, W.D. Comper, Dynamic Light Scattering Measurements of Diffusion in Polymer-Polymer-Solvent Systems, Macromolecules. 17 (1984) 2376–2380.

[113] R. Borsali, M. Duval, M. Benmouna, Quasi-Elastic Light Scattering from Ternary Mixtures of Polystyrene/Poly(dimethylsiloxane) /Solvents, Macromolecules. 22 (1989) 816–821.

[114] N. Nemoto, Y. Makita, Y. Tsunashima, M. Kurata, Dynamic Light Scattering Studies of Polymer Solutions. 3. Translational Diffusion and Internal Motion of High Molecular Weight Polystyrenes in Benzene at Infinite Dilution, Macromolecules. 17 (1984) 425–430.

[115] Y. Tsunashima, M. Hirata, N. Nemoto, M. Kurata, Dynamic Light Scattering Studies of Polymer Solutions. 5. Universal Behavior of Highly Swollen Chains at Infinite Dilution Observed for Polyisoprenes in Cyclohexane, Macromolecules. 20 (1987) 1992–1999.

[116] R.M. Murphy, Static and dynamic light scattering of biological macromolecules: what can we learn?, Curr. Opin. Biotechnol. 8 (1997) 25–30.

[117] D.S. Lyles, M.O. McKenzie, R.R. Hantgan, Stopped-Flow, Classical, and Dynamic Light Scattering Analysis of Matrix Protein Binding to Nucleocapsids of Vesicular Stomatitis Virus, Biochemistry. 35 (1996) 6508–6518.

[118] B.M.I. van der Zande, J.K.G. Dhont, M.R. Böhmer, A.P. Philipse, Colloidal Dispersions of Gold Rods Characterized by Dynamic Light Scattering and Electrophoresis, Langmuir. 16 (2000) 459–464.

[119] M. Mihai, E.S. Dragan, S. Schwarz, A. Janke, Dependency of Particle Sizes and Colloidal Stability of Polyelectrolyte Complex Dispersions on Polyanion Structure and Preparation Mode Investigated by Dynamic Light Scattering and Atomic Force Microscopy, J. Phys. Chem. B. 111 (2007) 8668–8675.

[120] F.E. Berger Bioucas, C. Damm, W. Peukert, M.H. Rausch, T.M. Koller, C. Giraudet, A.P. Fröba, Translational and Rotational Diffusion Coefficients of Gold Nanorods Dispersed in Mixtures of Water and Glycerol by Polarized Dynamic Light Scattering, J. Phys. Chem. B. 123 (2019) 9491–9502.

[121] W. Wu, M.S.G. Knoll, C. Giraudet, M. Heinrich Rausch, A.P. Fröba, Heterodyne dynamic light scattering for the characterization of particle dispersions, Appl. Opt. 62 (2023) 8007–8017.

[122] B.J. Ackerson, H.J.M. Hanley, Rayleigh scattering from a methane–ethane mixture, J. Chem. Phys. 73 (1980) 3568–3572.

[123] A.P. Fröba, S. Will, A. Leipertz, Diffusion Modes of an Equimolar Methane–Ethane Mixture from Dynamic Light Scattering, Int. J. Thermophys. 21 (2000) 603–620.

[124] M.A. Anisimov, V.A. Agayan, A.A. Povodyrev, J. V. Sengers, E.E. Gorodetskii, Two-exponential decay of dynamic light scattering in near-critical fluid mixtures, Phys. Rev. E - Stat. Physics, Plasmas, Fluids, Relat. Interdiscip. Top. 57 (1998) 1946–1961.

[125] G. Wu, M. Fiebig, A. Leipertz, Thermal diffusivity of transparent liquids by photon correlation spectroscopy—II. Measurements in binary mixtures with a small difference in the refractive index of both pure components, Int. J. Heat Mass Transf. 31 (1988) 1471–1475.

[126] E. Gulari, R.J. Brown, C.J. Pings, Measurement of mutual diffusion coefficients and thermal diffusivities by quasi-elastic light scattering, AIChE J. 19 (1973) 1196–1204.

[127] H. Saad, E. Gulari, Diffusion of Liquid Hydrocarbons in Supercritical CO_2 by Photon Correlation Spectroscopy, Berichte Der Bunsengesellschaft Für Phys. Chemie. 88 (1984) 834–837.

[128] J. Schmitz, L. Belkoura, D. Woermann, Diffusivity in 2-butoxyethanol/water mixtures of noncritical composition approaching the liquid/liquid coexistence curve, J. Chem. Phys. 101 (1994) 476–479.

[129] D.A. Ivanov, T. Grossmann, J. Winkelmann, Comparison of ternary diffusion coefficients obtained from dynamic light scattering and Taylor dispersion, Fluid Phase Equilib. 228–229 (2005) 283–291.

[130] A. Bardow, On the interpretation of ternary diffusion measurements in low-molecular weight fluids by dynamic light scattering, Fluid Phase Equilib. 251 (2007) 121–127.

[131] E. Gross, Change of Wavelength of Light due to Elastic Heat Waves at Scattering in Liquids, Nature. 126 (1930) 201–202.

[132] L. Brillouin, Diffusion de la lumière et des rayons X par un corps transparent homogène, Ann. Phys. 9 (1922) 88–122.

[133] E. Gross, Modification of Light Quanta by Elastic Heat Oscillations in Scattering Media, Nature. 129 (1932) 722–723.

[134] L. Landau, G. Placzek, Struktur der unverschobenen Streulinie, Z. Phys. Sowjetunion. 5 (1934) 172–173.

[135] A.T. Forrester, Photoelectric Mixing As a Spectroscopic Tool, J. Opt. Soc. Am. 51 (1961) 253–259.

[136] H.Z. Cummins, N. Knable, Y. Yeh, Observation of Diffusion Broadening of Rayleigh Scattered Light, Phys. Rev. Lett. 12 (1964) 150–153.

[137] S.S. Alpert, Time-Dependent Concentration Fluctuations Near the Critical Temperature Using a He-Ne Laser, Proc. Conf. Phenom. Neighborhood Crit. Points. N.B.S. Mis (1965).

[138] S.S. Alpert, Y. Yeh, E. Lipworth, Observation of Time-Dependent Concentration Fluctuations in a Binary Mixture Near the Critical Temperature Using a He-Ne Laser, Phys. Rev. Lett. 14 (1965) 486–488.

[139] N.C. Ford, G.B. Benedek, Observation of the Spectrum of Light Scattered from a Pure Fluid Near its Critical Point, Phys. Rev. Lett. 15 (1965) 649–653.

[140] R. Pecora, Doppler Shifts in Light Scattering from Pure Liquids and Polymer Solutions, J. Chem. Phys. 40 (1964) 1604–1614.

[141] J. V Sengers, Effects of Critical Fluctuations on the Thermodynamic and Transport Properties of Supercritical Fluids, in: E. Kiran, J.M.H.L. Sengers (Eds.), Springer Netherlands, Dordrecht, 1994: pp. 231–271.

[142] H.L. Swinney, D.L. Henry, Dynamics of Fluids near the Critical Point: Decay Rate of Order-Parameter Fluctuations, Phys. Rev. A. 8 (1973) 2586–2617.

[143] H.L. Swinney, H.Z. Cummins, Thermal Diffusivity of CO_2 in the Critical Region, Phys. Rev. 171 (1968) 152–160.

[144] P. Berge, P. Calmettes, C. Laj, B. Volochine, Experimental Evidence of the "Critical Region" of a Binary Mixture by Means of Inelastic Scattering of Light, Phys. Rev. Lett. 23 (1969) 693–694.

[145] P. Berge, P. Calmettes, B. Volochine, C. Laj, A study of the dynamics of concentration fluctuations in a binary mixture, by means of inelastic scattering of light, in the immediate vicinity of its critical temperature, Phys. Lett. A. 30 (1969) 7–8.

[146] B. Volochine, P. Berge, I. Lagues, Experimental Study of the Relaxation of Concentration Fluctuations in the "Critical Region" of a Binary Mixture, Phys. Rev. Lett. 25 (1970) 1414–1416.

[147] T.K. Lim, H.L. Swinney, K.H. Langley, T.A. Kachnowski, Rayleigh Linewidth in SF_6 Near the Critical Point, Phys. Rev. Lett. 27 (1971) 1776–1780.

[148] G.T. Feke, G.A. Hawkins, J.B. Lastovka, G.B. Benedek, Spectrum and Intensity of Light Scattered from Sulfur Hexafluoride along the Critical Isochore, Phys. Rev. Lett. 27 (1971) 1780–1783.

[149] G.T. Feke, J.B. Lastovka, G.B. Benedek, K.H. Langley, P.B. Elterman, Spectrum and intensity of light scattered from SF_6 along the coexistence curve, Opt. Commun. 7 (1973) 13–17.

[150] J.B. Lastovka, G.B. Benedek, Spectrum of Light Scattered Quasielastically from a Normal Liquid, Phys. Rev. Lett. 17 (1966) 1039–1042.

[151] I.M. Aref'ev, B.D. Kopylovskii, D.S. Mash, I.L. Fabelinskii, Determination of the Diffusion Coefficients by Heterodyning Light Scattered by Liquid Solutions, Sov. J. Exp. Theor. Phys. Lett. 5 (1967) 355.

[152] P. Berge, P. Calmettes, M. Dubois, C. Laj, Experimental Observation of the Complete Rayleigh Central Component of the Light Scattered by a Two-Component Fluid, Phys. Rev. Lett. 24 (1970) 89–90.

[153] M. Dubois, P. Berge, C. Laj, Measurement of the diffusion coefficient of small molecules by means of quasi-elastic scattering of light, Chem. Phys. Lett. 6 (1970) 226–230.

[154] M. DuBois, P. Berge, Experimental Study of Rayleigh Scattering Related to Concentration Fluctuations in Binary Solutions: Evidence of a Departure from Ideality, Phys. Rev. Lett. 26 (1971) 121.

[155] R.D. Mountain, Spectral Distribution of Scattered Light in a Simple Fluid, Rev. Mod. Phys. 38 (1966) 205–214.

[156] R.D. Mountain, Density fluctuations in fluids having an internal degree of freedom, J. Res. Natl. Bur. Stand. Sect. A, Phys. Chem. 72 (1968) 95.

[157] R.D. Mountain, Thermal relaxation and Brillouin scattering in liquids, J. Res. Natl. Bur. Stand. Sect. A, Phys. Chem. 70 (1966) 207.

[158] R.D. Mountain, J.M. Deutch, Light Scattering from Binary Solutions, J. Chem. Phys. 50 (1969) 1103–1108.

[159] A.M. Jamieson, A.G. Walton, Studies of viscous drag in binary liquid mixtures by quasielastic light scattering, J. Chem. Phys. 58 (1971) 1054–1060.

[160] M. Corti, V. Degiorgio, Measurement of the thermal diffusivity of pure fluids by Rayleigh scattering of laser light, J. Phys. C Solid State Phys. 8 (1975) 953.

[161] K.J. Czworniak, H.C. Andersen, R. Pecora, Light scattering measurement and theoretical interpretation of mutual diffusion coefficients in binary liquid mixtures, Chem. Phys. 11 (1975) 451–473.

[162] E. Gülari, A.F. Collings, R.L. Schmidt, C.J. Pings, Light Scattering and Shear Viscosity Studies of the Binary System 2,6-Lutidine-Water in the Critical Region, J. Chem. Phys. 56 (2003) 6169–6179.

[163] K. Hamano, T. Nomura, T. Kawazura, N. Kuwahara, Dynamics of concentration fluctuations for polydimethylsiloxane-diethyl carbonate, Phys. Rev. A. 26 (1982) 1153–1156.

[164] H.C. Burstyn, J. V Sengers, Decay rate of critical concentration fluctuations in a binary liquid, Phys. Rev. A. 25 (1982) 448–465.

[165] H.C. Burstyn, R.F. Chang, J. V Sengers, Nonexponential Decay of Critical Concentration Fluctuations in a Binary Liquid, Phys. Rev. Lett. 44 (1980) 410–413.

[166] H. Güttinger, D.S. Cannell, Correlation range and Rayleigh linewidth of xenon near the critical point, Phys. Rev. A. 22 (1980) 285–286.

[167] Y.-I. Miura, H. Meyer, A. Ikushima, The decay rate of critical fluctuations in3He-4He mixtures near the gas-liquid critical point, J. Low Temp. Phys. 55 (1984) 247–271.

[168] R.F. Chang, H. Burstyn, J. V Sengers, Correlation function near the critical mixing point of a binary liquid, Phys. Rev. A. 19 (1979) 866–882.

[169] R.F. Chang, H. Burstyn, J. V Sengers, A.J. Bray, Experimental Determination of the Critical Correlation Function for a Binary Liquid Mixture: Evidence for Universality, Phys. Rev. Lett. 37 (1976) 1481–1484.

[170] R.F. Chang, P.H. Keyes, J. V Sengers, C.O. Alley, Dynamics of Concentration Fluctuations Near the Critical Mixing Point of a Binary Fluid, Phys. Rev. Lett. 27 (1971) 1706–1709.

[171] H. Bohidar, S. Chopra, Experimental studies of entropy and concentration fluctuation by photon correlation technique, Opt. Commun. 36 (1981) 46–50.

[172] A. Leipertz, G. Wu, M. Fiebig, Spectroscopic determination of the thermal diffusivity of organic mixtures and refrigerants, in: Int. Symp. Heat Mass Transf. Refrig. Cryog., Begel House Inc., 1986.

[173] S. Will, A.P. Fröba, A. Leipertz, Thermal Diffusivity and Sound Velocity of Toluene Over a Wide Temperature Range, Int. J. Thermophys. 19 (1998) 403–414.

[174] A.P. Fröba, S. Will, A. Leipertz, Dynamic light scattering as universal measuring technique for determining material properties illustrated for the example of toluene, Chemie Ing. Tech. 71 (1999) 257–261.

[175] A.P. Fröba, S. Will, A. Leipertz, Determination of several thermophysical properties of toluene using a single experimental setup, Paper presented at the 5th Asian Thermophysical Properties Conference, 30 August–2 September, 1998, Seoul, South Korea.1, Fluid Phase Equilib. 161 (1999) 337–351.

[176] G. Wu, M. Fiebig, A. Leipertz, Thermal diffusivity of transparent liquids by photon correlation spectroscopy—III. Measurements in binary mixtures with large differences in the refractive index of the pure components, Int. J. Heat Mass Transf. 31 (1988) 2555–2558.

[177] A.P. Fröba, S. Will, A. Leipertz, Thermophysical Properties of Binary and Ternary Fluid Mixtures from Dynamic Light Scattering, Int. J. Thermophys. 22 (2001) 1349–1368.

[178] A.P. Fröba, A. Leipertz, Thermophysical Properties of the Refrigerant Mixtures R410A and R407C from Dynamic Light Scattering (DLS), Int. J. Thermophys. 24 (2003) 1185–1206.

[179] A.P. Fröba, H. Kremer, A. Leipertz, Thermophysical Properties of Binary Mixtures of R125 + R143a in Comparison with a Simple Prediction Method, Int. J. Thermophys. 25 (2004) 1115–1133.

[180] A.P. Fröba, H. Kremer, A. Leipertz, F. Flohr, C. Meurer, Thermophysical Properties of a Refrigerant Mixture of R365mfc (1,1,1,3,3-Pentafluorobutane) and Galden® HT 55 (Perfluoropolyether), Int. J. Thermophys. 28 (2007) 449–480.

[181] A. Heller, M.H. Rausch, F. Flohr, A. Leipertz, A.P. Fröba, Thermophysical Properties of the Refrigerant Mixtures R417A and R417B from Dynamic Light Scattering (DLS), Int. J. Thermophys. 33 (2012) 396–411.

[182] A.P. Fröba, C. Botero, H. Kremer, A. Leipertz, Thermophysical Properties of a Quaternary Refrigerant Mixture: Comparison of Dynamic Light Scattering Measurements with a Simple Prediction Method, Int. J. Thermophys. 28 (2007) 743–757.

[183] A. Leipertz, M. Hendrix, M. Fiebig, G. Wu, Spectroscopic determination of the thermal diffusivities of some pure transparent organic liquids, VDI. Ber. (1984) 163–179.

[184] K. Kraft, A. Leipertz, Thermal diffusivity and sound velocity of Round-Robin R134a, Fluid Phase Equilib. 125 (1996) 245–255.

[185] A.P. Fröba, S. Will, A. Leipertz, Thermal Diffusivity and Sound Speed of the Refrigerant R143a (1,1,1-Trifluoroethane), Int. J. Thermophys. 22 (2001) 1021–1033.

[186] A.P. Fröba, S. Will, A. Leipertz, Thermophysical properties of R143a (1,1,1-trifluoroethane), Int. J. Refrig. 24 (2001) 734–743.

[187] M. Hendrix, A. Leipertz, M. Fiebig, G. Simonsohn, Thermal diffusivity of transparent liquids by photon correlation spectroscopy—I. Results for toluene and methanol in an extended range of temperature and pressure, Int. J. Heat Mass Transf. 30 (1987) 333–339

[188] M. Ibreighith, M. Fiebig, A. Leipertz, G. Wu, Thermal Diffusivity of the Alternative Refrigerants R123, R134a, R142b and R152a in the Liquid Phase, Fluid Phase Equilib. 80 (1992) 323–332.

[189] K. Kraft, A. Leipertz, Thermal diffusivity and ultrasonic velocity of saturated R152a, Int. J. Thermophys. 15 (1994) 791–802.

[190] K. Kraft, A. Leipertz, Thermal diffusivity and ultrasonic velocity of saturated R125, Int. J. Thermophys. 15 (1994) 387–399.

[191] A.P. Fröba, K. Krzeminski, A. Leipertz, Thermophysical Properties of 1,1,1,3,3-Pentafluorobutane (R365mfc), Int. J. Thermophys. 25 (2004) 987–1004.

[192] A.P. Fröba, C. Botero, A. Leipertz, Thermal Diffusivity, Sound Speed, Viscosity, and Surface Tension of R227ea (1,1,1,2,3,3,3-Heptafluoropropane), Int. J. Thermophys. 27 (2006) 1609–1625.

[193] K. Kraft, M. Matos Lopes, A. Leipertz, Thermal diffusivity and thermal conductivity of toluene by photon correlation spectroscopy: A test of the accuracy of the method, Int. J. Thermophys. 16 (1995) 423–432.

[194] E. Reile, J. Straub, Measurements of thermal diffusivity in pure fluids and binary liquid-gas mixtures by dynamic light scattering, in: Proc. Symp. Thermophys. Prop., American Society of Mechanical Engineers, 1982: p. 463.

[195] P. Jany, J. Sträub, E. Reile, Messung der Temperaturleitfähigkeit reiner Fluide und binärer Gemische mit Hilfe der dynamischen Lichtstreuung, Wärme - Und Stoffübertragung. 18 (1984) 99–108.

[196] P. Jany, J. Straub, Thermal diffusivity of fluids in a broad region around the critical point, Int. J. Thermophys. 8 (1987) 165–180.

[197] B. Kruppa, P. Jany, J. Straub, Experimental apparatus for measuring the thermal diffusivity of pure fluids at high temperatures, Int. J. Thermophys. 9 (1988) 911–921.

[198] B. Kruppa, J. Straub, Measurement of thermal diffusivity of the refrigerants R22 and R134a by means of dynamic light scattering, Fluid Phase Equilib. 80 (1992) 305–321.

[199] B. Kruppa, J. Straub, Thermal diffusivity of the alternative refrigerant R152a, Int. J. Thermophys. 18 (1997) 807–823.

[200] M. Pitschmann, J. Straub, The Thermal Diffusivity of the Refrigerants R32, R125, and R143a, Int. J. Thermophys. 23 (2002) 877–904.

[201] B. Kruppa, J. Straub, Dynamic light scattering: An efficient method to determine thermal diffusivity of transparent fluids, Exp. Therm. Fluid Sci. 6 (1993) 28–38.

[202] K. Saitow, H. Ochiai, T. Kato, K. Nishikawa, Correlation time of density fluctuation for supercritical ethylene studied by dynamic light scattering, J. Chem. Phys. 116 (2002) 4985–4992.

[203] K. Saitow, D. Kajiya, K. Nishikawa, Dynamics of Density Fluctuation of Supercritical Fluid Mapped on Phase Diagram, J. Am. Chem. Soc. 126 (2004) 422–423.

[204] D. Kajiya, K. Nishikawa, K. Saitow, Time Evolution of Density Fluctuation in the Supercritical Region. 2. Comparison of Hydrogen- and Non-hydrogen-Bonded Fluids, J. Phys. Chem. A. 109 (2005) 7365–7370.

[205] K. Saitow, D. Kajiya, K. Nishikawa, Time Evolution of Density Fluctuation in Supercritical Region. I. Non-hydrogen-bonded Fluids Studied by Dynamic Light Scattering, J. Phys. Chem. A. 109 (2005) 83–91.

[206] J. Chen, H. Xing, T. Zhan, L. Chen, M. He, Y. Zhang, Measurement of thermal diffusivity of ethanol from (293 to 564) K and up to 10 MPa in vicinity of the critical point, Fluid Phase Equilib. 552 (2022) 113276.

[207] Y. Zhang, T. Zhan, J. Chen, X. Liu, M. He, Experimental investigation and modeling of thermophysical properties of ethyl decanoate at high temperatures, Fluid Phase Equilib. 501 (2019) 112274.

[208] S. Wang, Y. Zhang, M. He, S. Zhang, X. Zheng, Thermal diffusivity of di-isopropyl ether (DIPE) in the temperature range 298–530K and pressure up to 10MPa from dynamic light scattering (DLS), Fluid Phase Equilib. 376 (2014) 202–209.

[209] Y. Zhang, J. Chen, T. Zhan, X. Liu, M. He, Speed of sound and thermal diffusivity of ethyl myristate, J. Chem. Thermodyn. 140 (2020) 105899.

[210] Y. Zhang, Y. Chen, T. Zhan, Y. Zheng, X. Zheng, M. He, Measurement of thermal diffusivity for carbon dioxide (CO_2) at T = 293.15–406.15 K and pressures up to 11 MPa by dynamic light scattering (DLS), Fluid Phase Equilib. 474 (2018) 126–130.

[211] M. He, X. Zheng, Y. Zhang, Y. Chen, Measurement of speed of sound and thermal diffusivity of ethyl heptanoate using light scattering method, Fluid Phase Equilib. 431 (2017) 75–81.

[212] L. Chen, Y. Zhang, S. Wang, X. Zheng, M. He, Thermal Diffusivity of 2-Methoxy-2-methylpropane at Temperatures from (303.15 to 493.15) K and Pressures from (1.5 to 10) MPa, J. Chem. Eng. Data. 59 (2014) 3927–3931.

[213] Y. Zhang, X. Zheng, Y. Chen, M. He, Thermal Diffusivity of 2-Ethoxy-2-methylpropane (ETBE) and 2-Methoxy-2-methylbutane (TAME) at Temperatures from (293 to 523) K and Pressure up to 10 MPa, J. Chem. Eng. Data. 62 (2017) 893–901.

[214] S. Wang, Y. Zhang, M.-G. He, X. Zheng, L.-B. Chen, Thermal Diffusivity and Speed of Sound of Saturated Pentane from Light Scattering, Int. J. Thermophys. 35 (2014) 1450–1464.

[215] H. Xing, J. Chen, Y. Zhang, L. Chen, M. He, Y. Zhang, Measurement of Thermal Diffusivity of *n*-Pentane from (293–573) K and up to 10.0 MPa in the Near-Critical and Supercritical Regions, J. Chem. Eng. Data. 66 (2021) 4697–4705.

[216] Y. Zhang, X. Zheng, M. He, Y. Chen, Measurement of thermal diffusivity and speed of sound of dibutyl ether from 303.15 K to 688.15 K and up to 7.5 MPa, Fluid Phase Equilib. 427 (2016) 320–327.

[217] J. Cui, G. Zhao, S. Bi, J. Wu, Thermal diffusivity measurements of R1234yf and R1234ze(E) under saturation conditions using dynamic light scattering method, Int. J. Refrig. 86 (2018) 133–138.

[218] X. Tang, Y. Wang, J. Cui, X. Hu, S. Bi, J. Wu, Thermal Diffusivity Measurement of Trans-1-chloro-3,3,3-trifluoropropene (R1233zd (E)) and Dodecafluoro-2-methylpentan-3-one (Novec1230) by the Dynamic Light Scattering Method, J. Chem. Eng. Data. 65 (2020) 4236–4241.

[219] Z. Yuan, Y. Wang, G. Zhao, J. Yin, S. Ma, Experimental investigation of liquid thermal diffusivity for fatty acid methyl/ethyl esters by dynamic light scattering method, J. Chem. Thermodyn. 188 (2024) 107163.

[220] G. Zhao, Z. Yuan, X. Zhang, J. Yin, S. Ma, Saturated liquid kinematic viscosity, surface tension and thermal diffusivity of two low-GWP refrigerants 3,3,3-trifluoropropene (R1243zf) and trans-1-chloro-3,3,3-trifluoro-1-propene (R1233zd(E)) by light scattering method, Int. J. Refrig. 127 (2021) 194–202.

[221] G. Hiller, G. Simonsohn, Measuring Thermal Diffusivities Using Two Photomultipliers in Cross-Correlation - Photon Correlation Techniques in Fluid Mechanics, E.O. Schulz-DuBois (Ed.), Springer Berlin Heidelberg, 1983: pp. 377–383.

[222] K. McKeigue, E. Gulari, Light-scattering measurements of diffusion in binary solutions containing an associating component, J. Phys. Chem. 88 (1984) 3472–3479.

[223] M.A. Siddiqi, W. Krahn, K. Lucas, Mutual diffusion coefficients in some binary liquid mixtures, J. Chem. Eng. Data. 32 (1987) 48–50.

[224] H.W. Fiedel, G. Schweiger, K. Lucas, Mutual diffusion coefficients of the systems bromobenzene + acetonitrile, bromobenzene + hexane, and bromobenzene + ethanol, J. Chem. Eng. Data. 36 (1991) 169–170.

[225] G. Wu, M. Fiebig, A. Leipertz, Messung des binären Diffusionskoeffizienten in einem Entmischungssystem mit Hilfe der Photonen-Korrelationsspektroskopie, Wärme - Und Stoffübertragung. 22 (1988) 365–371.

[226] H. Saad, E. Gulari, Diffusion of carbon dioxide in heptane, J. Phys. Chem. 88 (1984) 136–139.

[227] J.M.H. Levelt Sengers, G. Morrison, R.F. Chang, Critical behavior in fluids and fluid mixtures, Fluid Phase Equilib. 14 (1983) 19–44.

[228] T.M. Bender, R. Pecora, Dynamic light scattering measurements of mutual diffusion coefficients of water-rich 2-butoxyethanol/ water systems, J. Phys. Chem. 92 (1988) 1675–1677.

[229] M.H. Rausch, J. Lehmann, A. Leipertz, A.P. Fröba, Mutual diffusion in binary mixtures of ionic liquids and molecular liquids by dynamic light scattering (DLS), Phys. Chem. Chem. Phys. 13 (2011) 9525–9533.

[230] M.H. Rausch, L. Hopf, A. Heller, A. Leipertz, A.P. Fröba, Binary diffusion coefficients for mixtures of ionic liquids [EMIM][$N(CN)_2$], [EMIM][NTf_2], and [HMIM][NTf_2] with acetone and ethanol by dynamic light scattering (DLS), J. Phys. Chem. B. 117 (2013) 2429–2437.

[231] M.H. Rausch, A. Heller, A.P. Fröba, Binary Diffusion Coefficients of Glycerol-Water Mixtures for Temperatures from 323 to 448 K by Dynamic Light Scattering, J. Chem. Eng. Data. 62 (2017) 4364–4370.

[232] A. Heller, M.H. Rausch, P.S. Schulz, P. Wasserscheid, A.P. Fröba, Binary Diffusion Coefficients of the Liquid Organic Hydrogen Carrier System Dibenzyltoluene/Perhydrodibenzyltoluene, J. Chem. Eng. Data. 61 (2016) 504–511.

[233] M.S.G. Knoll, C. Giraudet, C.J. Hahn, M.H. Rausch, A.P. Fröba, Simultaneous study of molecular and micelle diffusion in a technical microemulsion system by dynamic light scattering, J. Colloid Interface Sci. 544 (2019) 144–154.

[234] X.-Y. Tang, S.-S. Bi, Y. Wang, J.-W. Cui, J.-T. Wu, Experimental Study on Viscosity and Mutual Diffusivity of R32/PAG Lubricant System, K. Cheng Je Wu Li Hsueh Pao/Journal Eng. Thermophys. 42 (2021) 296–299.

[235] X. Tang, G. Ren, K. Zhang, S. Bi, Mutual diffusivities of difluoromethane and 2,3,3,3-tetrafluoropropylene dissolved in polyalkylene glycol lubricant, Int. J. Refrig. 139 (2022) 41–47.

[236] A. Leipertz, Transport properties of transparent liquids by photon-correlation spectroscopy, Int. J. Thermophys. 9 (1988) 897–909.

[237] W.B. Li, J. V Sengers, R.W. Gammon, P.N. Segrè, Measurement of transport properties of liquids with equilibrium and nonequilibrium Rayleigh scattering, Int. J. Thermophys. 16 (1995) 23–31.

[238] A. Heller, T.M. Koller, M.H. Rausch, M.S.H. Fleys, A.N.R. Bos, G.P. van der Laan, Z.A. Makrodimitri, I.G. Economou, A.P. Fröba, Simultaneous Determination of Thermal and Mutual Diffusivity of Binary Mixtures of *n*-Octacosane with Carbon Monoxide, Hydrogen, and Water by Dynamic Light Scattering, J. Phys. Chem. B. 118 (2014) 3981–3990.

[239] M.H. Rausch, A. Heller, J. Herbst, T.M. Koller, M. Bahlmann, P.S. Schulz, P. Wasserscheid, A.P. Fröba, Mutual and thermal diffusivity of binary mixtures of the ionic liquids [BMIM][$C(CN)_3$] and [BMIM][$B(CN)_4$] with dissolved CO_2 by dynamic light scattering, J. Phys. Chem. B. 118 (2014) 4636–4646.

[240] A. Heller, M.S.H. Fleys, J. Chen, G.P. Van Der Laan, M.H. Rausch, A.P. Fröba, Thermal and Mutual Diffusivity of Binary Mixtures of *n*-Dodecane and *n*-Tetracontane with Carbon Monoxide, Hydrogen, and Water from Dynamic Light Scattering (DLS), J. Chem. Eng. Data. 61 (2016) 1333–1340.

[241] T.M. Koller, A. Heller, M.H. Rausch, P. Wasserscheid, I.G. Economou, A.P. Fröba, Mutual and Self-Diffusivities in Binary Mixtures of [EMIM][$B(CN)_4$] with Dissolved Gases by Using Dynamic Light Scattering and Molecular Dynamics Simulations, J. Phys. Chem. B. 119 (2015) 8583–8592.

[242] T.M. Koller, T. Klein, J. Chen, A. Kalantar, G.P. van der Laan, M.H. Rausch, A.P. Fröba, Simultaneous Analysis of Equilibrium Fluctuations at the Surface and in the Bulk of a Binary Liquid Mixture by Dynamic Light Scattering, J. Phys. Chem. B. 121 (2017) 10950–10956.

[243] T. Klein, W. Wu, M.H. Rausch, C. Giraudet, T.M. Koller, A.P. Fröba, Influence of Liquid Structure on Fickian Diffusion in Binary Mixtures of *n*-Hexane and Carbon Dioxide Probed by Dynamic Light Scattering, Raman Spectroscopy, and Molecular Dynamics Simulations, J. Phys. Chem. B. 122 (2018) 7122–7133.

[244] W. Wu, T. Klein, M. Kerscher, M.H. Rausch, T.M. Koller, C. Giraudet, A.P. Fröba, Mutual and Thermal Diffusivities as well as Fluid-Phase Equilibria of Mixtures of 1-Hexanol and Carbon Dioxide, J. Phys. Chem. B. 124 (2020) 2482–2494.

[245] A. Heller, Dynamic Light Scattering for the Determination of Thermal and Mass Diffusivities in Binary and Ternary Fluid Mixtures in Chemical and Energy Engineering, Friedrich-Alexander-Universität Erlangen-Nürnberg, PhD thesis, 2017.

[246] J. Cui, S. Yan, J. Wu, S. Bi, Determination of thermal and mutual diffusivity of n-heptane with dissolved carbon dioxide by dynamic light scattering, Fluid Phase Equilib. 526 (2020) 112804.

[247] J. Cui, J. Wu, S. Bi, Liquid viscosity, interfacial tension, thermal diffusivity and mutual diffusivity of *n*-Tetradecane with dissolved carbon dioxide, Fluid Phase Equilib. 534 (2021) 112951.

[248] J. Cui, T. Yang, S. Bi, J. Wu, Liquid viscosity, interfacial tension, thermal and mutual diffusivities of mixtures of *n*-eicosane with dissolved carbon dioxide, J. Chem. Thermodyn. 190 (2024) 107212.

[249] J.-W. Cui, S.-S. Bi, G.-J. Zhao, J.-T. Wu, Simultaneously Determination of Dynamic Viscosity, Interfacial Tension, Diffusivity of Binary Mixtures by Dynamic Light Scattering Method, K. Cheng Je Wu Li Hsueh Pao/Journal Eng. Thermophys. 41 (2020) 266–270.

[250] P. Gao, G. Zhao, J. Yin, S. Ma, Simultaneous Measurement of Thermal and Mutual Diffusion Coefficients by Dynamic Light Scattering, Guangzi Xuebao/Acta Photonica Sin. 52 (2023).

[251] H. Behnejad, J. V Sengers, M.A. Anisimov, Thermodynamic behaviour of fluids near critical points, Appl. Thermodyn. Fluids. 8 (2010) 321–367.

[252] M.A. Anisimov, A.A. Povodyrev, J. V Sengers, Crossover critical phenomena in complex fluids, Fluid Phase Equilib. 158–160 (1999) 537–547.

[253] J.V. Sengers, J.M.H. Levelt Sengers, Concepts and methods for describing critical phenomena in fluids, NASA Contractor Report 149665, 1977.

[254] M.A. Anisimov, E.E. Gorodetskii, V.D. Kulikov, A.A. Povodyrev, J. V. Sengers, A general isomorphism approach to thermodynamic and transport properties of binary fluid mixtures near critical points, Phys. A Stat. Mech. Its Appl. 220 (1995) 277–324.

[255] M.A. Anisimov, E.E. Gorodetskii, V.D. Kulikov, J. V Sengers, Crossover between vapor-liquid and consolute critical phenomena, Phys. Rev. E. 51 (1995) 1199–1215.

[256] M.A. Anisimov, E.E. Gorodetskii, V.D. Kulikov, A.A. Povodyrev, J. V Sengers, Erratum to "A general isomorphism approach to thermodynamic and transport properties of binary fluid mixtures near critical points," Phys. A Stat. Mech. Its Appl. 223 (1996) 272.

[257] D.G. Leaist, L. Hao, Comparison of diffusion coefficients of multicomponent solutions from light scattering and macroscopic gradient techniques: sodium dodecyl sulfate micelles in aqueous salt solutions, J. Phys. Chem. 97 (1993) 7763–7768.

[258] D.A. Ivanov, J. Winkelmann, Static and dynamic light scattering measurements near the critical solution point of a ternary liquid mixture, Phys. Chem. Chem. Phys. 006 (2004) 3490–3499.

[259] D.A. Ivanov, J. Winkelmann, Multiexponential decay autocorrelation function in dynamic light scattering in near-critical ternary liquid mixture, J. Chem. Phys. 125 (2006) 104507.

[260] B. Das, B. Maitra, S.M. Mercer, M. Everist, D.G. Leaist, A comparison of diffusion coefficients for ternary mixed micelle solutions measured by macroscopic gradient and dynamic light scattering techniques, Phys. Chem. Chem. Phys. 10 (2008) 3083–3092.

[261] J.P. Boon, S. Yip, Molecular hydrodynamics, Dover Publications, New York, 1991.

[262] J.M. Ortiz de Zárate, J. V. Sengers, Hydrodynamic fluctuations, Elsevier, Amsterdam, 2006.

[263] C. Cohen, J.W.H. Sutherland, J.M. Deutch, Hydrodynamic Correlation Functions for Binary Mixtures, Phys. Chem. Liq. 2 (1971) 213–235.

[264] M. Piszko, T. Schaible, C. Bonten, A.P. Fröba, Mutual and Thermal Diffusivities in Polystyrene Melts with Dissolved Nitrogen by Dynamic Light Scattering, Macromolecules. 54 (2021) 5662–5672.

[265] M. Piszko, C. Giraudet, A.P. Fröba, Diffusivities of an Equimolar Methane–Propane Mixture Across the Two-Phase Region by Dynamic Light Scattering, Int. J. Thermophys. 41 (2020) 1–25.

[266] L.D. Landau, E.M. Lifshitz, Electrodynamics of Continuous Media, Eddison-Wesley Publ. Co., Inc., Reading, MA, 1960.

[267] D.S. Chung, K.Y. Lee, E. Mazur, Fourier-transform heterodyne spectroscopy of liquid and solid surfaces, Appl. Phys. B. 64 (1996) 1–13.

[268] A. Leipertz, A.P. Fröba, Diffusion Measurements in Fluids by Dynamic Light Scattering, in: Diffusion in Condensed Matter: Methods, Materials, Models, P. Heitjans, J. Kärger (Eds.), Springer Berlin Heidelberg, 2005: pp. 579–618.

[269] A. Bardow, V. Göke, H.-J. Koß, W. Marquardt, Ternary diffusivities by model-based analysis of Raman spectroscopy measurements, AIChE J. 52 (2006) 4004–4015.

[270] W.B. Li, R.W.G. Segré, J. V. Sengers, M. Lamvik, Determination of the temperature and concentration dependence of the refractive index of a liquid mixture, J. Chem. Phys. 101 (1994) 5058–5069.

[271] M. Gebhardt, W. Köhler, A. Mialdun, V. Yasnou, V. Shevtsova, Diffusion, thermal diffusion, and Soret coefficients and optical contrast factors of the binary mixtures of dodecane, isobutylbenzene, and 1,2,3,4-tetrahydronaphthalene, J. Chem. Phys. 138 (2013) 114503.

[272] C. Giraudet, L. Marlin, D. Bégué, F. Croccolo, H. Bataller, Concentration dependent refractive index of CO_2/CH_4 mixture in gaseous and supercritical phase, J. Chem. Phys. 144 (2016).

[273] H.A. Lorentz, The Theory of Electrons and its Applications to the Phenomena of Light and Radiant Heat, 2nd ed., Leipzig: B.G. Teubner, 1916.

[274] C.M.M. Giraudet, Contributions à l'étude de la thermo diffusion de mélanges binaires en conditions de réservoirs, Université de Pau et des Pays de l'Adour (UPPA), PhD thesis, 2015.

[275] T.N. Olney, N.M. Cann, G. Cooper, C.E. Brion, Absolute scale determination for photoabsorption spectra and the calculation of molecular properties using dipole sum-rules, Chem. Phys. 223 (1997) 59–98.

[276] NIST Computational Chemistry Comparison and Benchmark Database NIST Standard Reference Database Number 101 Release 19, April 2018, Editor: Russell D. Johnson III.

[277] O. Kunz, W. Wagner, The GERG-2008 wide-range equation of state for natural gases and other mixtures: An expansion of GERG-2004, J. Chem. Eng. Data. 57 (2012) 3032–3091.

[278] A.M. Abudour, S.A. Mohammad, R.L. Robinson, K.A.M. Gasem, Volume-translated Peng-Robinson equation of state for liquid densities of diverse binary mixtures, Fluid Phase Equilib. 349 (2013) 37–55.

[279] E.W. Lemmon, I.H. Bell, M.L. Huber, M.O. McLinden, NIST Standard Reference Database 23: Reference Fluid Thermodynamic and Transport Properties-REFPROP, Version 10.0, National Institute of Standards and Technology, (2018).

[280] M. Piszko, P.S. Schmidt, M.H. Rausch, A.P. Fröba, Thermal Diffusivity and Fick Diffusion Coefficient in Mixtures of Hydrogen and Methane by Dynamic Light Scattering, Int. J. Thermophys. 44 (2023) 146.

[281] M. Piszko, C.J. Kankanamge, M.H. Rausch, T. Klein, A.P. Fröba, Dynamic Light Scattering for Studying Mutual Diffusion Coefficients in Electrolyte Systems Comprised Entirely of Ions, J. Electrochem. Soc. 167 (2020) 133502.

[282] M. Piszko, W. Wu, S. Will, M.H. Rausch, C. Giraudet, A.P. Fröba, Thermal and mutual diffusivities of fuel-related binary liquid mixtures under pre-combustion conditions, Fuel. 242 (2019) 562–572.

[283] M. Piszko, F.D. Lenahan, C. Dennstädt, T. Klein, A.P. Fröba, Mutual and Thermal Diffusivities in Binary Mixtures of *n*-Hexane or 1-Hexanol with Krypton, R143a, or Sulfur Hexafluoride by Using Dynamic Light Scattering and Molecular Dynamics Simulations, J. Chem. Eng. Data. 68 (2023) 1343–1357.

[284] T. Klein, M. Piszko, C.J. Kankanamge, G. Kasapis, A.P. Fröba, Fick Diffusion Coefficient in Binary Mixtures of [HMIM][NTf_2] and Carbon Dioxide by Dynamic Light Scattering and Molecular Dynamics Simulations, J. Phys. Chem. B. 125 (2021) 5100–5113

[285] T. Klein, M. Piszko, M. Lang, J. Mehler, P.S. Schulz, M.H. Rausch, T.M. Koller, A.P. Fröba, Diffusivities in Binary Mixtures of [AMIM][NTf_2] Ionic Liquids with the Dissolved Gases H_2, He, N_2, CO, CO_2, or Kr Close to Infinite Dilution, J. Chem. Eng. Data. 65 (2020) 4116–4129.

[286] M. Piszko, F.D. Lenahan, S.-L. Steinacker, T. Klein, A.P. Fröba, Diffusivities in Binary Mixtures of Ammonia Dissolved in *n*-Hexane, 1-Hexanol, or Cyclohexane Determined by Dynamic Light Scattering and Molecular Dynamics Simulations, J. Chem. Eng. Data. 68 (2023) 2585–2598.

[287] M. Piszko, P.S. Schmidt, M.H. Rausch, A.P. Fröba, Diffusivities in Water or Aqueous Solutions of Sodium Chloride with Dissolved Hydrogen and Methane, Int. J. Hydrogen Energy. 68 (2024) 499–510.

[288] F.D. Lenahan, M. Piszko, T. Klein, A.P. Fröba, Diffusivities in Binary Mixtures of *n*-Decane, *n*-Hexadecane, *n*-Octacosane, 2-Methylpentane, 2,2-Dimethylbutane, Cyclohexane, Benzene, Ethanol, 1-Decanol, Ethyl Butanoate, or *n*-Hexanoic Acid with Dissolved He or Kr Close to Infinite Dilution, J. Chem. Eng. Data. 67 (2022) 622–635.

[289] M. Piszko, K. Batz, M.H. Rausch, C. Giraudet, A.P. Fröba, Diffusivities of Binary Mixtures Consisting of Carbon Dioxide, Methane, and Propane by Dynamic Light Scattering, J. Chem. Eng. Data. 65 (2020) 1068–1082.

[290] M. Piszko, F.D. Lenahan, L. Friedl, T. Klein, A.P. Fröba, Mutual and Thermal Diffusivities in Mixtures of Cyclohexane, *n*-Hexadecane, *n*-Octacosane, or *n*-Hexanoic Acid with Carbon Dioxide Obtained by Dynamic Light Scattering and Molecular Dynamics Simulations, J. Chem. Eng. Data. 67 (2022) 3059–3076.

[291] M. Piszko, F.D. Lenahan, S. Hahn, M.H. Rausch, T.M. Koller, T. Klein, A.P. Fröba, Diffusivities in Binary Mixtures of *n*-Hexane or 1-Hexanol with Dissolved CH_4, Ne, Kr, R143a, SF_6, or R236fa Close to Infinite Dilution, J. Chem. Eng. Data. 66 (2021) 2218–2232.

[292] M. Piszko, F.D. Lenahan, T. Klein, A.P. Fröba, Diffusivities in Binary Mixtures of Cyclohexane or Ethyl Butanoate with Dissolved CH_4 or R143a Close to Infinite Dilution, J. Chem. Eng. Data. 68 (2023) 339–348.

[293] P. Calmettes, C. Laj, Dynamics of Entropy Fluctuations in a Critical Binary Mixture, Phys. Rev. Lett. 36 (1976) 1372–1375.

[294] P.N. Segrè, J. V. Sengers, Nonequilibrium fluctuations in liquid mixtures under the influence of gravity, Physica A. 198 (1993) 46–77.

[295] M.R. Moldover, J. V. Sengers, R.W. Gammon, R.J. Hocken, Gravity effects in fluids near the gas-liquid, Rev. Mod. Phys. 51 (1979) 79.

[296] I. Lizarraga, C. Giraudet, F. Croccolo, M. Bou-ali, H. Bataller, Mass diffusion and thermal diffusivity of the decane-pentane mixture under high pressure as a ground-based study for SCCO project, Microgravity - Sci. Technol. 28 (2016) 545–552.

[297] I. Medina, Determination of diffusion coefficients for supercritical fluids, J. Chromatogr. A. 1250 (2012) 124–140.

[298] C. Giraudet, H. Bataller, F. Croccolo, High-pressure mass transport properties measured by dynamic near-field scattering of non-equilibrium fluctuations, Eur. Phys. J. E. 37 (2014) 1–7.

[299] J. Luettmer-Strathmann, J. V Sengers, Transport Properties of Fluid Mixtures in the Critical Region I, 15 (1994) 1241–1249.

[300] J. V Sengers, J.G. Shanks, Experimental Critical-Exponent Values for Fluids, (2009) 857–877.

[301] P. Zangi, M.H. Rausch, A.P. Fröba, Binary Diffusion Coefficients for Gas Mixtures of Propane with Methane and Carbon Dioxide Measured in a Loschmidt Cell Combined with Holographic Interferometry, Int. J. Thermophys. 40 (2019) 18.

[302] S. Lee, A. Sardesai, Liquid phase methanol and dimethyl ether synthesis from syngas, Top. Catal. 32 (2005) 197–207.

[303] Q. Fei, M.T. Guarnieri, L. Tao, L.M.L. Laurens, N. Dowe, P.T. Pienkos, Bioconversion of natural gas to liquid fuel: Opportunities and challenges, Biotechnol. Adv. 32 (2014) 596–614.

[304] F.G. Acién Fernández, J.M. Fernández Sevilla, E. Molina Grima, Photobioreactors for the production of microalgae, Rev. Environ. Sci. Bio/Technology. 12 (2013) 131–151.

[305] S.T. Summerfelt, B.J. Vinci, R.H. Piedrahita, Oxygenation and carbon dioxide control in water reuse systems, Aquac. Eng. 22 (2000) 87–108.

[306] F.D. Lenahan, M. Piszko, T. Klein, A.P. Fröba, Molecular Dynamics Simulations of Liquid Ethane up to 298.15 K, Mol. Phys. 121:14 (2023).

[307] H. Lawrence Clever, R. Battino, J.H. Saylor, P.M. Gross, The solubility of helium, neon, argon and krypton in some hydrocarbon solvents, J. Phys. Chem. 61 (1957) 1078–1082.

[308] P.J. Hesse, R. Battino, P. Scharlin, E. Wilhelm, Solubility of gases in liquids. 20. Solubility of He, Ne, Ar, Kr, N_2, O_2, CH_4, CF_4, and SF_6 in *n*-Alkanes *n*-C_lH_{2l+2} ($6 \le l \le 16$) at 298.15 K, J. Chem. Eng. Data. 41 (1996) 195–201.

[309] S. Bo, R. Battino, E. Wilhelm, Solubility of Gases in Liquids. 19. Solubility of He, Ne, Ar, Kr, Xe, N_2, O_2, CH_4, CF_4, and SF_6 in Normal 1-Alkanols *n*-$C_lH_{2l+1}OH$ ($1 \le l \le 11$) at 298.15 K, J. Chem. Eng. Data. 38 (1993) 611–616.

[310] P.J. Lin, J.F. Parcher, Direct Gas Chromatographic Determination of the Solubility of Light Gases in Liquids. Henry's Law Constants for Eleven Gases in *n*-Hexadecane, *n*-Octacosane, and *n*-Hexatriacontane, J. Chromatogr. Sci. 20 (1982) 33–38.

[311] J.H. Jander, M. Piszko, V.W. Kühl, Julius, M.H. Rausch, A.P. Fröba, Solubility and Liquid Density of Binary Mixtures of n-Hexane or 1-Hexanol with Krypton, Sulfur Hexafluoride, or R143a, J. Chem. Eng. Data. 68 (2023) 813–834.

[312] J. Newman, K.E. Thomas-Alyea, Electrochemical Systems, 3rd ed., John Wiley & Sons, Inc, New Jersey, 2004.

[313] A. Kovač, M. Paranos, D. Marciuš, Hydrogen in energy transition: A review, Int. J. Hydrogen Energy. 46 (2021) 10016–10035.

[314] A.M. Abdalla, S. Hossain, O.B. Nisfindy, A.T. Azad, M. Dawood, A.K. Azad, Hydrogen production, storage, transportation and key challenges with applications: A review, Energy Convers. Manag. 165 (2018) 602–627.

[315] X. Li, C.J. Raorane, C. Xia, Y. Wu, T.K.N. Tran, T. Khademi, Latest approaches on green hydrogen as a potential source of renewable energy towards sustainable energy: Spotlighting of recent innovations, challenges, and future insights, Fuel. 334 (2023) 126684.

[316] S.E. Hosseini, M.A. Wahid, Hydrogen from solar energy, a clean energy carrier from a sustainable source of energy, Int. J. Energy Res. 44 (2020) 4110–4131.

[317] C. Acar, I. Dincer, Review and evaluation of hydrogen production options for better environment, J. Clean. Prod. 218 (2019) 835–849.

[318] H. Ishaq, I. Dincer, Comparative assessment of renewable energy-based hydrogen production methods, Renew. Sustain. Energy Rev. 135 (2021) 110192.

[319] S.E. Hosseini, M.A. Wahid, Hydrogen production from renewable and sustainable energy resources: Promising green energy carrier for clean development, Renew. Sustain. Energy Rev. 57 (2016) 850–866.

[320] J. Kurtz, S. Sprik, T.H. Bradley, Review of transportation hydrogen infrastructure performance and reliability, Int. J. Hydrogen Energy. 44 (2019) 12010–12023.

[321] M.R. Usman, Hydrogen storage methods: Review and current status, Renew. Sustain. Energy Rev. 167 (2022) 112743.

[322] A.M. Elberry, J. Thakur, A. Santasalo-Aarnio, M. Larmi, Large-scale compressed hydrogen storage as part of renewable electricity storage systems, Int. J. Hydrogen Energy. 46 (2021) 15671–15690.

[323] G. Valenti, 2 - Hydrogen liquefaction and liquid hydrogen storage, in: R.B. Gupta, A. Basile, T.N.B.T.-C. of H.E. Veziroğlu (Eds.), Woodhead Publ. Ser. Energy, Woodhead Publishing, 2016: pp. 27–51.

[324] A. Kumar, P. Muthukumar, P. Sharma, E.A. Kumar, Absorption based solid state hydrogen storage system: A review, Sustain. Energy Technol. Assessments. 52 (2022) 102204.

[325] D. Teichmann, W. Arlt, P. Wasserscheid, R. Freymann, A future energy supply based on Liquid Organic Hydrogen Carriers (LOHC), Energy Environ. Sci. 4 (2011) 2767–2773.

[326] J.H. Jander, P.S. Schmidt, C. Giraudet, P. Wasserscheid, M.H. Rausch, A.P. Fröba, Hydrogen solubility, interfacial tension, and density of the liquid organic hydrogen carrier system diphenylmethane/dicyclohexylmethane, Int. J. Hydrogen Energy. 46 (2021) 19446–19466.

[327] F.E. Berger Bioucas, M. Piszko, M. Kerscher, P. Preuster, M.H. Rausch, T.M. Koller, P. Wasserscheid, A.P. Fröba, Thermal Conductivity of Hydrocarbon Liquid Organic Hydrogen Carrier Systems: Measurement and Prediction, J. Chem. Eng. Data. 65 (2020) 5003–5017.

[328] M. Panfilov, 4 - Underground and pipeline hydrogen storage, in: R.B. Gupta, A. Basile, T.N.B.T.-C. of H.E. Veziroğlu (Eds.), Woodhead Publ. Ser. Energy, Woodhead Publishing, 2016: pp. 91–115.

[329] E.I. Epelle, W. Obande, G.A. Udourioh, I.C. Afolabi, K.S. Desongu, U. Orivri, B. Gunes, J.A. Okolie, Perspectives and prospects of underground hydrogen storage and natural hydrogen, Sustain. Energy Fuels. 6 (2022) 3324–3343.

[330] A. Aftab, A. Hassanpouryouzband, Q. Xie, L.L. Machuca, M. Sarmadivaleh, Toward a Fundamental Understanding of Geological Hydrogen Storage, Ind. Eng. Chem. Res. 61 (2022) 3233–3253.

[331] D.G. Caglayan, N. Weber, H.U. Heinrichs, J. Linßen, M. Robinius, P.A. Kukla, D. Stolten, Technical potential of salt caverns for hydrogen storage in Europe, Int. J. Hydrogen Energy. 45 (2020) 6793–6805.

[332] S.M. Jafari Raad, Y. Leonenko, H. Hassanzadeh, Hydrogen storage in saline aquifers: Opportunities and challenges, Renew. Sustain. Energy Rev. 168 (2022) 112846.

[333] N.S. Muhammed, M.B. Haq, D.A. Al Shehri, A. Al-Ahmed, M.M. Rahman, E. Zaman, S. Iglauer, Hydrogen storage in depleted gas reservoirs: A comprehensive review, Fuel. 337 (2023) 127032.

[334] M. Lysyy, M. Fernø, G. Ersland, Seasonal hydrogen storage in a depleted oil and gas field, Int. J. Hydrogen Energy. 46 (2021) 25160–25174.

[335] M. Zamehrian, B. Sedaee, Underground hydrogen storage in a partially depleted gas condensate reservoir: Influence of cushion gas, J. Pet. Sci. Eng. 212 (2022) 110304.

[336] M. Kanaani, B. Sedaee, M. Asadian-Pakfar, Role of Cushion Gas on Underground Hydrogen Storage in Depleted Oil Reservoirs, J. Energy Storage. 45 (2022) 103783.

[337] E.R. Peterson, Measurement of thermal conductivity of aqueous organic liquids using the relative transient hot-wire technique, Oklahoma State University, PhD thesis, 1985.

[338] W.J. de Blok, J.M.H. Fortuin, Method for determining diffusion coefficients of slightly soluble gases in liquids, Chem. Eng. Sci. 36 (1981) 1687–1694.

[339] P.T.H.M. Verhallen, L.J.P. Oomen, A.J.J.M. v. d. Elsen, J. Kruger, J.M.H. Fortuin, The diffusion coefficients of helium, hydrogen, oxygen and nitrogen in water determined from the permeability of a stagnant liquid layer in the quasi-steady state, Chem. Eng. Sci. 39 (1984) 1535–1541.

[340] R.T. Ferrell, D.M. Himmelblau, Diffusion coefficients of hydrogen and helium in water, AIChE J. 13 (1967) 702–708.

[341] B. Jähne, G. Heinz, W. Dietrich, Measurement of the diffusion coefficients of sparingly soluble gases in water, J. Geophys. Res. Ocean. 92 (1987) 10767–10776.

[342] S. Wang, T. Zhou, Z. Pan, J.P.M. Trusler, Diffusion Coefficients of N_2O and H_2 in Water at Temperatures between 298.15 and 423.15 K with Pressures up to 30 MPa, J. Chem. Eng. Data. 68 (2023) 1313–1319.

[343] I.N. Tsimpanogiannis, S. Maity, A.T. Celebi, O.A. Moultos, Engineering Model for Predicting the Intradiffusion Coefficients of Hydrogen and Oxygen in Vapor, Liquid, and Supercritical Water based on Molecular Dynamics Simulations, J. Chem. Eng. Data. 66 (2021) 3226–3244.

[344] S. Chabab, P. Théveneau, C. Coquelet, J. Corvisier, P. Paricaud, Measurements and predictive models of high-pressure H_2 solubility in brine (H_2O+NaCl) for underground hydrogen storage application, Int. J. Hydrogen Energy. 45 (2020) 32206–32220.

[345] M. Frost, E. Karakatsani, N. von Solms, D. Richon, G.M. Kontogeorgis, Vapor–Liquid Equilibrium of Methane with Water and Methanol. Measurements and Modeling, J. Chem. Eng. Data. 59 (2014) 961–967.

[346] H. Guo, Y. Chen, W. Lu, L. Li, M. Wang, In situ Raman spectroscopic study of diffusion coefficients of methane in liquid water under high pressure and wide temperatures, Fluid Phase Equilib. 360 (2013) 274–278.

[347] D.R. Caldwell, Thermal and Fickian diffusion of sodium chloride in a solution of oceanic concentration, Deep Sea Res. Oceanogr. Abstr. 20 (1973) 1029–1039.

[348] H.S. Harned, C.L.J. Hildreth, The Differential Diffusion Coefficients of Lithium and Sodium Chlorides in Dilute Aqueous Solution at 25°, J. Am. Chem. Soc. 73 (1951) 650–652.

[349] J.A. Rard, D.G. Miller, The mutual diffusion coefficients of NaCl–H_2O and $CaCl_2$–H_2O at 25°C from Rayleigh interferometry, J. Solution Chem. 8 (1979) 701–716.

[350] V. Vitagliano, P.A. Lyons, Diffusion Coefficients for Aqueous Solutions of Sodium Chloride and Barium Chloride, J. Am. Chem. Soc. 78 (1956) 1549–1552.

[351] L.A. Woolf, Isothermal diffusion measurement on the systems water—sodium chloride, water—pentaerythritol, and water—pentaerythritol—sodium chloride at 25°, J. Phys. Chem. 67 (1963) 273–277.

[352] J.H. Han, C. Dae Han, Bubble nucleation in polymeric liquids. I. Bubble nucleation in concentrated polymer solutions, J. Polym. Sci. Part B Polym. Phys. 28 (1990) 743–761.

[353] D. Tammaro, G. D'Avino, E. Di Maio, R. Pasquino, M.M. Villone, D. Gonzales, M. Groombridge, N. Grizzuti, P.L. Maffettone, Validated modeling of bubble growth, impingement and retraction to predict cell-opening in thermoplastic foaming, Chem. Eng. J. 287 (2016) 492–502..

[354] E.J. Barlow, W.E. Langlois, Diffusion of Gas from a Liquid into an Expanding Bubble, IBM J. Res. Dev. 6 (1962) 329–337.

[355] J. Stange, Einfluss rheologischer Eigenschaften auf das Schäumverhalten von Polypropylenen unterschiedlicher molekularer Struktur, Friedrich-Alexander-Universität Erlangen-Nürnberg, PhD thesis, 2006.

[356] Y. Sato, M. Yurugi, K. Fujiwara, S. Takishima, H. Masuoka, Solubilities of carbon dioxide and nitrogen in polystyrene under high temperature and pressure, Fluid Phase Equilib. 125 (1996) 129–138.

[357] L. García, 4 - Hydrogen production by steam reforming of natural gas and other nonrenewable feedstocks, in: V. Subramani, A. Basile, T.N.B.T.-C. of H.E. Veziroğlu (Eds.), Woodhead Publ. Ser. Energy, Woodhead Publishing, Oxford, 2015: pp. 83–107.

[358] N. Sánchez-Bastardo, R. Schlögl, H. Ruland, Methane Pyrolysis for Zero-Emission Hydrogen Production: A Potential Bridge Technology from Fossil Fuels to a Renewable and Sustainable Hydrogen Economy, Ind. Eng. Chem. Res. 60 (2021) 11855–11881.

[359] G. Iervolino, V. Vaiano, J.J. Murcia, A.E. Lara, J.S. Hernández, H. Rojas, J.A. Navío, M.C. Hidalgo, Photocatalytic production of hydrogen and methane from glycerol reforming over Pt/TiO_2–Nb_2O_5, Int. J. Hydrogen Energy. 46 (2021) 38678–38691.

[360] D. Haeseldonckx, W. D'haeseleer, The use of the natural-gas pipeline infrastructure for hydrogen transport in a changing market structure, Int. J. Hydrogen Energy. 32 (2007) 1381–1386.

[361] T.R. Marrero, E.A. Mason, Gaseous Diffusion Coefficients, J. Phys. Chem. Ref. Data. 1 (1972) 3–118.

[362] J.A.P. Lima, E. Marín, M.G. da Silva, M.S. Sthel, S.L. Cardoso, H. Vargas, L.C.M. Miranda, Application of the thermal wave resonator to the measurement of the thermal diffusivity of gas mixtures, Rev. Sci. Instrum. 72 (2001) 1580–1582.

[363] J.W. Leachman, R.T. Jacobsen, S.G. Penoncello, E.W. Lemmon, Fundamental Equations of State for Parahydrogen, Normal Hydrogen, and Orthohydrogen, J. Phys. Chem. Ref. Data. 38 (2009) 721–748.

[364] M.J. Assael, J.-A.M. Assael, M.L. Huber, R.A. Perkins, Y. Takata, Correlation of the Thermal Conductivity of Normal and Parahydrogen from the Triple Point to 1000 K and up to 100 MPa, J. Phys. Chem. Ref. Data. 40 (2011) 33101.

[365] U. Setzmann, W. Wagner, A New Equation of State and Tables of Thermodynamic Properties for Methane Covering the Range from the Melting Line to 625 K at Pressures up to 1000 MPa, J. Phys. Chem. Ref. Data. 20 (1991) 1061–1155.

[366] D.G. Friend, J.F. Ely, H. Ingham, Tables for the thermophysical properties of methane, NIST Technical Note 1325, 1989.

[367] O. Kunz, R. Klimeck, W. Wagner, M. Jaeschke, The GERG-2004 Wide-Range Equation of State for Natural Gases and Other Mixtures, Düsseldorf, 2007.

[368] R.D. McCarty, J. Hord, H.M. Roder, Selected Properties of Hydrogen, National Engineering Lab (NBS), Boulder, 1981.

Appendix: Publications

Publication A

Piszko, M.; Wu, W.; Will, S.; Rausch, M. H.; Giraudet, C.; Fröba, A. P. *Thermal and Mutual Diffusivities of Fuel-Related Binary Liquid Mixtures under Pre-Combustion Conditions*. Fuel **2019**, *242*, 562–572.

Publication B

Bioucas, F. E. B.; Piszko, M.; Kerscher, M.; Preuster, P.; Rausch, M. H.; Koller, T. M.; Wasserscheid, P.; Fröba, A. P. *Thermal Conductivity of Hydrocarbon Liquid Organic Hydrogen Carrier Systems: Measurement and Prediction*. J. Chem. Eng. Data **2020**, *65*, 5003–5017.

Publication C

Piszko, M.; Batz, K.; Rausch, M. H.; Giraudet, C.; Fröba, A. P. *Diffusivities of Binary Mixtures Consisting of Carbon Dioxide, Methane, and Propane by Dynamic Light Scattering*. J. Chem. Eng. Data **2020**, *65*, 1068–1082.

Publication D

Piszko, M.; Giraudet, C.; Fröba, A. P. *Diffusivities of an Equimolar Methane–Propane Mixture Across the Two-Phase Region by Dynamic Light Scattering*. Int. J. Thermophys. **2020**, *41*, 1–25.

Publication E

Piszko, M.; Kankanamge, C. J.; Rausch, M. H.; Klein, T.; Fröba, A. P. *Dynamic Light Scattering for Studying Mutual Diffusion Coefficients in Electrolyte Systems Comprised Entirely of Ions*. J. Electrochem. Soc. **2020**, *167*, 133502

Publication F

Piszko, M.; Lenahan, F. D.; Hahn, S.; Rausch, M. H.; Koller, T. M.; Klein, T.; Fröba, A. P. *Diffusivities in Binary Mixtures of n-Hexane or 1-Hexanol with Dissolved CH_4, Ne, Kr, R143a, SF_6, or R236fa* Close to Infinite Dilution. J. Chem. Eng. Data **2021**, *66*, 2218–2232.

Publication G

Piszko, M.; Schaible, T.; Bonten, C.; Fröba, A. P. Mutual and *Thermal Diffusivities in Polystyrene Melts with Dissolved Nitrogen by Dynamic Light Scattering*. Macromolecules **2021**, *54*, 5662–5672

Publication H

Lenahan, F. D.; Piszko, M.; Klein, T.; Fröba, A. P. *Diffusivities in Binary Mixtures of n-Decane, n-Hexadecane, n-Octacosane, 2-Methylpentane, 2,2-Dimethylbutane, Cyclohexane, Benzene, Ethanol, 1-Decanol, Ethyl Butanoate, or n-Hexanoic Acid with Dissolved He or Kr Close to Infinite Dilution*. J. Chem. Eng. Data **2022**, *67*, 622–635.

Publication I

Piszko, M.; Lenahan, F. D.; Friedl, L.; Klein, T.; Fröba, A. P. *Mutual and Thermal Diffusivities in Mixtures of Cyclohexane, n-Hexadecane, n-Octacosane, or n-Hexanoic Acid with Carbon Dioxide Obtained by Dynamic Light Scattering and Molecular Dynamics Simulations*. J. Chem. Eng. Data **2022**, *67*, 3059–3076.

Publication J

Piszko, M.; Lenahan, F. D.; Dennstädt, C.; Klein, T.; Fröba, A. P. *Mutual and Thermal Diffusivities in Binary Mixtures of n-Hexane or 1-Hexanol with Krypton, R143a, or Sulfur Hexafluoride by Using Dynamic Light Scattering and Molecular Dynamics Simulations*. J. Chem. Eng. Data **2023**, *68*, 1343–1357.

Publication K

Piszko, M.; Schmidt, P. S.; Rausch, M. H.; Fröba, A. P. *Thermal Diffusivity and Fick Diffusion Coefficient in Mixtures of Hydrogen and Methane by Dynamic Light Scattering*. Int. J. Thermophys. **2023**, *44*, 146.

Publication L

Piszko, M.; Schmidt, P. S.; Rausch M. H.; Fröba, A. P. *Diffusivities in Water or Aqueous Solutions of Sodium Chloride with Dissolved Hydrogen and Methane*. Int. J. Hydrogen Energy **2024**, *68*, 499–510.

This thesis explores which factors influence the feasibility of a simultaneous determination of thermal and mutual diffusivities in homogeneous molecular fluid mixtures by dynamic light scattering (DLS). The focus is primarily on binary fluid mixtures, but certain aspects related to multicomponent mixtures are also discussed. Considering both the theory and the experimental implementation of DLS, selected model systems consisting of methane and propane, as well as binary mixtures of liquids with dissolved gases, are studied in this work, allowing fundamental investigations of different influencing factors. Furthermore, various systems relevant for process and energy technologies are investigated, which often have a technical nature. These include mixtures related to biofuels, electrolytes, liquid organic hydrogen carriers, geological hydrogen storage, natural gas, and polymer melts with dissolved blowing agent. Investigations are conducted across a wide range of thermodynamic states, encompassing temperatures between (280 and 560) K, pressures between (0.030 and 20) MPa, and compositions spanning mole fractions between about (0.002 and 0.995). Besides the main aim, this endeavor not only significantly expands the database of reliable diffusivity data but frequently showcases, for the first time, the applicability of DLS to the respective system. Additionally, a signal attribution strategy is developed, which is universally applicable to any binary fluid mixture.

ISBN 978-3-96147-795-1

9 783961 477951

FAU UNIVERSITY PRESS 2025